

Cooperative Control for Heterogeneous Underactuated Autonomous Vehicle Networks

by

Bo Wang

Department of Mechanical Engineering
Villanova University
Villanova, PA 19085

Dissertation
Submitted to
College of Engineering
Villanova University

In Partial Fulfillment of the Requirements for the
Degree of Doctor of Philosophy

Villanova University
December, 2022

Copyright ©2022 by Bo Wang
All Rights Reserved

Statement by Author

This dissertation has been submitted in partial fulfillment of the requirements for an advanced degree at Villanova University.

Brief quotations from this dissertation are allowable without special permission, provided that accurate acknowledgment of source is made. Requests for permission for extended quotation from or reproduction of this manuscript in whole or in part may be granted by the head of the major department or the Associate Dean for Graduate Studies and Research of the College of Engineering when in his or her judgment the proposed use of the material is in the interests of scholarship. In all other instances, however, permission must be obtained from the author.

Dedication

*To Hashem Ashrafiou
and Sergey G. Nersesov
with thanks.*

Acknowledgments

First and foremost, I would like to thank my advisors Hashem Ashrafiuon and Sergey Nersesov for their continuous support during my Ph.D., and their precious advice, help, and motivation. They introduced me to the field of underactuated systems and keep me focused all these years. This dissertation would not have been possible without the cooperation of my advisors.

Besides, I would like to thank the members of my dissertation committee, Dr. Antonio Loria, Prof. Miroslav Krstić, and Prof. Garrett Clayton, for the valuable and very insightful comments they provided on this dissertation. I particularly wish to thank Antonio for his Ph.D. lectures in 2020, which enhanced my understanding in stability theory and introduced me to the field of nonlinear time-varying systems. I particularly would like to thank Prof. Miroslav Krstić for his assistance and guidance on extremum seeking control problems. His advice and encouragement towards my work have been invaluable.

I would like to thank my lab mates Aarya Deb, Marc Kohlhepp, Charles Yoo, Steven Williams, Jacob Delancy, and many more, for their great help in building and maintaining vital lab equipment.

I also would like to take a moment to mention my friends Drs. Chong Li, Guangwei Wang, Bowen Yi, Chengxi Zhang, and Ruzhou Yang for the inspiring and fruitful discussion with them. They walk ahead of me and light the way for me.

I am incredibly grateful to my family. My parents gave me their unconditional love and support during all these years. While I never had the opportunity to see my family during my three-and-a-half years of studies at Villanova, my heart has always been with them. They never stopped believing in me and did everything they could to help me achieve my goals.

At last, my most special thanks go to Yang Xu, who has accompanied me and has given me the strength to keep going.

Abstract

The cooperative control problem of multi-vehicle systems has attracted great attention within the fields of control engineering due to increasing potential military, industrial, and civilian applications. The advantages of multi-vehicle systems over single vehicles include higher efficiency, robustness, and flexibility. This work is devoted to developing distributed control approaches that are applicable to *heterogeneous underactuated* multi-vehicle systems.

Heterogeneous networks are multi-agent systems that contain different dynamical models. A multi-vehicle system usually contains different types of vehicles that may possess different parameters and dynamics. For instance, a combination of ground, marine, and aerial vehicles can be used for military operations to increase the striking force from multiple sources. Nevertheless, efforts to develop cooperative control approaches applicable to *heterogeneous* multi-vehicle systems have been limited. Moreover, *nonholonomicity* and *underactuation* are two main obstacles in the control design for multi-vehicle systems. The problem of cooperative control of underactuated networks is far more complicated than control of fully-actuated networks.

This study attempts to solve the cooperative control problem for heterogeneous underactuated multi-vehicle systems in a distributed fashion. We investigate the following problems for both *planar* and *spatial* underactuated multi-vehicle systems:

- 1) *Robust formation control.* By exploiting the structural properties of the planar vehicle model, a robust formation control framework is proposed for planar underactuated vehicle networks.
- 2) *Formation stabilization and tracking control.* A time-varying control strategy is presented to solve the simultaneous formation stabilization and tracking control problem for planar vehicles based on persistency of excitation.
- 3) *Source seeking control.* We propose a source seeking scheme for generic force-controlled planar underactuated vehicles by surge force tuning. The controller requires only real-time measurements of the source signal and ensures practical stability with respect to the linear motion coordinates for the closed-loop system.
- 4) *Formation control using bearing measurements.* We investigate the formation control problem for heterogeneous spatial underactuated vehicle networks without requiring any relative position measurements and subject to switching topologies.

In addition to the above theoretical analysis and control designs, we also conduct experiments on real multi-vehicle systems, including nonholonomic mobile robots, underactuated surface vessels, and quadcopters, to validate our control algorithms.

Contents

Abstract	vi
Nomenclature	ix
1 Introduction	1
1.1 Background & Motivation	1
1.2 Literature Review	3
1.2.1 On Underactuated Vehicle Systems	3
1.2.2 On Formation Control of Multi-Vehicle Systems	6
1.3 Overview of the Dissertation	8
2 Modeling of Underactuated Vehicle Networks	11
2.1 Generic Model of Underactuated Vehicles	11
2.1.1 Model of Planar Underactuated Vehicles	11
2.1.2 Model of Spatial Underactuated Vehicles	15
2.2 Notations from Graph Theory	17
2.3 Feasible Trajectory Generation	18
3 Robust Formation Control for Planar Underactuated Vehicle Networks	22
3.1 Problem Formulation	22
3.2 Reduced-Order Error Dynamics	24
3.3 Robust Formation Control Designs	27
3.3.1 A First-Order Sliding Mode Approach	27
3.3.2 A Super-Twisting Sliding Mode Approach	30
3.4 Numerical Simulations	34
3.4.1 Example 1	34
3.4.2 Example 2	36
3.5 Conclusion	37
4 Formation Stabilization and Tracking Control for Planar Underactuated Vehicle Networks	39
4.1 Introduction	39
4.2 Problem Formulation	40
4.3 Formation Stabilization and Tracking Control Design	42

4.4	Applications and Simulation Results	48
4.4.1	Applications	48
4.4.2	Numerical Simulations	49
4.5	Concluding Remarks	52
5	Source Seeking for Planar Underactuated Vehicles	53
5.1	Introduction	53
5.2	Problem Statement	55
5.2.1	Control/Optimization Objective	55
5.2.2	Shifted Passivity	55
5.3	Symmetric Product Approximations	57
5.3.1	Motivational Example	57
5.3.2	Symmetric Product Approximations	60
5.4	Source Seeking for Underactuated Vehicles	64
5.4.1	Source Seeking Scheme	64
5.4.2	Stability Analysis	65
5.5	Simulations	67
5.6	Experimental Results	68
5.7	Conclusions	69
6	Range Observer-Based Formation Control for Spatial Underactuated Vehicle Networks	72
6.1	Introduction	72
6.2	Range Observer Design	74
6.3	Formation Control Development	76
6.3.1	Generalized Slotine-Li Controller	76
6.3.2	Formation Control Design	81
6.4	Numerical Simulation	83
6.5	Conclusions	86
7	Conclusions & Future Work	87
7.1	Conclusions	87
7.2	Future Work	88
Appendices		90
A	Basic Notions	90
A.1	Partial-State Stability Notions	90
A.2	Technical Lemmas	95
A.3	The Variation of Constants Formula	97
Bibliography		98

Nomenclature

Notations

$\mathbb{Z}_{>0}$ ($\mathbb{Z}_{\geq 0}$)	The set of all positive (non-negative) integers.
\mathbb{R}	The set of all real numbers.
$\mathbb{R}_{>0}$ ($\mathbb{R}_{\geq 0}$)	The set of all positive (non-negative) real numbers.
\mathbb{R}^n	The set of all n -tuples for any $n \in \mathbb{Z}_{>0}$.
$ x $	The Euclidean norm of $x \in \mathbb{R}^n$, i.e., $ x = (\sum_{i=1}^n x_i ^2)^{1/2}$.
C^k	Class of functions f whose the first k derivatives exist and are continuous.
\mathcal{K}	Class of C^0 and strictly increasing functions $f : \mathbb{R}_{\geq 0} \rightarrow \mathbb{R}_{\geq 0}$ with $f(0) = 0$.
\mathcal{K}_∞	Class of functions $f \in \mathcal{K}$ with $f(\infty) = \infty$.
\mathcal{L}	Class of C^0 and strictly decreasing functions $f : \mathbb{R}_{\geq 0} \rightarrow \mathbb{R}_{\geq 0}$ with $f(\infty) = 0$.
\mathcal{KL}	Class of C^0 functions $f : \mathbb{R}_{\geq 0} \times \mathbb{R}_{\geq 0} \rightarrow \mathbb{R}_{\geq 0}$ with $f(\cdot, s) \in \mathcal{K}$ and $f(r, \cdot) \in \mathcal{L}$.

Abbreviations

PE	Persistency of Excitation
US	Uniform Stability
UAS	Uniform Asymptotic Stability
UES	Uniform Exponential Stability
UGAS	Uniform Global Asymptotic Stability
UGES	Uniform Global Exponential Stability
ISS	Input-to-State Stability
SPUAS	Semi-global Practical Uniform Asymptotic Stability
P-SPUAS	Partial Semi-global Practical Uniform Asymptotic Stability
GUUB	Global Uniform Ultimate Boundedness

Chapter 1

Introduction

1.1 Background & Motivation

The research problems to be discussed in this dissertation fall into the broad scope of cooperative control and networked systems, which have attracted great attention in the control community in the last two decades. In general, solving cooperative control problems for multi-agent systems consists of designing control input for each agent in the network so that the group of agents is able to accomplish a common task, for instance, synchronization, following a group leader, and forming a geometric pattern, or flocking motion. The central themes in the research of cooperative control for networked systems include understanding the role of cooperation, the mechanism of information sharing among agents, the stability of a global task arising from local interactions, and the robustness against measurement/communication perturbations, etc. [1].

In this dissertation, we focus on the cooperative control problem of multi-vehicle systems. The cooperative control problem of multi-vehicle systems has attracted great attention within the fields of control engineering due to increasing potential military, industrial, and civilian applications. Potential applications include reconnaissance, mine clearance, and search and rescue missions, to name a few. Such tasks cannot be performed by a single vehicle due to its limited capability and vulnerability to malfunctions. Operating multiple vehicles as a team can enhance efficiency and flexibility, and increase robustness to individual agent failures [2, 3].

Based on different mechanisms of information sharing, we distinguish the *centralized* and *distributed* control approaches in multi-vehicle coordination. The centralized approaches require centralized planning and coordination and attempt to control each vehicle in the network directly. In this case, each vehicle is assumed to be able to sense its global position, and the cooperative control problem is reduced to the stabilization of each system separately to

its reference behavior. The centralized schemes may reduce the performance of multi-vehicle systems and increase implementation costs. In contrast to centralized schemes, distributed control approaches need only local neighbor-to-neighbor interactions, which are significantly more scalable and robust in practice, and thus, distributed schemes have more autonomy and can save implementation costs. One of the objectives of this work is to develop distributed control approaches, where only local information is used to achieve global tasks. Some excellent surveys for recent progress on distributed control of multi-agent systems can be found in [3–6].

Heterogeneous networks are multi-agent systems that contain agents with different dynamical models. In practice, a multi-vehicle system usually contains different types of vehicles that may possess different parameters and dynamics due to the variety of sizes, capabilities, and mediums of operation. For instance, a combination of ground, marine, and aerial vehicles can be used for military operations to increase the striking force from multiple sources. Thus, it is more practical if a group of vehicles can cooperate with each other regardless of the parameters or even structures of their dynamic models. To address this problem, several analysis and design approaches have been presented in recent years for heterogeneous multi-agent systems such as for heterogeneous linear systems [7] and for heterogeneous nonlinear systems in normal form [8]. Nevertheless, efforts to develop cooperative control approaches applicable to heterogeneous multi-vehicle systems have been limited.

Moreover, *nonholonomicity* and *underactuation* are two main obstacles in the control design for multi-vehicle systems. Most real vehicles are underactuated, where by underactuated it is commonly meant that the number of independent actuators of a vehicle is strictly lower than the number of its degrees of freedom. The problem of cooperative control of underactuated multi-vehicle systems is far more complicated than control of fully-actuated multi-vehicle systems. In particular, since fully-actuated mechanical systems are feedback equivalent to the double-integrator dynamics, the cooperative control of fully-actuated multi-vehicle systems is equivalent to the cooperative control of double-integrator networks. However, the control problem for underactuated systems is far more difficult. For example, planar underactuated vehicles with zero gravitational and buoyant fields do not meet the Brockett's necessary condition, and thus, cannot be asymptotically stabilized by any continuous pure-state feedback.

This work is devoted to developing distributed control approaches that are applicable to heterogeneous underactuated multi-vehicle systems. In particular, we model the vehicles in the network as generic planar or spatial underactuated rigid bodies and allow them to have nonidentical dynamics. We mainly consider the formation control problem because it is the basis of other cooperative control algorithms such as estimation-based formation control, flocking, containment control, cyclic pursuit, etc. We also consider in this work distributed

obstacle avoidance and source seeking problems for underactuated vehicle systems.

1.2 Literature Review

1.2.1 On Underactuated Vehicle Systems

In mechanics, the *degrees of freedom* of a mechanical system is the number of independent parameters that define its configuration. A mechanical system is *underactuated* if it has fewer number of independent actuators than its degrees of freedom. Planar and spatial vehicle systems with first-order or second-order nonintegrable constraints are typical underactuated systems, which include, but are not limited to, wheeled mobile robots, surface vessels, underwater vehicles, helicopters, quadcopters, spacecraft, etc.

Nonholonomic Ground Vehicles. Studies of underactuated mechanical systems can be traced back to three decades ago when control of nonholonomic systems was of great interest to scientists, and they generates interesting control problems for which traditional control theory was not applicable [9]. Mechanical systems with nonholonomic constraints do not meet the Brockett's necessary condition [10], and thus, cannot be asymptotically stabilized by any continuous pure-state feedback. For nonholonomic systems, set-point stabilization and trajectory tracking usually are studied as two separate problems. Early works mainly focus on the stabilization problem of nonholonomic systems using time-varying approaches [11], discontinuous approaches [12], and hybrid approaches [13]. See the seminal survey paper [14] for the early developments in stabilization and motion planning of nonholonomic systems. Wheeled mobile robots are typical examples of mechanical systems with nonholonomic constraints. An excellent overview of the kinematic model of wheeled mobile robots can be found in [15], which discusses its structural properties, such as controllability, feedback linearizability, and feedback stabilizability, and proposes several controllers to solve the stabilization, trajectory tracking, and path following problems. For the stabilization problem, as pointed out in [14], the rates of convergence provided by smooth time-periodic feedback laws are necessarily non-exponential, and the feedback laws which provide faster convergence rates must necessarily be non-smooth. However, controlling kinematic nonholonomic systems with discontinuous (velocity) controls may be difficult to implement. An alternative pursuit in this direction is to consider the stabilization problem in polar coordinates. In [16], smooth time-invariant feedback is proposed to regulate the kinematic mobile robot to a set point with a fast convergence rate, even though the closed-loop system loses its stability at the origin.

For the trajectory tracking problem of nonholonomic systems, another obstruction is

that there exists no universal continuous controller (even time-varying) that can track an arbitrary feasible trajectory [17]. In [18], the global trajectory tracking problem was solved for the simplified mobile robot dynamic model using the backstepping technique under the condition that either the reference linear velocity or the reference angular velocity does not converge to zero. In [19], a simple linear global tracking controller was proposed for both the kinematic model and the simplified dynamic model of a mobile robot based on a cascaded system approach under the condition that the reference angular velocity is PE. This is the first time that the PE condition has appeared explicitly in control of nonholonomic systems, and nowadays PE conditions in control of nonholonomic systems are ubiquitous. Later, many nonlinear tracking controllers were proposed for nonholonomic mobile robots in the literature, for instance, using robust and adaptive technique [20], dynamic feedback linearization [21], and finite-time design [22], etc. Recently, using an observer-based dynamic feedback linearization method, the trajectory tracking control problem for nonholonomic mobile robots was solved using only Cartesian position measurements in [23].

The problem of *simultaneous stabilization and tracking* refers to finding a single control law that can solve both stabilization and tracking problems simultaneously without changing the controller structure [24]. This problem was first addressed for nonholonomic mobile robots in [25] using a saturation feedback and backstepping technique. Then, an output feedback controller [26] and an adaptive controller [27] were proposed using the same backstepping idea as in [25], where a sinusoidal signal is introduced in the angular velocity virtual control to handle the set-point stabilization. In [28], a controller was proposed for simultaneous stabilization and tracking of a mobile robot by introducing a time-varying signal, where the signal facilitates the conversion from a stabilization controller to a tracking controller adaptively and smoothly. Using the same saturation feedback idea in [25], an input-restricted robust controller was proposed in [29] to handle the parameter uncertainty and input constraints for mobile robots. In [30], a uniform δ -persistently exciting ($u\delta$ -PE) controller was proposed for nonholonomic mobile robots and UGAS for the origin of the closed-loop system was established for the first time in the literature.

Underactuated Marine Vehicles. Another type of underactuated vehicle is the planar vehicle with second-order nonintegrable constraints, i.e., acceleration constraints. Surface vessels are typical examples of this kind of underactuated vehicle. Similar to nonholonomic systems, planar underactuated vehicles with zero gravitational and buoyant field also cannot be asymptotically stabilized by continuous pure-state feedback [31], and there does not exist universal continuous controller (even time-varying) that can track an arbitrary feasible trajectory. Thus, in contrast with the case of fully-actuated systems, set-point stabilization cannot

be considered as a special case of trajectory tracking for planar underactuated vehicles.

The local stabilization problem was solved for surface vessels using discontinuous feedback (σ -process) in [32] and using time-varying feedback in [33]. A global practical stabilization controller was proposed in [34] for surface vessels using a combined averaging and backstepping approach. The global asymptotic stabilization problem for surface vessels was first solved in [35] using a smooth time-varying controller based on backstepping and Lyapunov design. Later, smooth time-varying and global exponential stabilization controllers were proposed for surface vessels in [36], and a time-invariant discontinuous and global asymptotic stabilization controller was proposed in [37].

The semi-global exponential tracking controller was presented for surface vessels in [38] using backstepping design. Based on Lyapunov's direct method, the global asymptotic tracking problem for surface vessels was first solved in [39] under the condition that the reference angular velocity is PE. In [40], the PE condition was relaxed and the reference trajectory is allowed to be a straight line. A simple exponential tracking control law was proposed in [41] based on the cascaded systems approach under the PE condition.

For the simultaneous stabilization and tracking control problem, unlike nonholonomic mobile robots, a surface vessel with only two available controls is under a nonintegrable second-order nonholonomic constraint and is not transformable into a chained system. Thus, the controllers designed specifically for mobile robots [25–30] cannot be extended to underactuated surface vessels directly. The simultaneous stabilization and tracking problem for underactuated surface vessels was first addressed in [42] using high-gain feedback, which achieves tracking and stabilization in the sense of global uniform ultimate boundedness (GUUB). Based on Lyapunov's direct method and backstepping technique, a time-varying controller was developed in [43] which guarantees the global asymptotic convergence of the stabilization and tracking errors to the origin. Then, an output-feedback controller [44] was designed using the same backstepping idea as in [43]. However, the designs in [43, 44] are quite complicated, computationally demanding, and are heavily dependent on particular ship dynamics with linear hydrodynamic damping, which makes those approaches less practical. It is noted that while there are many approaches to design controllers for different kinds of planar underactuated vehicles, they are heavily dependent on the particular structures of the vehicles. In [45], a trajectory tracking control framework was proposed for the generic planar underactuated vehicles that can be applied to various forms of planar vehicles.

Underactuated Spatial Vehicles. In contrast to the underactuated ground and marine vehicles, Brockett's necessary condition is not an obstacle for the stabilization problem of underactuated spatial vehicles, and the stabilization problem can be seen as a special case of tra-

jectory tracking control problem for underactuated spatial vehicles. Quadcopters are typical examples of underactuated spatial vehicles. Linear controllers such as PID controller [46, 47] and LQR controller [46] are commonly used in quadcopter systems due to their simplicity. Numerous nonlinear tracking controllers for quadcopters have been proposed in the literature such as feedback linearization controller [48], sliding mode controller [48, 49], flatness-based controller [50], etc. However, due to the configuration space of the quadcopter system being $\text{SE}(3)$, the above control designs [46–50] based on Euler angles exhibit singularities when representing complex rotational maneuvers of a quadcopter. To avoid singularities, geometric tracking controllers were proposed in [51, 52] for quadcopters to achieve almost global asymptotic tracking. Recently, using similar ideas from [45], the trajectory tracking control problem was solved for generic spatial vehicles with one degree of underactuation in [53], and spatial vehicles with two degrees of underactuation in [54].

1.2.2 On Formation Control of Multi-Vehicle Systems

Controlled collective behaviors of multi-vehicle systems are of particular interest in recent years due to their potential applications ranging from industry to military [2, 3]. The distributed formation control problem, which can be considered as classical trajectory tracking or stabilization control problem extended to the multi-agent systems, is one of the most actively studied topics within the field of control engineering. The distributed formation control consists of making all the agents form a predefined geometrical configuration through *local* interactions with or without a group reference [3]. In other words, each follower uses only *local* information/measurements to achieve a *global* formation task.

According to fundamental ideas in control schemes, formation control can be classified as leader-follower strategy, virtual structure approach and behavior-based method [55]. Among various control schemes, the leader-follower strategy is of particular significance in many applications due to its simplicity and scalability [56]. Within this framework, many research articles have addressed the formation control problem for planar underactuated vehicles [57–59] and for spatial underactuated vehicles [60, 61]. In the survey paper [5], multi-agent formation control strategies were reviewed and categorized into position-based, displacement-based and distance-based approaches depending on the sensing capability and the interaction topology. In the position-based approach, such as in [62–64], agents sense their positions with respect to a global coordinate system, and interactions are not necessarily required because the desired formation can be achieved by position control of individual agents. Distance-based coordination approaches, such as [65], do not need the local coordinate systems to be aligned with each other, but the interaction graph has to be rigid or persistent and must contain

redundant connections. The displacement-based approach balances the sensing capability and the interaction requirements, and thus, is particularly useful in applications where the GPS signal is not available while onboard sensors can provide measurements necessary for feedback. In the displacement-based approach, the desired formation is specified by the inter-agent positions, which implies that agents need to know their orientation in the global coordinate system.

Various consensus and formation control approaches were proposed in the literature for vehicles modeled as single and double integrators [66–69], linear systems [70], fully-actuated rigid body attitude dynamics [71, 72], and fully-actuated Euler-Lagrangian systems [73]. For underactuated multi-vehicle networks, several cooperative control methods have been developed in the literature according to different models of vehicles. Leader-follower formation control of multiple nonholonomic mobile robots was considered in [56, 57, 64, 74–76]. We refer the readers to the survey paper [77] for a comprehensive literature review of formation control of ground vehicles. Leader–follower cooperative control of multiple underactuated surface vessels was considered in [58, 62, 63], and cooperative control of underactuated aircraft was considered in [78–80]. While this brief discussion is not intended to be a comprehensive review, it is found that although most of the control strategies in the existing work can successfully be applied to *homogeneous* underactuated multi-vehicle networks, these control designs heavily depend on the specific structures of vehicle dynamics and hence can hardly be applied to control *heterogeneous* networks of underactuated vehicles. In practice, however, it is useful if a group of vehicles can cooperate with each other regardless of the model parameters or even structures of their dynamic models.

Only a few works discuss the formation control problem of *heterogeneous underactuated* networks. In [81], the formation–containment control problem was considered for heterogeneous underactuated autonomous underwater vehicles (AUVs) in three-dimensional space based on a simplified 5-DOF model. In [82, 83], an integral sliding mode control law and an LQR consensus protocol were proposed for heterogeneous multi-vehicle systems consisting of quadrotors and wheeled mobile robots based on the linearized models. Recently, in [84], a coordinated trajectory tracking controller was developed based on cascaded system theory and Lyapunov analysis for the marine aerial-surface heterogeneous system composed of a quadrotor and a (fully-actuated) surface vehicle. Nevertheless, in the above-mentioned works [81–84], the vehicle models in the heterogeneous networks are either simplified, linearized, or partially assumed to be fully actuated.

1.3 Overview of the Dissertation

We briefly summarize the main results of this document, chapter by chapter, and cite related publications.

- Chapter 1: We provide an introduction to the topics studied in this dissertation, including background, motivation, literature review, and summary of contributions.
- Chapter 2: We provide generic rigid-body models of both planar and spatial underactuated vehicles including wheeled mobile robots, surface vessels, and quadcopters. Then, graph theory is used to model the network structure of multi-vehicle systems. Since an underactuated system cannot be commanded to track arbitrary trajectories, we also discuss feasible trajectory generation using the constraints of vehicle dynamics.
- Chapter 3: We investigate distributed robust formation control problems for networks of heterogeneous planar underactuated vehicles without global position measurements. We exploit the cascaded structure of the kinematics and dynamics of generic vessel models to develop structured reduced-order error dynamics for group cooperation. By incorporating graph theory, sliding-mode control techniques, and the PE concept, a distributed robust formation control framework is developed without requiring global position measurements, where agents in the network may possess completely different dynamic models. These results were originally presented in [(ii), (iii), (x)].
- Chapter 4: We solve the leader–follower simultaneous formation stabilization and tracking control problem for heterogeneous planar underactuated vehicle networks without global position measurements. Using partial stability theory, Matrosov’s theorem, and the PE concept, a smooth formation control scheme is proposed to simultaneously address the formation stabilization and formation tracking problems without switching. These results were originally presented in [(i), (iv), (v), (xi)].
- Chapter 5: We extend source seeking algorithms, in the absence of position and velocity measurements, and with the tuning of the surge input, from velocity-actuated (unicycle) kinematic models to force-actuated generic Euler-Lagrange dynamic underactuated models. In the design and analysis, we employ a symmetric product approximation, averaging, passivity, and partial-state stability theory. The proposed control law requires only real-time measurement of the source signal at the current position of the vehicle and ensures SPUAS with respect to the linear motion coordinates for the closed-loop system. These results were originally presented in [(xv), (xvi)].

- Chapter 6: We solve the distributed formation control problem for heterogeneous spatial underactuated vehicle networks subject to switching topologies. A distributed finite-time sliding mode observer is designed to estimate the ranges between vehicles based on the bearing angles, and thus, the control design does not require relative position measurements. A transformation is proposed to define continuous reference velocity trajectories under switching topologies. Then, a distributed formation protocol is presented which guarantees the global asymptotic convergence for the closed-loop system. These results were originally presented in [(xiv), (xvii)].
- Chapter 7: We provide concluding remarks and opportunities for future work.

List of publications

The following is an exhaustive list of publications written during the past three and a half years, that are either published, accepted for publication, or still under review. It contains but is not restricted to the contents of this document.

Journal Papers

- i./ B. Wang, H. Ashrafiou, and S. G. Nersesov, “The use of partial stability in the analysis of interconnected systems,” *ASME J. Dyn. Syst. Meas. Contr.*, vol. 143, p. 044501, 2021.
- ii./ B. Wang, S. G. Nersesov, and H. Ashrafiou, “Time-varying formation control for heterogeneous planar underactuated multivehicle systems,” *ASME J. Dyn. Syst. Meas. Contr.*, vol. 144, no. 4, p. 041006, 2022.
- iii./ B. Wang, S. Nersesov, and H. Ashrafiou, “Robust formation control and obstacle avoidance for heterogeneous underactuated surface vessel networks,” *IEEE Trans. Control Netw. Syst.*, vol. 9, no. 1, pp. 125–137, 2022.
- iv./ B. Wang, H. Ashrafiou, and S. Nersesov, “Leader-follower formation stabilization and tracking control for heterogeneous planar underactuated vehicle networks,” *Syst. Control Lett.*, vol. 156, p. 105008, 2021.
- v./ B. Wang, S. Nersesov, and H. Ashrafiou, “Formation regulation and tracking control for nonholonomic mobile robot networks using polar coordinates,” *IEEE Contr. Syst. Lett.*, vol. 6, pp. 1909–1914, 2021.
- vi./ G. Wang, B. Wang, and C. Zhang, “Fixed-time third-order super-twisting-like sliding mode motion control for piezoelectric nanopositioning stage,” *Mathematics*, vol. 9, no. 15, p. 1770, 2021.

- vii./ G. Wang, B. Wang, J. Zhao, and M. Tao, "Robust Tracking for Nanopositioning Stages Using Sliding Mode Control with Active Disturbance Rejection: Design and Implementation," *J. Vib. Control*, 2022. (OnlineFirst).
- viii./ C. Li, Y. Wang, C.K. Ahn, C. Zhang, and B. Wang, "Milli-Hertz Frequency Tuning Architecture Towards High Repeatable Micromachined Axi-Symmetry Gyroscopes," Submitted to *IEEE Trans. Ind. Electron.*, 2022. (Early Access).

Conference Papers

- ix./ B. Wang, S. Nersesov, and H. Ashrafiuon, "A unified approach to stabilization, trajectory tracking, and formation control of planar underactuated vehicles," in *Proc. Amer. Contr. Conf.*, (Denver, CO, USA), pp. 5269–5274, IEEE, 2020.
- x./ B. Wang, S. Nersesov, and H. Ashrafiuon, "Formation control for underactuated surface vessel networks," in *Proc. ASME Dyn. Syst. Control Conf.*, (Pittsburgh, PA, USA), pp. DSCL2020-3178, ASME, 2020.
- xi./ B. Wang, S. Nersesov, and H. Ashrafiuon, "Singularity-free decentralized formation tracking control for heterogeneous underactuated surface vessels," in *Proc. Amer. Contr. Conf.*, (New Orleans, LA, USA), pp. 3296–3301, IEEE, 2021.
- xii./ B. Wang, H. Ashrafiuon, and S. Nersesov, "Leader-follower formation stabilization control for planar underactuated vehicle networks," in *Proc. IEEE Conf. Decis. Control*, (Austin, TX, USA), pp. 5703–5708, IEEE, 2021.
- xiii./ B. Wang, S. Nersesov, and H. Ashrafiuon, "Quasi-LPV Control Design for a Class of Underactuated," in *Proc. Amer. Contr. Conf.*, pp. 1904–1909, Atlanta, GA, June 2022.
- xiv./ B. Wang, S. Nersesov, and H. Ashrafiuon, "Formation Control for Heterogeneous Spatial Underactuated Vehicles Using Bearing Measurements," *Modeling, Estimation and Control Conference (MECC)*, 2022. (Accepted).
- xv./ B. Wang, S. Nersesov, H. Ashrafiuon, P. Naseradinmousavi, and M. Krstić, "Source Seeking for Planar Underactuated Vehicles by Surge Force Tuning," *IEEE Conf. Decis. Control*, 2022. (Accepted).

Papers Under Review

- xvi./ B. Wang, S. Nersesov, H. Ashrafiuon, P. Naseradinmousavi, and M. Krstić, "Underactuated source seeking by surge force tuning: Theory and boat experiments," Submitted to *IEEE Trans. Control Syst. Technol.*, 2022. See also: arXiv preprint, vol. arXiv:220504589.
- xvii./ B. Wang, S. Nersesov, and H. Ashrafiuon, "Range Observer-Based Formation Control for Heterogeneous Spatial Underactuated Vehicle Networks," Submitted to *Int. J. Adapt. Control Signal Process.*, 2022.

Chapter 2

Modeling of Underactuated Vehicle Networks

2.1 Generic Model of Underactuated Vehicles

2.1.1 Model of Planar Underactuated Vehicles

A generic planar underactuated vehicle can be modeled as a 3-DOF planar rigid body with two independent control inputs. Let \mathcal{F}_s denote the fixed inertial frame attached to the ground, and \mathcal{F}_b the body-fixed frame attached to the center of mass of the vehicle. The position of the vehicle in \mathcal{F}_s is described by (x, y) , and the orientation of the vehicle is represented by θ , as shown in Figure 2.1. The equations of motion of the planar underactuated vehicle are given by Euler-Lagrangian (EL) form

$$\dot{q} = J(q)v, \quad (2.1a)$$

$$M\dot{v} + C(v)v + D(v)v = Gu, \quad (2.1b)$$

where $q = [x, y, \theta]^\top \in \mathbb{R}^3$ is the configuration of the vehicle; $v = [v_x, v_y, \omega]^\top \in \mathbb{R}^3$ is the generalized velocity vector consisting of the linear velocity (v_x, v_y) in the body-fixed frame and the angular velocity ω ; $u = [u_1, u_2]^\top \in \mathbb{R}^2$ is the control input vector; $J(q)$ is the kinematic transformation matrix given by

$$J(q) = \begin{bmatrix} \cos(\theta) & -\sin(\theta) & 0 \\ \sin(\theta) & \cos(\theta) & 0 \\ 0 & 0 & 1 \end{bmatrix}; \quad (2.2)$$

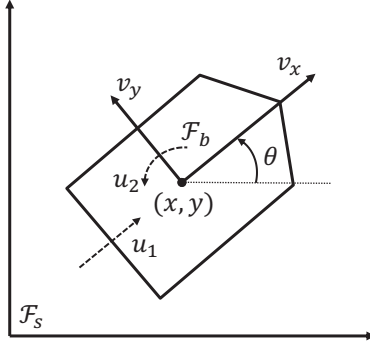


Figure 2.1: Top view of the planar underactuated vehicle.

M is the inertia matrix; $C(v)$ is the Coriolis and centrifugal matrix; $D(v)$ is the damping matrix; and G is the input matrix. Without loss of generality, we assume that

$$G = \begin{bmatrix} 1 & 0 \\ 0 & a_y \\ 0 & a_\omega \end{bmatrix}, \quad (2.3)$$

The constant coefficients a_y and $a_\omega \neq 0$ determine the contribution of u_2 to sway and yaw motions, respectively. All matrices above are assumed to be in appropriate dimensions. Three well-known properties associated with the EL system (2.1a)-(2.1b) are as follows.

Property 2.1 ([85,86]). *For a single rigid body, the inertia matrix M is constant, symmetric, and positive definite, and the Coriolis and centrifugal matrix $C(v)$ is skew-symmetric. The components of vector $C(v)v$ are homogeneous polynomials in $\{v_x, v_y, \omega\}$ of degree 2.*

Property 2.2 ([85]). *The damping matrix $D(v)$ is symmetric and positive semi-definite.*

Property 2.3 ([87]). *For the system (2.1a)-(2.1b), the differential equation*

$$M\dot{s} + C(v)s + D(v)s = G\tau \quad (2.4)$$

defines an the input-output mapping $\tau \mapsto G^\top s$, which is passive with the storage function $E_K := \frac{1}{2}s^\top Ms$. Furthermore, if $D(\cdot)$ is positive definite, then the mapping $\tau \mapsto G^\top s$ is output strictly passive.

The EL system (2.1a)-(2.1b) can model a wide class of planar underactuated vehicles in practical applications such as nonholonomic mobile robots [19, 88], surface vessels [39, 45], underwater vehicles [44], etc. In particular, the general planar vehicle model is represented

by the kinematic and force-balance equations of motion as

$$\begin{cases} \dot{x} = v_x \cos \theta - v_y \sin \theta, \\ \dot{y} = v_x \sin \theta + v_y \cos \theta, \\ \dot{\theta} = \omega, \\ \dot{v}_x = f_x(v_x, v_y, \omega, \theta, t) + \delta_x(t) + \tau_1, \\ \dot{v}_y = f_y(v_x, v_y, \omega, \theta, t) + \delta_y(t) + a_y \tau_2, \\ \dot{\omega} = f_\omega(v_x, v_y, \omega, \theta, t) + \delta_\omega(t) + a_\omega \tau_2, \end{cases} \quad (2.5)$$

where $f_x(\cdot), f_y(\cdot), f_\omega(\cdot)$ are known locally Lipschitz continuous functions, and $\delta_x(\cdot), \delta_y(\cdot), \delta_\omega(\cdot)$ stand for the unknown but bounded model uncertainties and disturbances, i.e.,

$$|\delta_x(t)| \leq \Delta_x, \quad |\delta_y(t)| \leq \Delta_y, \quad |\delta_\omega(t)| \leq \Delta_\omega, \quad (2.6)$$

for all $t \geq 0$, where $\Delta_x, \Delta_y, \Delta_\omega$ are known positive constants.

Specific vehicle models including mobile robots, surface vessels, and planar vertical takeoff and landing (PVTOL) aircraft are presented in the form of (2.5) as follows.

Wheeled Mobile Robots. The force-balance equations for a mobile robot (Fig. 2.2 (a)) with nonholonomic constraint $v_y = d\omega$ are given by [57]

$$\begin{aligned} \dot{v}_x &= \frac{md}{\tilde{m}}\omega^2 + \frac{1}{\tilde{m}r}(\tau_L + \tau_R) + \delta_x(t), \\ \dot{\omega} &= -\frac{md}{\tilde{I}}\omega v_x + \frac{a}{2\tilde{I}r}(\tau_R - \tau_L) + \delta_\omega(t). \end{aligned}$$

where m , r and a are mass, wheel radius, and axle length, respectively. $\tilde{m} = m + 2J/r^2$, $\tilde{I} = I + md^2 + a^2J/r^2$, where I and J are robot and wheel moment of inertia, respectively. τ_L and τ_R represent the differential torques applied to the left and right wheels, respectively. Note that, the nonholonomic constraint is $v_y = d\omega$, where the constant $d > 0$ represents the distance from the center of mass of the robot to its axle.

Surface Vessel with Diagonal Mass Matrix. The force-balance equations of an underactuated surface vessel (Fig. 2.2 (b)) model with nonlinear hydrodynamic damping are given

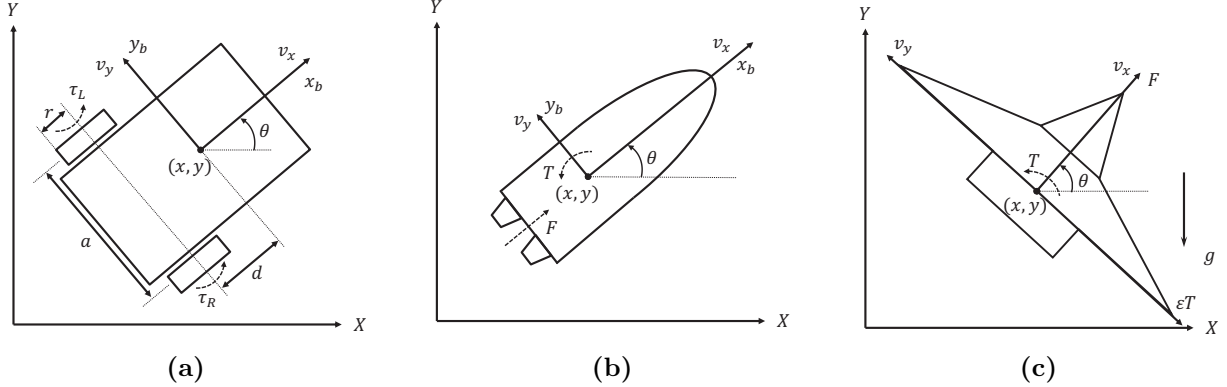


Figure 2.2: Underactuated planar vehicle models: (a) nonholonomic mobile robot, (b) marine surface vessel, (c) PVTOL aircraft.

by [45]

$$\begin{aligned}\dot{v}_x &= \frac{m_{22}}{m_{11}}v_y\omega - \frac{d_{11}}{m_{11}}|v_x|^{\alpha_{11}}\text{sign}(v_x) + \frac{F}{m_{11}} + \delta_x(t), \\ \dot{v}_y &= -\frac{m_{11}}{m_{22}}v_x\omega - \frac{d_{22}}{m_{22}}|v_y|^{\alpha_{22}}\text{sign}(v_y) + \delta_y(t), \\ \dot{\omega} &= \frac{m_d}{m_{33}}v_xv_y - \frac{d_{33}}{m_{33}}|\omega|^{\alpha_{33}}\text{sign}(\omega) + \frac{T}{m_{33}} + \delta_\omega(t),\end{aligned}$$

where the parameters m_{kk} 's ($k = 1, 2, 3$) are positive constants representing the mass and inertia parameters of the surface vessel including the added mass effects. The hydrodynamic damping is represented by the power law parameters d_{kk} and α_{kk} , ($k = 1, 2, 3$). The terms F and T are the control inputs, which represent the surge force and the yaw moment, respectively. This model is also applicable to linear hydrodynamic damping with $\alpha_{11} = \alpha_{22} = \alpha_{33} = 1$.

Surface Vessel with Coupled Mass Matrix. The force-balance equations of an underactuated surface vessel (Fig. 2.2 (b)) model with couple mass matrix are given by [45]

$$\begin{bmatrix} m_{11} & 0 & 0 \\ 0 & m_{22} & m_{23} \\ 0 & m_{23} & m_{33} \end{bmatrix} \begin{bmatrix} \dot{v}_x \\ \dot{v}_y \\ \dot{\omega} \end{bmatrix} + \begin{bmatrix} -m_{22}v_y\omega - m_{23}\omega^2 \\ m_{11}v_x\omega \\ -m_dv_xv_y + m_{23}v_x\omega \end{bmatrix} + \begin{bmatrix} d_{11} & 0 & 0 \\ 0 & d_{22} & d_{23} \\ 0 & d_{23} & d_{33} \end{bmatrix} \begin{bmatrix} v_x \\ v_y \\ \omega \end{bmatrix} = \begin{bmatrix} F \\ 0 \\ T \end{bmatrix}.$$

The parameters m_{23} , d_{23} are non-negative and represent the off-diagonal terms of the mass and damping matrices

PVTOL Aircraft. The force-balance equations for PVTOL aircraft (Fig. 2.2 (c)) controlled by the force F and moment T are given as [89]

$$\begin{aligned}\ddot{x} &= \frac{F}{m} \cos \theta + \frac{\epsilon T}{m} \sin \theta, \\ \ddot{y} &= \frac{F}{m} \sin \theta - \frac{\epsilon T}{m} \cos \theta - g, \\ \ddot{\theta} &= \frac{T}{I}.\end{aligned}$$

After including uncertainties, the equations in form (2.5) are given by

$$\begin{aligned}\dot{v}_x &= \omega v_y - g \sin \theta + \frac{F}{m} + \delta_x(t), \\ \dot{v}_y &= -\omega v_x - g \cos \theta - \frac{\epsilon T}{m} + \delta_y(t), \\ \dot{\omega} &= \frac{T}{I} + \delta_\omega(t)\end{aligned}$$

where m, I are the mass and the moment of inertia of the aircraft, respectively. The parameter g is the gravity constant and the constant $\epsilon > 0$ represents the coupling between the yaw moment and the lateral force on the aircraft.

2.1.2 Model of Spatial Underactuated Vehicles

A generic spatial vehicle is modeled as a 6-DOF rigid body moving in three-dimensional Euclidean space. Let $\{\mathcal{I}\}$ denote an earth-fixed inertial frame, and $\{\mathcal{B}\}$ the body-fixed frame attached to the vehicle, where the origin is located at the center of mass of the vehicle, as shown in Figure 2.3. The position of the vehicle in the earth-fixed frame $\{\mathcal{I}\}$ is represented by $\xi = [x, y, z]^\top$, and the attitude is represented by the Euler angles $\eta = [\phi, \theta, \psi]^\top$ of $\{\mathcal{B}\}$ relative to $\{\mathcal{I}\}$, where ϕ, θ, ψ represent the roll, pitch, and yaw angles, respectively. Let $v = [v_x, v_y, v_z]^\top$ and $\omega = [\omega_x, \omega_y, \omega_z]^\top$ denote the linear and angular velocity vectors of the vehicle, respectively, resolved in its body-fixed frame. The kinematics of the vehicle is described by [90]

$$\begin{bmatrix} \dot{\xi} \\ \dot{\eta} \end{bmatrix} = \begin{bmatrix} R(\eta) & 0 \\ 0 & T(\eta) \end{bmatrix} \begin{bmatrix} v \\ \omega \end{bmatrix} \quad (2.7)$$

where $R(\cdot) \in \text{SO}(3)$ is the rotation matrix parameterized by Euler angles $\eta = [\phi, \theta, \psi]^\top$, i.e.,

$$R(\eta) = \begin{bmatrix} c_\theta c_\psi & s_\phi s_\theta c_\psi - c_\phi s_\psi & c_\phi s_\theta c_\psi + s_\phi s_\psi \\ c_\theta s_\psi & s_\phi s_\theta s_\psi + c_\phi c_\psi & c_\phi s_\theta s_\psi - s_\phi c_\psi \\ -s_\theta & s_\phi c_\theta & c_\phi c_\theta \end{bmatrix}, \quad (2.8)$$

and the matrix $T(\cdot)$ is given by

$$T(\eta) = \begin{bmatrix} 1 & s_\phi t_\theta & c_\phi t_\theta \\ 0 & c_\phi & -s_\phi \\ 0 & \frac{s_\phi}{c_\theta} & \frac{c_\phi}{c_\theta} \end{bmatrix}. \quad (2.9)$$

Note that the matrix $T(\eta)$ becomes singular when $\theta = \pm\pi/2$, and thus, we restrict the use of Euler angles to $|\phi| < \pi/2$ and $|\theta| < \pi/2$ to avoid aggressive maneuvers and singularity [54].

We consider the spatial vehicle model with two degrees of underactuation. More precisely, we assume that each vehicle has only one control thrust (force) and three control torques. The dynamic EL model of the vehicle can be written as

$$\begin{bmatrix} mI_3 & 0 \\ 0 & I \end{bmatrix} \begin{bmatrix} \dot{v} \\ \dot{\omega} \end{bmatrix} + \begin{bmatrix} \omega \times (mv) \\ \omega \times (I\omega) \end{bmatrix} + \begin{bmatrix} D_v & 0 \\ 0 & D_\omega \end{bmatrix} \begin{bmatrix} v \\ \omega \end{bmatrix} = \begin{bmatrix} F + R(\eta)^\top G \\ \tau \end{bmatrix}, \quad (2.10)$$

where m is the total mass of the vehicle; $I \in \mathbb{R}^{3 \times 3}$ is the diagonal inertia matrix; $D_v, D_\omega \in \mathbb{R}^{3 \times 3}$ are constant, positive semi-definite damping matrices; F is the control thrust force; $G = [0, 0, G_z]^\top$ is the total force of gravity and the buoyancy (if exists); $\tau = [\tau_\phi, \tau_\theta, \tau_\psi]^\top$ is the control torque vector. Note that the vehicle system (2.7)-(2.10) is in the EL form. The system is underactuated because it has six DOF, i.e., three translational DOF and three rotational DOF, however, it only has four independent control inputs, i.e., one control thrust force, and three control torques. Without any loss of generality, we assume that the control thrust is in the direction of one of the three body-fixed axes, i.e., $F = [F_x, 0, 0]^\top$, $F = [0, F_y, 0]^\top$, or $F = [0, 0, F_z]^\top$. It should be noted that the full nonlinear vehicle model (2.7)-(2.10) can represent a wide class of spatial underactuated vehicles including AUVs ($F = [F_x, 0, 0]^\top$) and quadrotors ($F = [0, 0, F_z]^\top$) [54].

Taking time derivative of (2.7), substituting (2.10), and using the properties that $R(\eta)^\top = R(\eta)^{-1}$, $\dot{R}(\eta) = R(\eta)(\omega)_\times$, and $(\omega)_\times v = \omega \times v$, we obtain the equations of motion in the

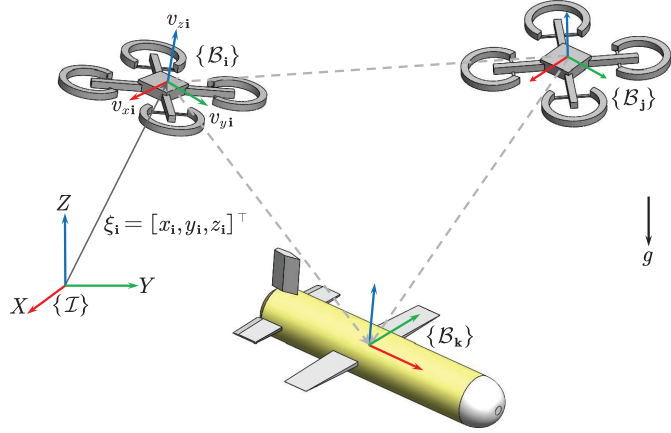


Figure 2.3: Illustration of the leader-follower formation of heterogeneous spatial underactuated vehicle networks, where the network consists of two quadrotors and an AUV.

earth-fixed frame:

$$\ddot{\xi} = R(\eta)u + \frac{G}{m} - D_\xi(\eta)\dot{\xi}, \quad (2.11)$$

$$\ddot{\eta} = \tilde{\tau}, \quad (2.12)$$

where $D_\xi(\eta) = (1/m)R(\eta)D_vR(\eta)^\top$; $u = F/m$ and

$$\tilde{\tau} = [\tilde{\tau}_\phi, \tilde{\tau}_\theta, \tilde{\tau}_\psi]^\top = \dot{T}(\eta)\omega - T(\eta)I^{-1}[\omega \times (I\omega) + D_\omega\omega - \tau] \quad (2.13)$$

are the new control inputs. Note that $u = [u_x, 0, 0]^\top$, $[0, u_y, 0]^\top$, or $[0, 0, u_z]^\top$ according to the specific configuration of the thrust actuator, where $u_{(.)} = F_{(.)}/m$.

2.2 Notations from Graph Theory

Consider a network of $N + 1$ heterogeneous underactuated vehicles, where the vehicles are numbered $\mathbf{i} = 0, 1, \dots, N$ with $\mathbf{0}$ representing the group leader, which can be either a virtual vehicle or an actual vehicle, and $\mathbf{1}, \dots, \mathbf{N}$ the followers. For multi-agent systems considered in this paper, we use the bold and non-italicized subscript \mathbf{i} to denote the index of an agent. The information exchange among the N vehicles is modeled as a time-varying directed graph $\mathcal{G}(t) = (\mathcal{V}, \mathcal{E}(t), \mathcal{A}(t))$, where each vehicle is considered as a node in the graph, i.e., the vertex set $\mathcal{V} = \{\mathbf{1}, \dots, \mathbf{N}\}$; $\mathcal{E}(t) \subseteq \mathcal{V} \times \mathcal{V}$ is the edge set; and $\mathcal{A}(t) \in \mathbb{R}^{(N+1) \times (N+1)}$ is the weighted adjacency matrix [2]. The set of neighboring nodes with edges connected to the node \mathbf{i} is denoted by $\mathcal{N}_{\mathbf{i}}(t) = \{\mathbf{j} \in \mathcal{V} : (\mathbf{i}, \mathbf{j}) \in \mathcal{E}_t\}$, where (\mathbf{i}, \mathbf{j}) represents that node \mathbf{i} obtains information

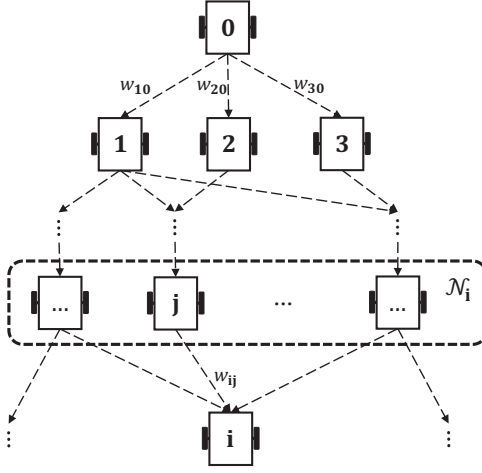


Figure 2.4: Communication graph of $N + 1$ heterogeneous vehicle network.

from node \mathbf{j} via communication. The weighted adjacency matrix $\mathcal{A}(t) = [a_{ij}(t)]$ is defined as $a_{ij}(t) > 0$ if $\mathbf{j} \in \mathcal{N}_i(t)$ and $a_{ij}(t) = 0$ otherwise, for each $t \geq 0$. The physical meaning of the weighting coefficients $a_{ij}(t)$ is in the different levels of importance of the agent neighbors' information states. We assume that the graph $\mathcal{G}(t)$ has no self-loop or loop for each $t \geq 0$ and that the group leader does not receive any communication from other nodes. For more details on algebraic graph theory, see [2, 3]. The directed graph $\mathcal{G}(t)$ considered in this paper can be switching in formation control of the heterogeneous multi-vehicle systems. We make the following assumption on the adjacency matrix $\mathcal{A}(t)$.

Assumption 2.1. (i) $\mathcal{A}(t)$ is piecewise continuous for all $t \geq 0$; (ii) each nonzero entry $a_{ij}(t)$ is bounded, i.e., there exist positive constants \underline{a}, \bar{a} such that $\underline{a} < a_{ij}(t) < \bar{a}$; (iii) Let $t_0 = 0$ and let t_1, t_2, \dots be the switching times for $\mathcal{A}(t)$. The directed switching graph $\mathcal{G}(t)$ has a directed spanning tree across each interval $[t_i, t_{i+1})$, $\forall i \in \mathbb{Z}_{\geq 0}$, i.e., there exists at least one directed path starting from the group leader to any other node in the network.

2.3 Feasible Trajectory Generation

The formation control problem is to design a distributed control protocol such that the network of heterogeneous vehicles moves together following the leader and asymptotically converge to a predefined geometric pattern, which can be either time-invariant or time-varying. Take planar underactuated vehicles for example. The desired geometric pattern of the vehicle formation is defined by a set of time-varying offset vectors $d_{ij}(t) \in \mathbb{R}^3$, $i, j = 0, 1, \dots, N$, $\forall t \geq 0$. We denote the configuration variables of agent i as $q_i = [x_i, y_i, \theta_i]^\top$.

Planar formation control problem. Design distributed control laws for each follower agent without global position measurements such that: i.) the solutions of the closed-loop system are uniformly bounded; ii.) all the vehicles in the network can maintain a prescribed formation in the sense that

$$\lim_{t \rightarrow \infty} \left[q_i - \sum_{j \in \mathcal{N}_i} a_{ij} [q_j + d_{ij}(t)] \right] = 0, \quad \forall i \in \mathcal{V}. \quad (2.14)$$

Unlike fully-actuated systems, underactuated systems cannot be commanded to track arbitrary trajectories. Similarly, the desired configuration trajectory also cannot be assigned arbitrarily in formation. In other words, the time-varying offset $d_{ij}(t) = [d_{ij}^x(t), d_{ij}^y(t), d_{ij}^\theta(t)]^\top$ cannot be assigned to each vehicle arbitrarily. For a planar vehicle with one degree of underactuation, the time-varying offset vector can only be independently specified for two elements. The first two elements $d_{ij}^x(t)$ and $d_{ij}^y(t)$ are specified for the formation, which assigns the desired position trajectory of the follower agent i relative to that of its neighbor $j \in \mathcal{N}_i$. Then, the orientation offset $d_{ij}^\theta(t)$ must be determined from the vehicle dynamics. Specifically, let us denote the desired position trajectory assigned to agent i from all agents $j \in \mathcal{N}_i$ by

$$\bar{x}_i(t) := \sum_{j \in \mathcal{N}_i} a_{ij} [x_j + d_{ij}^x(t)], \quad \bar{y}_i(t) := \sum_{j \in \mathcal{N}_i} a_{ij} [y_j + d_{ij}^y(t)]. \quad (2.15)$$

Then, the feasible orientation trajectory $\bar{\theta}_i(t)$ needs to be determined based on the nonholonomic constraint of agent i . It follows from (2.5) that the desired orientation trajectory $\bar{\theta}_i(t)$ is a solution of the following second-order ordinary differential equation

$$\dot{\bar{v}}_{yi}(t) = f_{yi}(\bar{v}_{xi}(t), \bar{v}_{yi}(t), \bar{\omega}_i(t), \bar{\theta}_i(t), t) + \frac{a_{yi}}{a_{\omega i}} [\dot{\bar{\omega}}_i(t) - f_{\omega i}(\bar{v}_{xi}(t), \bar{v}_{yi}(t), \bar{\omega}_i(t), \bar{\theta}_i(t), t)], \quad (2.16)$$

subject to initial conditions $\bar{\theta}_i(0) = \bar{\theta}_{i,0}$ and $\dot{\bar{\theta}}_i(0) = \dot{\bar{\theta}}_{i,0}$, and $\bar{v}_{xi}(t)$, $\bar{v}_{yi}(t)$, and $\bar{\omega}_i(t)$ are given by

$$\begin{bmatrix} \bar{v}_{xi}(t) \\ \bar{v}_{yi}(t) \\ \bar{\omega}_i(t) \end{bmatrix} = \begin{bmatrix} \cos \bar{\theta}_i(t) & \sin \bar{\theta}_i(t) & 0 \\ -\sin \bar{\theta}_i(t) & \cos \bar{\theta}_i(t) & 0 \\ 0 & 0 & 1 \end{bmatrix} \begin{bmatrix} \dot{\bar{x}}_i(t) \\ \dot{\bar{y}}_i(t) \\ \dot{\bar{\theta}}_i(t) \end{bmatrix},$$

It is noted that no global position measurement is required in (2.16). Next, the feasible orientation trajectory $\bar{\theta}_i(t)$ can be calculated by numerically integrating equation (2.16) given any smooth position offset $[d_{ij}^x(t), d_{ij}^y(t)]^\top$. Furthermore, the feasible orientation offset variable $d_{ij}^\theta(t)$ is selected as $d_{ij}^\theta(t) = \bar{\theta}_i(t) - \theta_j(t)$.

Remark 2.1. The second-order ordinary differential equation (2.16) reduces into a first-

order ordinary differential equation in the case of $a_{yi} = 0$. We emphasize that only the local motion information (velocity and acceleration) is used in feasible trajectory generation. The formation is achieved if $x_i \rightarrow \bar{x}_i(t)$, $y_i \rightarrow \bar{y}_i(t)$, and $\theta_i \rightarrow \bar{\theta}_i(t)$. In the control design, we will use the differences $(x_i - \bar{x}_i(t))$ and $(y_i - \bar{y}_i(t))$ for feedback purpose, and only relative position measurements $(x_i - x_j)$ and $(y_i - y_j)$ are required to construct these difference signals.

For spatial vehicles, the desired geometric pattern of the vehicle network in terms of spatial positions is defined by a set of constant position offset vectors $\{d_{ij} = [d_{ij}^x, d_{ij}^y, d_{ij}^z]^\top \in \mathbb{R}^3 : i, j \in \mathcal{V}, i \neq j\}$.

Spatial formation control problem. Under Assumption 2.1, design a controller for each follower (2.11)-(2.12) without global position measurements such that: (i) the state trajectories of the closed-loop system are bounded for all $t \geq 0$; (ii) all the vehicles in the network can maintain a prescribed formation in the sense that for all $i \in \mathcal{V}$,

$$\lim_{t \rightarrow +\infty} \sum_{j \in \mathcal{N}_i(t)} |\xi_i(t) - \xi_j(t) - d_{ij}| = 0. \quad (2.17)$$

For the 6-DOF spatial vehicle model (2.11)-(2.12) with two degrees of underactuation, the desired trajectories can only be independently specified for four configuration variables [54]. Considering the formation objective (2.17), in addition to controlling the three position variables, one attitude variable also can be independently controlled. The other two attitude variables must be determined from the constraints imposed due to underactuation.

The vehicle model (2.11)-(2.12) has three possible structural heterogeneities, which correspond to the three possible configurations of the thrust actuator, i.e., $u_i = [u_{xi}, 0, 0]^\top$, $[0, u_{yi}, 0]^\top$, or $[0, 0, u_{zi}]^\top$. Introducing a virtual input $\nu_i = [\nu_{xi}, \nu_{yi}, \nu_{zi}]^\top \in \mathbb{R}^3$ in the position dynamics, we have

$$\ddot{\xi}_i = \nu_i + g_i(\eta_i, u_i, \dot{\xi}_i, \nu_i), \quad (2.18)$$

where $g_i(\eta_i, u_i, \dot{\xi}_i, \nu_i) = R(\eta_i)u_i + G_i/m_i - D_{\xi_i}(\eta_i)\dot{\xi}_i - \nu_i$. The desired attitude trajectory $\eta_{id}(t) = [\phi_{id}(t), \theta_{id}(t), \psi_{id}(t)]^\top$ and the thrust $u_i(t)$ are selected such that $g_i(\eta_{id}(t), u_i(t), \dot{\xi}_i, \nu_i) = 0$, for all $t \geq 0$. Specifically, denoting $\mu_i = [\mu_{xi}, \mu_{yi}, \mu_{zi}]^\top = D_{\xi_i}(\eta_i)\dot{\xi}_i + \nu_i - G_i/m_i$, the desired trajectories $\eta_{id}(t)$ and the thrust $u_i(t)$ are selected such that $R(\eta_{id}(t))u_i(t) = \mu_i(t)$. Note that the signal $\mu_i(t)$ is available. For the three cases, we propose the attitude resolution as follows:

Case 1. ($u_i = [u_{xi}, 0, 0]^\top$; ϕ_i is independently controlled.) Given $\phi_{id}(t) = \phi_i(t)$ and $\nu_i(t)$, the

thrust and desired attitude signals are selected as

$$u_{xi} = \sqrt{\mu_{xi}^2 + \mu_{yi}^2 + \mu_{zi}^2}, \quad (2.19)$$

$$\theta_{id} = \arcsin(-u_{xi}^{-1} \mu_{zi}), \quad (2.20)$$

$$\psi_{id} = \arctan(\mu_{xi}^{-1} \mu_{yi}). \quad (2.21)$$

Case 2. ($u_i = [0, u_{yi}, 0]^\top$; θ_i is independently controlled.) Given $\theta_{id}(t) = \theta_i(t)$ and $\nu_i(t)$, the thrust and desired attitude signals are selected as

$$u_{yi} = \sqrt{\mu_{xi}^2 + \mu_{yi}^2 + \mu_{zi}^2}, \quad (2.22)$$

$$\phi_{id} = \arcsin[\mu_{zi} u_{yi}^{-1} \sec(\theta_{id})], \quad (2.23)$$

$$\psi_{id} = \arccos[u_{yi} (\mu_{xi} \sin(\phi_{id}) \sin(\theta_{id}) + \mu_{yi} \cos(\phi_{id})) (\mu_{xi}^2 + \mu_{yi}^2)^{-1}]. \quad (2.24)$$

Case 3. ($u_i = [0, 0, u_{zi}]^\top$; ψ_i is independently controlled.) Given $\psi_{id}(t) = \psi_i(t)$ and $\nu_i(t)$, the thrust and desired attitude signals are selected as

$$u_{zi} = \sqrt{\mu_{xi}^2 + \mu_{yi}^2 + \mu_{zi}^2}, \quad (2.25)$$

$$\phi_{id} = \arcsin[u_{zi}^{-1} (\mu_{xi} \sin(\psi_{id}) - \mu_{yi} \cos(\psi_{id}))], \quad (2.26)$$

$$\theta_{id} = \arctan[\mu_{zi}^{-1} (\mu_{xi} \cos(\psi_{id}) + \mu_{yi} \sin(\psi_{id}))]. \quad (2.27)$$

Remark 2.2. Note that the position subsystem (2.18) and the attitude subsystem (2.12) form a cascaded structure. That is, the (double-integrator) attitude subsystem (2.12) is decoupled from (2.18), and is controlled independently by $\tilde{\tau}_i$. Due to the simple double-integrator dynamics of (2.12), it is trivial to design control law $\tilde{\tau}_i$ such that $|\eta_i(t) - \eta_{id}(t)| \rightarrow 0$ as $t \rightarrow +\infty$. If the thrust u_i and $\eta_{id}(t)$ are selected as above, the interconnection term $g_i(\eta_i(t), u_i, \dot{\xi}_i, \nu_i)$ in (2.18) also tends to zero as $|\eta_i(t) - \eta_{id}(t)| \rightarrow 0$. Then, the position subsystem (2.18) reduces to the double-integrator dynamics $\ddot{\xi}_i = \nu_i$, and the position control input ν_i can be independently designed. The attitude resolution **Case 3** is frequently used in the quadrotor control design [61, 90, 91].

Chapter 3

Robust Formation Control for Planar Underactuated Vehicle Networks

In this chapter, we propose a displacement-based framework for coordinated motion and apply it to the formation control of networks of heterogeneous planar underactuated vehicles. All vehicles in the network are modeled as generic three degree-of-freedom planar rigid bodies with two control inputs, and are allowed to have nonidentical dynamics. Moreover, we allow for the *time-varying* geometric pattern of the vehicles to capture the changes in vehicle arrangements as well as obstacle and collision avoidance. By exploiting the cascaded structure of the planar vehicle model, a transformation is introduced to define the reduced-order error dynamics. Two formation control solutions are presented by the application of sliding mode techniques without global position measurements. The proposed formation control laws guarantee the UGAS for the closed-loop system subject to bounded disturbances.

3.1 Problem Formulation

Consider the generic planar vehicle model given by the kinematic and force-balance equations of motion as

$$\begin{cases} \dot{x}_i = v_{xi} \cos \theta_i - v_{yi} \sin \theta_i, \\ \dot{y}_i = v_{xi} \sin \theta_i + v_{yi} \cos \theta_i, \\ \dot{\theta}_i = \omega_i, \\ \dot{v}_{xi} = f_{xi}(v_{xi}, v_{yi}, \omega_i, \theta_i, t) + \delta_{xi}(t) + \tau_{1i}, \\ \dot{v}_{yi} = f_{yi}(v_{xi}, v_{yi}, \omega_i, \theta_i, t) + \delta_{yi}(t) + a_{yi}\tau_{2i}, \\ \dot{\omega}_i = f_{\omega i}(v_{xi}, v_{yi}, \omega_i, \theta_i, t) + \delta_{\omega i}(t) + a_{\omega i}\tau_{2i}, \end{cases} \quad (3.1)$$

where $[v_{xi}, v_{yi}]^\top$ represents the body-fixed velocity, ω_i is the angular velocity, τ_{1i} and τ_{2i} are the control inputs. The constant coefficients a_{yi} and $a_{\omega i} \neq 0$ determine the contribution of τ_{2i} to sway and yaw motions, respectively. In addition, $f_{xi}(\cdot)$, $f_{yi}(\cdot)$, $f_{\omega i}(\cdot)$ are known locally Lipschitz continuous functions, and $\delta_{xi}(\cdot)$, $\delta_{yi}(\cdot)$, $\delta_{\omega i}(\cdot)$ stand for the unknown but bounded model uncertainties and disturbances, i.e.,

$$|\delta_{xi}(t)| \leq \Delta_{xi}, \quad |\delta_{yi}(t)| \leq \Delta_{yi}, \quad |\delta_{\omega i}(t)| \leq \Delta_{\omega i}, \quad (3.2)$$

for all $t \geq 0$, where $\Delta_{xi}, \Delta_{yi}, \Delta_{\omega i}$ are known positive constants.

From rigid body dynamics, the term $f_{yi}(\cdot)$ in the sway force-balance equation in (2.5) consists of quadratic Coriolis and centrifugal force terms $f_{yi}^C(\cdot)$ and damping terms $f_{yi}^D(\cdot)$, i.e. $f_{yi} = f_{yi}^C + f_{yi}^D$. The Coriolis force has the form $-m_i \vec{\omega}_i \times \vec{v}_i$, and the centrifugal force has the form $-m_i \vec{\omega}_i \times (\vec{\omega}_i \times \vec{r}_i)$, where m_i is the mass of the rigid body, $\vec{\omega}_i$ is the angular velocity vector, \vec{r}_i and \vec{v}_i are the position and velocity vectors relative to the rotating reference frame, respectively. Thus, the components of Coriolis and centrifugal forces in the sway direction are only functions of v_{xi} and ω_i , that is, $f_{yi}^C = f_{yi}^C(v_{xi}, \omega_i)$, and the directions of the forces are opposed to the y_{bi} direction. Furthermore, the component of the damping force in the direction y_{bi} is only related to v_{yi} , that is $f_{yi}^D = f_{yi}^D(v_{yi})$, and its direction is opposite to the direction of v_{yi} . Based on the above discussion, we make the following assumption on the underactuated force-balance equation of the vehicle dynamics considered in this chapter.

Assumption 3.1. There exists a constant $\eta_i > 0$ related to the inertia parameters such that

$$\frac{\partial f_{yi}(v_{xi}, v_{yi}, \omega_i, \theta_i, t)}{\partial v_{xi}} = -\eta_i \omega_i, \quad (3.3)$$

and the direction of hydrodynamic damping force is opposite to the direction of v_{yi} , that is,

$$\frac{\partial f_{yi}(v_{xi}, v_{yi}, \omega_i, \theta_i, t)}{\partial v_{yi}} \leq 0. \quad (3.4)$$

Consider a network of $N + 1$ heterogeneous planar underactuated vehicles, where the vehicles are numbered $i = 0, 1, \dots, N$ with $\mathbf{0}$ representing the group leader, and $\mathbf{1}, \dots, \mathbf{N}$ the followers. The network topology is associated with a directed graph $\mathcal{G} = (\mathcal{V}, \mathcal{E})$ having $N + 1$ nodes with node dynamics (2.5), where $\mathcal{V} = \{0, 1, \dots, N\}$ and $\mathcal{E} \subseteq \mathcal{V} \times \mathcal{V}$ are the set of vertices and edges, respectively. The set of neighboring nodes that communicate their information to node i is denoted by $\mathcal{N}_i = \{j \mid (j, i) \in \mathcal{E}\}$. Let w_{ij} be a real number associated with the edge (j, i) for any $i, j \in \mathcal{V}$, representing the weighting coefficients of the communication between the vehicles. We assume that $w_{ij} > 0$ if $(j, i) \in \mathcal{E}$ and $w_{ij} = 0$, otherwise such that $\sum_{j \in \mathcal{N}_i} w_{ij} = 1$.

Assumption 3.2. There exists at least one directed path starting from the group leader to any other agent in the network captured by the communication graph \mathcal{G} , which implies that the graph \mathcal{G} contains a directed spanning tree. The group leader does not receive information from any other agent. Moreover, we assume that no self-loop or loop is allowed in the graph.

The formation control problem is to design a distributed control protocol such that the network of heterogeneous planar vehicles moves together following the leader and asymptotically converge to a predefined geometric pattern, which can be either time-invariant or time-varying. The desired geometric pattern of the vehicle formation is defined by a set of time-varying offset vectors $d_{ij}(t) \in \mathbb{R}^3$, $i, j = 0, 1, \dots, N$, $\forall t \geq 0$. We denote the configuration variables of agent i as $q_i = [x_i, y_i, \theta_i]^\top$.

Formation control problem: Design distributed control laws for each follower agent without global position measurements such that: i.) the solutions of the closed-loop system are uniformly bounded; ii.) all the vehicles in the network can maintain a prescribed formation in the sense that

$$\lim_{t \rightarrow \infty} \left[q_i - \sum_{j \in \mathcal{N}_i} w_{ij} [q_j + d_{ij}(t)] \right] = 0, \quad \forall i \in \mathcal{V}. \quad (3.5)$$

Denote the desired position trajectory assigned to agent i from all agents $j \in \mathcal{N}_i$ by

$$\bar{x}_i(t) := \sum_{j \in \mathcal{N}_i} w_{ij} [x_j + d_{ij}^x(t)], \quad \bar{y}_i(t) := \sum_{j \in \mathcal{N}_i} w_{ij} [y_j + d_{ij}^y(t)]. \quad (3.6)$$

Then, the feasible orientation trajectory $\bar{\theta}_i(t)$ is obtained from the feasible reference trajectory generation procedure given in Section 2.3. The feasible velocities $\bar{v}_{xi}(t)$, $\bar{v}_{yi}(t)$, and $\bar{\omega}_i(t)$ are given by

$$\begin{bmatrix} \bar{v}_{xi}(t) \\ \bar{v}_{yi}(t) \\ \bar{\omega}_i(t) \end{bmatrix} = \begin{bmatrix} \cos \bar{\theta}_i(t) & \sin \bar{\theta}_i(t) & 0 \\ -\sin \bar{\theta}_i(t) & \cos \bar{\theta}_i(t) & 0 \\ 0 & 0 & 1 \end{bmatrix} \begin{bmatrix} \dot{\bar{x}}_i(t) \\ \dot{\bar{y}}_i(t) \\ \dot{\bar{\theta}}_i(t) \end{bmatrix}.$$

3.2 Reduced-Order Error Dynamics

In this section, we introduce a transformation that results in structured reduced-order error dynamics. Define the formation errors $z_i = [z_{1i}, z_{2i}, z_{3i}]^\top$ for agents $i = 1, \dots, N$ as

$$z_i = J(\theta_i)^\top [(\dot{q}_i - \dot{\bar{q}}_i) - \Lambda (q_i - \bar{q}_i)], \quad (3.7)$$

where $\bar{q}_i := [\bar{x}_i, \bar{y}_i, \bar{\theta}_i]^\top$, the matrix

$$J(\theta_i) := \begin{bmatrix} \cos \theta_i & -\sin \theta_i & 0 \\ \sin \theta_i & \cos \theta_i & 0 \\ 0 & 0 & 1 \end{bmatrix}, \quad (3.8)$$

and $\Lambda := \text{diag}\{\lambda_1, \lambda_2, \lambda_3\}$ with $\lambda_1, \lambda_2, \lambda_3 < 0$. The idea is that when the error vector $z_i(t)$ asymptotically converges to 0, all configuration errors asymptotically converge to 0 as $t \rightarrow \infty$, as stated in the following lemma.

Lemma 3.1. Consider the error z_i defined in (3.7), where $\Lambda := \text{diag}\{\lambda_1, \lambda_2, \lambda_3\}$ with $\lambda_1, \lambda_2, \lambda_3 < 0$. If the error $|z_i(t)| \rightarrow 0$ as $t \rightarrow \infty$, then the formation error $|q_i(t) - \bar{q}_i(t)| \rightarrow 0$ as $t \rightarrow \infty$.

Proof. Since $J(\theta_i)^\top$ is an orthogonal matrix, $|z_i(t)| \rightarrow 0$ implies $|(\dot{q}_i - \dot{\bar{q}}_i) - \Lambda (q_i - \bar{q}_i)| \rightarrow 0$, which also can be written as a perturbed linear system:

$$\dot{\tilde{q}}_i = \Lambda \tilde{q}_i + \zeta_i(t), \quad \lim_{t \rightarrow \infty} |\zeta_i(t)| = 0, \quad (3.9)$$

where $\tilde{q}_i := q_i - \bar{q}_i(t)$, and $\zeta_i(t) = J(\theta_i)z_i(t)$. The nominal part $\dot{\tilde{q}}_i = \Lambda \tilde{q}_i$ of the perturbed linear system is exponentially stable, and the perturbation term $\zeta_i(t)$ converges to zero as $t \rightarrow \infty$. Then, by the converging-input-converging-state (CICS) property of stable linear systems [92], we conclude that $|\tilde{q}_i(t)| \rightarrow 0$, and $|\dot{\tilde{q}}_i(t)| \rightarrow 0$ as $t \rightarrow \infty$. \square

Thus, the control objective is then to design a controller which asymptotically stabilizes the formation errors $z_i(t)$ for all agents $i = 1, \dots, N$. The reduced-order error dynamics for agent i are calculated by taking derivative of (3.7) along the trajectory of (3.1) as:

$$\dot{z}_i = \dot{J}(\theta_i)^\top (\dot{\tilde{q}}_i - \Lambda \tilde{q}_i) + J(\theta_i)^\top (\ddot{\tilde{q}}_i - \Lambda \dot{\tilde{q}}_i). \quad (3.10)$$

Substituting equation (3.1) for agents i and j into the error dynamics (3.10), and using the following feedback transformation

$$\begin{aligned} \tau_{1i} = & -f_{xi} + \omega_i v_{yi} + \cos(\theta_i - \bar{\theta}_i) (\dot{v}_{xi} - \bar{\omega}_i \bar{v}_{yi}) + \sin(\theta_i - \bar{\theta}_i) (\dot{v}_{yi} + \bar{\omega}_i \bar{v}_{xi}) + \lambda_1 v_{xi} \\ & - \lambda_1 [\bar{v}_{xi} \cos(\theta_i - \bar{\theta}_i) + \bar{v}_{yi} \sin(\theta_i - \bar{\theta}_i)] + u_{1i}, \end{aligned} \quad (3.11)$$

$$\tau_{2i} = \frac{1}{a_{\omega i}} [-f_{\omega i} + \dot{\omega}_i + \lambda_3 (\omega_i - \bar{\omega}_i) + u_{2i}], \quad (3.12)$$

the reduced-order error dynamics (3.10) can be written as

$$\begin{bmatrix} \dot{z}_{1i} \\ \dot{z}_{2i} \\ \dot{z}_{3i} \end{bmatrix} = \begin{bmatrix} \omega_i z_{2i} \\ -\omega_i z_{1i} \\ 0 \end{bmatrix} + \begin{bmatrix} u_{1i} \\ \Psi_i \\ u_{2i} \end{bmatrix} + \begin{bmatrix} \delta_{xi}(t) \\ \delta_{yi}(t) \\ \delta_{\omega i}(t) \end{bmatrix}, \quad (3.13)$$

where

$$\begin{aligned} \Psi_i &= \dot{v}_{yi} + \omega_i v_{xi} + \sin(\theta_i - \bar{\theta}_i) (\dot{v}_{xi} - \bar{\omega}_i \bar{v}_{yi}) - \cos(\theta_i - \bar{\theta}_i) (\dot{v}_{yi} + \bar{\omega}_i \bar{v}_{xi}) - \lambda_2 v_{yi} \\ &\quad + \lambda_2 [-\bar{v}_{xi} \sin(\theta_i - \bar{\theta}_i) + \bar{v}_{yi} \cos(\theta_i - \bar{\theta}_i)]. \end{aligned} \quad (3.14)$$

The error dynamics (3.13) has only three states for each agent that must be stabilized to achieve the desired formation. Next, we will design the new control inputs $[u_{1i}, u_{2i}]^\top$ to stabilize the reduced-order error dynamics (3.13) for all agents $i = 1, \dots, N$. The control law will be distributed and will not use global position measurements since (3.13) only depends on the relative pose of agent i with respect to its neighbor j and their velocities and accelerations in their own body-fixed frames measured by onboard sensors such as Lidar, camera, inertial measurement unit (IMU), speedometer, etc.

It is noted that the reduced-order error system (3.13) has two structural properties: i.) the first term in the right-hand side is reminiscent of the skew-symmetric structure, which is commonly seen in the model reference adaptive control systems [93]; ii.) the nominal part of (3.13) is reminiscent of a cascaded system, i.e., z_{3i} -dynamics are decoupled from (z_{1i}, z_{2i}) -dynamics, and $z_{3i}(t) \rightarrow 0$ implies that the interconnected term $\Psi_i(t) \rightarrow 0$. These two structural properties are used later in the control design. The next lemma characterizes the cascaded-like property of the error dynamics (3.13), which suggests separating control of the linear and angular dynamics, and is important in the control design.

Lemma 3.2. Under feedback transformation (3.11)-(3.12), if both $z_{3i}(t)$ and $||[u_{1i}(t), u_{2i}(t)]||$ converge to zero exponentially as $t \rightarrow \infty$, and $\bar{\omega}_i(t)$ is bounded and PE, then the interconnected term $\Psi_i(t) \rightarrow 0$ exponentially as $t \rightarrow \infty$.

Proof. It follows from Lemma 3.1 that $z_{3i}(t) \rightarrow 0$ exponentially implies $(\theta_i(t) - \bar{\theta}_i(t)) \rightarrow 0$ and $(\dot{\theta}_i(t) - \dot{\bar{\theta}}_i(t)) \rightarrow 0$ exponentially as $t \rightarrow \infty$. Consequently, $\sin(\theta_i(t) - \bar{\theta}_i(t)) \rightarrow 0$ and $\cos(\theta_i(t) - \bar{\theta}_i(t)) \rightarrow 1$ exponentially. Then, from (3.11) we have

$$(\dot{v}_{xi} - \dot{\bar{v}}_{xi}) = \lambda_1 (v_{xi} - \bar{v}_{xi}) + \bar{\omega}_i (v_{yi} - \bar{v}_{yi}) + o_x(t), \quad (3.15)$$

where $o_x(t) \rightarrow 0$ exponentially, and from the model (3.1), we have

$$(\dot{v}_{y\mathbf{i}} - \bar{\dot{v}}_{y\mathbf{i}}) = f_{y\mathbf{i}}(v_{x\mathbf{i}}, v_{y\mathbf{i}}, \omega_{\mathbf{i}}, \theta_{\mathbf{i}}, t) + a_{y\mathbf{i}}\tau_{2\mathbf{i}} - f_{y\mathbf{i}}(\bar{v}_{x\mathbf{i}}, \bar{v}_{y\mathbf{i}}, \bar{\omega}_{\mathbf{i}}, \bar{\theta}_{\mathbf{i}}, t) - a_{y\mathbf{i}}\bar{\tau}_{2\mathbf{i}}. \quad (3.16)$$

Then, the feedback transformation (3.12) implies that $(\tau_{2\mathbf{i}} - \bar{\tau}_{2\mathbf{i}}) \rightarrow 0$, and (3.15) and (3.16) can be written as

$$\begin{bmatrix} \dot{v}_{x\mathbf{i}} - \bar{\dot{v}}_{x\mathbf{i}} \\ \dot{v}_{y\mathbf{i}} - \bar{\dot{v}}_{y\mathbf{i}} \end{bmatrix} = \begin{bmatrix} \lambda_1 & \bar{\omega}_{\mathbf{i}}(t) \\ -\eta_{\mathbf{i}}\bar{\omega}_{\mathbf{i}}(t) & \mathcal{A}_{22}(t) \end{bmatrix} \begin{bmatrix} v_{x\mathbf{i}} - \bar{v}_{x\mathbf{i}} \\ v_{y\mathbf{i}} - \bar{v}_{y\mathbf{i}} \end{bmatrix} + o(t), \quad (3.17)$$

where $\mathcal{A}_{22}(t) = \partial f_{y\mathbf{i}} / \partial v_{y\mathbf{i}} \leq 0$ and $|o(t)| \rightarrow 0$ exponentially. Note that, the system (3.17) can be seen as a linear time-varying system under an exponentially converging input $o(t)$, and the nominal part of (3.17) with $\mathcal{A}_{22}(t) \equiv 0$ is reminiscent of the system (A.25) in Lemma A.1. Since $\lambda_1 < 0$ and $\mathcal{A}_{22}(t) \leq 0$, referring to Lemma A.1, the comparison lemma, and CICS property of linear systems, we conclude that system (3.17) is UGES provided that $\bar{\omega}_{\mathbf{i}}(t)$ is bounded and PE. On the other hand, it follows from (3.14) that

$$\Psi_{\mathbf{i}} \rightarrow (\dot{v}_{y\mathbf{i}} - \bar{\dot{v}}_{y\mathbf{i}}) - \lambda_2(v_{y\mathbf{i}} - \bar{v}_{y\mathbf{i}}) + \bar{\omega}_{\mathbf{i}}(t)(v_{x\mathbf{i}} - \bar{v}_{x\mathbf{i}}), \quad (3.18)$$

and from the UGES of (3.17), we conclude that $\Psi_{\mathbf{i}}(t) \rightarrow 0$ exponentially as $t \rightarrow \infty$. \square

3.3 Robust Formation Control Designs

We begin this section by noting that different control laws may be applied to stabilize the error dynamics (3.13), for instance, sliding mode control, backstepping design, or linear high-gain feedback. While *any* nonlinear control technique may be applicable under this framework, in the current work, we choose sliding mode control due to its simplicity and robustness, which only requires boundedness of unknown modeling uncertainties and disturbances.

3.3.1 A First-Order Sliding Mode Approach

First, it is noted that the error dynamics (3.13) is structured such that the angular error $z_{3\mathbf{i}}$ is decoupled from the positioning error $[z_{1\mathbf{i}}, z_{2\mathbf{i}}]^\top$, and thus can be independently controlled. Therefore, we choose the simplest sliding mode control law as

$$u_{2\mathbf{i}} = -k_{2\mathbf{i}} \operatorname{sign}(z_{3\mathbf{i}}), \quad (3.19)$$

where $k_{2i} > \Delta_{\omega_i}$ implying that z_{3i} is stabilized to zero in finite time. It follows from Lemma 3.1 that angular error will converge to zero as $t \rightarrow \infty$. Next, consider the linear error dynamics (z_{1i}, z_{2i}) . We define the sliding variable in the following form:

$$s_i(z_{1i}, z_{2i}, t) = -\omega_i z_{1i} + \Psi_i(t) + c_i z_{2i}, \quad (3.20)$$

where $c_i > 0$ is a constant. Referring to (3.13), the dynamics on the sliding manifold $\{s_i = 0\}$ are given by

$$\dot{z}_{2i} = -c_i z_{2i} + \delta_{yi}(t), \quad (3.21)$$

where the nominal part is an exponential stable linear system. If the mismatched uncertainty $\delta_{yi}(\cdot)$ has a linear growth bound with respect to z_{2i} , then the dynamics on the sliding manifold is globally exponential stable.

To derive the control law, let us consider the Lyapunov candidate $V_i(s_i) = \frac{1}{2}s_i^2$ and take its time derivative along (z_{1i}, z_{2i}) -trajectories as

$$\dot{V}_i(t, z_{1i}, z_{2i}) = s_i \left[\frac{\partial s_i}{\partial z_{1i}} (\omega_i z_{2i} + u_{1i} + \delta_{xi}(t)) + \frac{\partial s_i}{\partial t} + \frac{\partial s_i}{\partial z_{2i}} (-\omega_i z_{1i} + \Psi_i(t) + \delta_{yi}(t)) \right]. \quad (3.22)$$

Following standard sliding mode control approach and assuming $\partial s_i / \partial z_{1i} \neq 0$, we choose the control law as

$$u_{1i} = -\omega_i z_{2i} - \left(\frac{\partial s_i}{\partial z_{1i}} \right)^{-1} \left[\frac{\partial s_i}{\partial z_{2i}} (-\omega_i z_{1i} + \Psi_i) + \frac{\partial s_i}{\partial t} + k_{1i} \text{sign}(s_i) \right], \quad (3.23)$$

which guarantees

$$\dot{V}_i(t, z_{1i}, z_{2i}) \leq |s_i| \left[-k_{1i} + \left| \frac{\partial s_i}{\partial z_{1i}} \right| \Delta_{xi} + \left| \frac{\partial s_i}{\partial z_{2i}} \right| \Delta_{yi} \right]. \quad (3.24)$$

The robustness gain k_{1i} is chosen such that

$$k_{1i} > \left| \frac{\partial s_i}{\partial z_{1i}} \right| \Delta_{xi} + \left| \frac{\partial s_i}{\partial z_{2i}} \right| \Delta_{yi}. \quad (3.25)$$

Then, trajectories will converge to the sliding manifold $\{s_i = 0\}$ in finite time. On the sliding manifold, the dynamics are represented by (3.21) and exponential stability can be established under the linear growth bound assumption that $|\delta_{yi}(\cdot)| \leq \kappa_i |z_{2i}|$, where κ_i is a positive constant [93, Lemma 9.1]. Note that $|\partial s_i / \partial z_{1i}| = |\omega_i(t)|$ and $|\partial s_i / \partial z_{2i}| = c_i$. For each vehicle i , the maximum angular velocity must be bounded in practice, i.e., $|\omega_i(t)| \leq \omega_{Mi}$ for

all $t \geq 0$, and can be measured by experiments in advance. Thus, the robustness gain k_{1i} can be simply chosen such that $k_{1i} > \omega_{Mi}\Delta_{xi} + c_i\Delta_{yi}$ in practice. The following theorem presents the main results.

Theorem 3.1. *Consider a network of heterogeneous planar underactuated vehicles, where the node dynamics given by (3.1), with the directed spanning tree communication topology. Assume that the linear and angular velocities and accelerations of the leader are bounded, the angular velocity for each follower \mathbf{i} is nonzero, i.e., $\omega_i(t) \neq 0$ for all $t \geq 0$, and the mismatched uncertainty $\delta_{yi}(\cdot)$ has a linear growth bound, i.e., $|\delta_{yi}(t)| \leq \kappa_i|z_{2i}|$ with $\kappa_i > 0$. Then, under the control law (3.11), (3.12), (3.19) and (3.23) with control gains $c_i > 0$, $k_{2i} > \Delta_{\omega_i}$, and k_{1i} satisfying (3.25), the origin of error dynamics (3.13) is UGAS.*

Proof. Consider the Lyapunov function candidate for the error dynamics (3.13) as $W_i = V_i(s_i) + \frac{1}{2}z_{3i}^2$. From (3.19) and (3.24), it follows that, along the trajectories of (3.13),

$$\dot{W}_i \leq - \left(k_{1i} - \left| \frac{\partial s_i}{\partial z_{1i}} \right| \Delta_{xi} - \left| \frac{\partial s_i}{\partial z_{2i}} \right| \Delta_{yi} \right) |s_i| - (k_{2i} - \Delta_{\omega_i}) |z_{3i}| \leq 0, \quad (3.26)$$

which implies that the closed-loop system is globally stable, and thus the formation error z_i is bounded over the time interval $[0, +\infty)$. Again, the variables $z_{3i}(t)$ and $s_i(t)$ converge to zero in finite time. It is noted that $z_{3i} \rightarrow 0$ for all $i = 1, \dots, N$ implies that the error in an angular motion for each agent will converge to zero as $t \rightarrow \infty$. Next, $s_i(t)$ converges to zero in finite time implies that all trajectories will reach the sliding manifold, and on the manifold, $z_{2i}(t) \rightarrow 0$ exponentially under the linear growth bound condition $|\delta_{yi}(t)| \leq \kappa_i|z_{2i}|$, [93, Lemma 9.1]. Also, on the sliding manifold, we have $z_{1i} \rightarrow \Psi_i/\omega_i$, and with the assumption $\partial s_i / \partial z_{1i} \neq 0$, we only need to verify that $\Psi_i(t) \rightarrow 0$ as $t \rightarrow \infty$. It also follows from (3.20) that $\partial s_i / \partial z_{1i} \neq 0$ is equivalent to $\omega_i(t) \neq 0$. Since $z_{3i}(t) \rightarrow 0$ in finite time for all $i = 1, \dots, N$, then $(\theta_i - \bar{\theta}_i) \rightarrow 0$ and $(\dot{\theta}_i - \dot{\bar{\theta}}_i) \rightarrow 0$ as $t \rightarrow \infty$ with an exponential convergence rate λ_3 . This implies that the orientations of all vehicles in the network are aligned with the predefined offset $d_{ij}^\theta(t)$. Then, the control law (3.19) suggests that $u_{2i}(t)$ reaches zero in finite time, and similarly, on the sliding manifold $\{s_i = 0\}$ we have $u_{2i}(t) \rightarrow 0$ exponentially as $t \rightarrow \infty$. It follows from Lemma 3.2 that $\Psi_i(t) \rightarrow 0$ exponentially as $t \rightarrow \infty$, and consequently $z_{1i}(t) \rightarrow 0$ as $t \rightarrow \infty$. Therefore, the UGES of the closed-loop error dynamics has been established. Finally, we conclude that the time-varying formation of heterogeneous planar underactuated vehicle network is achieved by Lemma 3.1. \square

Remark 3.1. As mentioned above, the singularity condition $\partial s_i / \partial z_{1i}(t) \neq 0$ implies that $\omega_i(t) \neq 0$. In case of $\omega_i(t) = 0$, the (z_{1i}, z_{2i}) -dynamics are uncoupled, that is, z_{2i} cannot be

controlled by the control input u_{1i} . In this situation, a hybrid control law can be used to avoid the singularity. Selecting $s_i = z_{1i}$, the control law (3.23) is replaced with $u_{1i} = -k_{1i} \text{sign}(s_i)$, where $k_{1i} > \Delta_{xi}$. Then, the origin of the (z_{1i}, z_{3i}) -subsystem is UGAS. Furthermore, disturbance observers (DOB) are widely used in the literature to estimate disturbances [94, 95]. An efficient solution for counteracting the mismatched disturbances is known as disturbance observer-based sliding mode control (DOB-SMC) [96]. Thus, if the mismatched uncertainty $\delta_{yi}(t)$ is non-vanishing, a DOB-SMC may be employed. In this case, the sliding variable (3.20) can be designed as $s_i(z_{1i}, z_{2i}, t) = -\omega_i z_{1i} + \Psi_i(t) + c_i z_{2i} + \hat{\delta}_{yi}(t)$, where $\hat{\delta}_{yi}(t)$ is the estimation of the $\delta_{yi}(t)$. Then, the error dynamics (3.21) become $\dot{z}_{2i} = -c_i z_{2i} + [\delta_{yi}(t) - \hat{\delta}_{yi}(t)]$, and correspondingly, the origin of the closed-loop system is UGAS if $\delta_{yi}(t) - \hat{\delta}_{yi}(t) \rightarrow 0$ as $t \rightarrow \infty$.

Remark 3.2. It is noted that $\dot{v}_{xi}(t)$, $\dot{v}_{yi}(t)$, and $\dot{\omega}_i(t)$ are required in the control law (3.11)-(3.12), which means that the acceleration information of each vehicle should be known. In some practical applications, acceleration can be measured directly by onboard sensors. In other cases, the acceleration can be estimated in real-time using observers or differentiators. Various differentiators can be used to estimate the accelerations, for instance, the sliding mode differentiator [97], or the high-gain differentiator [98], etc. Furthermore, the estimation errors can be viewed as a part of the disturbances $\delta_{xi}(t)$, $\delta_{yi}(t)$, $\delta_{\omega i}(t)$, which can be handled by the proposed controller.

3.3.2 A Super-Twisting Sliding Mode Approach

The super-twisting control takes advantage of the structural properties of the error system (3.13), and only a mild condition on the angular velocity is needed as we shall see later. We choose the super-twisting control laws as

$$\begin{cases} u_{1i} = -k_{1i}|z_{1i}|^{\frac{1}{2}} \text{sign}(z_{1i}) + \xi_{1i}, \\ \dot{\xi}_{1i} = -k_{2i} \text{sign}(z_{1i}), \end{cases} \quad (3.27)$$

$$\begin{cases} u_{2i} = -k_{3i}|z_{3i}|^{\frac{1}{2}} \text{sign}(z_{3i}) + \xi_{2i}, \\ \dot{\xi}_{2i} = -k_{4i} \text{sign}(z_{3i}), \end{cases} \quad (3.28)$$

where k_{1i} , k_{2i} , k_{3i} and k_{4i} are positive control gains.

It follows that under control law (3.27), the closed-loop (z_{1i}, z_{2i}) -dynamics are given by

$$\begin{aligned} \dot{z}_{1i} &= -k_{1i}|z_{1i}|^{\frac{1}{2}} \text{sign}(z_{1i}) + \rho_{1i} + \omega_i z_{2i}, \\ \dot{\rho}_{1i} &= -k_{2i} \text{sign}(z_{1i}) + \dot{\delta}_{xi}, \\ \dot{z}_{2i} &= -\omega_i z_{1i} + \Psi_i + \delta_{yi}, \end{aligned} \quad (3.29)$$

where $\rho_{1i} := \xi_{1i} + \delta_{xi}$. Furthermore, under control law (3.28), the closed-loop z_{3i} -dynamics are given by

$$\begin{aligned}\dot{z}_{3i} &= -k_{3i}|z_{3i}|^{\frac{1}{2}} \operatorname{sign}(z_{3i}) + \rho_{2i}, \\ \dot{\rho}_{2i} &= -k_{4i} \operatorname{sign}(z_{3i}) + \dot{\delta}_{\omega i},\end{aligned}\tag{3.30}$$

where $\rho_{2i} := \xi_{2i} + \delta_{\omega i}$. Note that the closed-loop system (3.29)-(3.30) has a cascade-like structure, i.e., z_{3i} enters the (z_{1i}, z_{2i}) -dynamics via the interconnection term Ψ_i . In other words, the position error $(z_{1i}, \rho_{1i}, z_{2i})$ -dynamics do not affect the angular error (z_{3i}, ρ_{2i}) -dynamics. Stabilizing (z_{3i}, ρ_{2i}) -dynamics implies $\omega_i - \bar{\omega}_i(t) \rightarrow 0$ as $t \rightarrow \infty$. If the group leader has a PE angular velocity $\omega_0(t)$, it follows from the directed spanning tree topology that each follower has a PE angular velocity ω_i , which is independent of position errors (z_{1i}, z_{2i}) . Consequently, ω_i can be viewed as a PE time-varying function $\omega_i(t)$ in $(z_{1i}, \rho_{1i}, z_{2i})$ -dynamics. It is also important to note that, the controllers (3.11), (3.12), (3.27), (3.28) are completely distributed and independent of global position measurements. The next theorem provides the main result of this subsection.

Theorem 3.2. *Consider a network of $N + 1$ heterogeneous underactuated surface vessels with the communication graph \mathcal{G} , the node dynamics given by (3.1), and the error dynamics given by (3.13). Assume that the angular velocity of the group leader is PE, i.e., there exist two constants $T > 0, \mu > 0$ such that $\omega_0(t)$ satisfies*

$$\int_t^{t+T} |\omega_0(\tau)| d\tau \geq \mu, \quad \forall t \geq 0.$$

- (i.) *Then, without perturbations, (i.e., $\delta_{xi} \equiv \delta_{yi} \equiv \delta_{\omega i} \equiv 0$), under the super-twisting control laws (3.27), (3.28) with positive gains k_{1i}, k_{2i}, k_{3i} and k_{4i} , the origin of closed-loop error system (3.29)-(3.30) is UGAS.*
- (ii.) *If the perturbations $\delta_{xi}(\cdot), \delta_{yi}(\cdot), \delta_{\omega i}(\cdot)$ are bounded with bounded derivatives such that (3.2) holds, and the unmatched uncertainty $\delta_{yi}(\cdot)$ vanishes with respect to z_{2i} , i.e., $|\delta_{yi}(\cdot)| \leq \kappa_i |z_{2i}|$ with $\kappa_i > 0$, then with $k_{2i} > \Delta_{xi}$, $k_{4i} > \Delta_{\omega i}$, and k_{1i}, k_{3i} sufficiently large, the origin of the closed-loop error system (3.29)-(3.30) is UGAS.*

Finally, together with the feedback transformation (3.11)-(3.12), the robust formation control problem is solved.

Proof. (i.) Note first that the “upper left corner” of system (3.29) (i.e., under $z_{2i} \equiv 0$) and system (3.30) are standard super-twisting systems. If the control gains $k_{1i}, k_{2i}, k_{3i}, k_{4i}$ are

positive, then the corresponding strict Lyapunov functions can be constructed [99, Theorem 1]. That is, for *every* positive definite matrix $Q_{1i} > 0$ and $Q_{3i} > 0$, the algebraic Lyapunov equations

$$A_{1i}^\top P_{1i} + P_{1i} A_{1i} = -Q_{1i}, \quad A_{3i}^\top P_{3i} + P_{3i} A_{3i} = -Q_{3i} \quad (3.31)$$

have unique positive definite solutions $P_{1i} > 0$ and $P_{3i} > 0$, where

$$A_{1i} = \begin{bmatrix} -\frac{1}{2}k_{1i} & \frac{1}{2} \\ -k_{2i} & 0 \end{bmatrix}, \quad A_{3i} = \begin{bmatrix} -\frac{1}{2}k_{3i} & \frac{1}{2} \\ -k_{4i} & 0 \end{bmatrix}.$$

Then, $V_{1i}(z_{1i}, \rho_{1i}) = \zeta_{1i}^\top P_{1i} \zeta_{1i}$ and $V_{3i}(z_{3i}, \rho_{2i}) = \zeta_{3i}^\top P_{3i} \zeta_{3i}$ are strict Lyapunov functions for system (3.29) with $z_{2i} \equiv 0$ and (3.30), respectively, where $\zeta_{1i} = [|z_{1i}|^{1/2}, \rho_{1i}]^\top$ and $\zeta_{3i} = [|z_{3i}|^{1/2}, \rho_{2i}]^\top$, and their time derivatives are negative definite

$$\dot{V}_{1i} = -|z_{1i}|^{-1/2} \zeta_{1i}^\top Q_{1i} \zeta_{1i}, \quad \dot{V}_{3i} = -|z_{3i}|^{-1/2} \zeta_{3i}^\top Q_{3i} \zeta_{3i}.$$

Thus, the origin of the system (3.30) is finite-time stable and $z_{3i}(t)$ reaches zero in finite time. It follows from the definition of z_{3i} that $(\theta_i - \bar{\theta}_i) \xrightarrow{\text{exp}} 0$ and $(\omega_i - \bar{\omega}_i) \xrightarrow{\text{exp}} 0$ as $t \rightarrow \infty$. Then, consider the nominal part of (3.29), (i.e., (3.29) with $\Psi_i \equiv 0$). It follows from Lemma A.1 in Appendix that system (3.29) with $\Psi_i \equiv 0$ is UGES. Next, it follows from $s_{(i-j)} \xrightarrow{\text{exp}} 0$ and $c_{(i-j)} \xrightarrow{\text{exp}} 1$ that (3.14) reduces to

$$\Psi_i \xrightarrow{\text{exp}} (\dot{v}_{yi} - \dot{\bar{v}}_{yi}) + \lambda_2 (v_{yi} - \bar{v}_{yi}) + \bar{\omega}_i (v_{xi} - \bar{v}_{xi}), \quad (3.32)$$

and (3.11) reduces to

$$(\dot{v}_{xi} - \dot{\bar{v}}_{xi}) \xrightarrow{\text{exp}} -\lambda_1 (v_{xi} - \bar{v}_{xi}) + \bar{\omega}_i (v_{yi} - \bar{v}_{yi}). \quad (3.33)$$

From the vehicle model, we have

$$\begin{aligned} (\dot{v}_{yi} - \dot{\bar{v}}_{yi}) &= f_{yi}(v_{xi}, v_{yi}, \omega_i) - f_{yi}(\bar{v}_{xi}, \bar{v}_{yi}, \bar{\omega}_i) \\ &= [f_{yi}^C(v_{xi}, \omega_i) - f_{yi}^C(\bar{v}_{xi}, \bar{\omega}_i)] + [f_{yi}^D(v_{yi}) - f_{yi}^D(\bar{v}_{yi})]. \end{aligned} \quad (3.34)$$

Then, (3.33) and (3.34) can be written as

$$\begin{bmatrix} \dot{v}_{xi} - \dot{\bar{v}}_{xi} \\ \dot{v}_{yi} - \dot{\bar{v}}_{yi} \end{bmatrix} = \begin{bmatrix} -\lambda_1 & \bar{\omega}_i(t) \\ -\eta_i \bar{\omega}_i(t) & \mathcal{D}_i(t) \end{bmatrix} \begin{bmatrix} v_{xi} - \bar{v}_{xi} \\ v_{yi} - \bar{v}_{yi} \end{bmatrix} + o(t), \quad (3.35)$$

where $o(\cdot) : \mathbb{R} \rightarrow \mathbb{R}^2$ and $|o(t)| \xrightarrow{\text{exp}} 0$; $\mathcal{D}_i(t) := [f_{yi}^D(v_{yi}) - f_{yi}^D(\bar{v}_{yi})]/[v_{yi} - \bar{v}_{yi}]$. It follows from the vehicle model that $\mathcal{D}_i(t) \leq 0$ for all $t \geq 0$. Then, from Lemma A.1 again, we conclude that the origin of system (3.35) is UGES, which implies that $\Psi_i \xrightarrow{\text{exp}} 0$. Finally, we conclude that the origin of full dynamics (3.29)-(3.30) is UGAS using the output injection lemma [100, Proposition 3] by considering that $\Psi_i \in \mathcal{L}_2$ is the uniformly integrable output.

(ii.) If $\delta_{yi} \equiv 0$ and if the gains $k_{2i} > \Delta_{xi}$, $k_{4i} > \Delta_{\omega i}$, and k_{1i}, k_{3i} are sufficiently large, then it follows from [99, Theorem 2] that for *some* positive definite matrices $Q_{1i} > 0$ and $Q_{3i} > 0$, the algebraic Lyapunov equations (3.31) have positive definite solutions $P_{1i} > 0$ and $P_{3i} > 0$, and thus V_{1i}, V_{3i} are the strict Lyapunov functions for system (3.29) with $z_{2i} \equiv 0$ and (3.30), respectively. If $\delta_{yi}(\cdot)$ vanishes with respect to z_{2i} , then it follows from [93, Lemma 9.1] that the origin of nominal part of the system (3.29) is UGES if k_{1i}, k_{3i} are sufficiently large. Then, the rest of the proof is the same as (i.) and the origin of error dynamics (3.29)-(3.30) is UGAS.

Finally, we conclude that the robust formation control problem is solved from Lemma 3.1. \square

Remark 3.3. A selection rule for the gains k_{1i}, k_{3i} is such that the “upper left corner” of system (3.29) (i.e., $z_{2i} \equiv 0$) and system (3.30) are finite-time stable. The selection rule for sufficiently large control gains k_{1i}, k_{3i} is given by [101]

$$k_{1i} > \sqrt{\frac{2(k_{2i} + \Delta_{xi})^2}{k_{2i} - \Delta_{xi}}}, \quad k_{3i} > \sqrt{\frac{2(k_{4i} + \Delta_{\omega i})^2}{k_{4i} - \Delta_{\omega i}}}.$$

Remark 3.4. Although in Theorem 3.2 (ii.) we assume that unmatched uncertainty $\delta_{yi}(\cdot)$ vanishes with respect to z_{2i} to guarantee the *asymptotic stability* of the error system, it should be noted that sea currents and waves are non-vanishing perturbations in practice. Other perturbations $\delta_{xi}(\cdot), \delta_{\omega i}(\cdot)$ are assumed to be simply bounded with bounded derivatives since control inputs directly affect surge and yaw motion. In order to stabilize the lateral dynamics, we have to make an assumption about vanishing lateral perturbations due to the fact that the vehicles are underactuated. Note that asymptotic stability is less practical under unknown unmatched disturbances. However, as pointed out in [102], in marine practice the hydrodynamic damping forces in the v_{yi} -equation of (3.1) are dominant in the sway direction. As a result, the sway velocity of the surface vessel is passively bounded, and thus it is uniformly ultimately bounded [103] if $\delta_{yi}(\cdot)$ is a non-vanishing perturbation. Moreover, as shown in recent works on underactuated systems [104, 105], it is still possible to reject the unknown unmatched perturbations $\delta_{yi}(\cdot)$ using disturbance observer based sliding mode control.

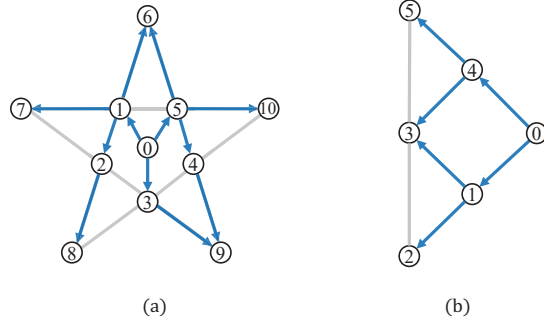


Figure 3.1: Communication topology graphs in the simulations: (a) Example 1, (b) Example 2.

3.4 Numerical Simulations

In this section, two numerical simulations are provided to verify the performance of the proposed formation control approaches. All the parameters are given in SI units.

3.4.1 Example 1

Consider a network of eleven heterogeneous planar underactuated vehicles with the indices $\mathbf{i} = 0, 1, \dots, 10$. Agent **0** is the leader and agents **1** to **10** are the followers with the communication topology graph as shown in Figure 3.1 (a). Agent **6** and agent **9** have two communication edges such that **6** follows **1** and **5**, and **9** follows **3** and **4**. Note that we assume that the communication from agent **5** to agent **6** is more important than the communication from agent **1** to agent **6**, and that the communication from agent **4** to agent **9** is more important than the communication from agent **3** to agent **9**. Therefore, we set the weighting coefficients $w_{61} = 0.4$, $w_{65} = 0.6$, $w_{93} = 0.3$, $w_{94} = 0.7$, while the remaining coefficients are all set to 1.

We assume that agents **0** to **3** are identical underactuated surface vessels modeled with diagonal mass matrix and linear hydrodynamic damping ($\alpha_{11,i} = \alpha_{22,i} = \alpha_{33,i} = 1$). The parameters of agents **0** to **3** are given as

$$\begin{aligned} m_{11,i} &= 1.412, \quad m_{22,i} = 1.982, \quad m_{33,i} = 0.354, \\ d_{11,i} &= 3.436, \quad d_{22,i} = 12.99, \quad d_{33,i} = 0.864. \end{aligned} \tag{3.36}$$

Agents **4** to **6** are also identical underactuated surface vessels modeled with diagonal mass

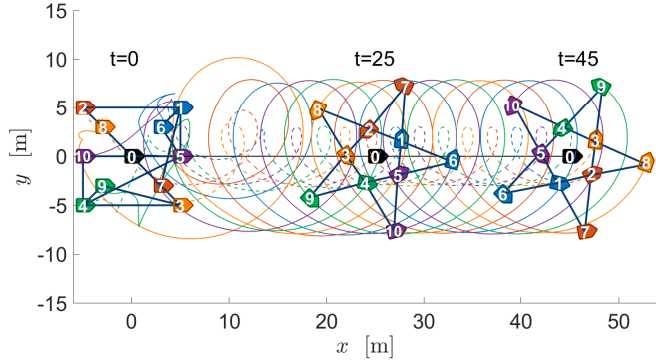


Figure 3.2: Illustration of the trajectories of the eleven planar vehicles in Example 1.

matrix model and nonlinear hydrodynamic damping with the parameters given as

$$\begin{aligned} m_{11,i} &= 1.317, \quad m_{22,i} = 3.832, \quad m_{33,i} = 0.926, \\ d_{11,i} &= 5.252, \quad d_{22,i} = 14.138, \quad d_{33,i} = 2.262, \\ \alpha_{11,i} &= 1.510, \quad \alpha_{22,i} = 1.747, \quad \alpha_{33,i} = 1.592. \end{aligned} \quad (3.37)$$

Agents **7** to **10** are identical nonholonomic mobile robots with the parameters given as

$$\begin{aligned} m_i &= 3.0, \quad I_i = 0.025, \quad J_i = 6 \times 10^{-6}, \\ a_i &= 0.33, \quad d_i = 0.08, \quad r_i = 0.05. \end{aligned} \quad (3.38)$$

In this simulation, the leader is commanded to follow a straight line in the x -direction with desired velocity 1 m/s. The geometric shape of the desired formation for the ten follower vehicles is a pentagram, where the center of the pentagram is located at the leader. Then, the positions of the ten follower agents are to be driven to the ten vertices of the pentagram, as shown in Figure 3.1(a). The radius of the circumscribed circle of the inner five vertices is set to 3 m, and the corresponding radius of the circumscribed circle of the outer five vertices is 9.434 m. The pentagram rotates counterclockwise around its center with a constant angular velocity of 0.5 rad/s, making the formation time-varying. All vehicles start from rest at zero orientation, while their initial positions can be observed in Figure 3.2.

To demonstrate robustness, we applied disturbances $\delta_{xi}(t) = 0.25 \sin(t) + 0.5 \sin(20t)$ and $\delta_{\omega i}(t) = 0.4 \sin(t) + 0.5 \sin(10t)$. We also assume that the communication between agents **5** and **6**, and the communication between agents **4** and **9** suddenly breaks at $t = 5$ s. We use the first-order sliding mode approach proposed in Section 3.3.1. The control gains and disturbance bounds for all agents were selected as $\lambda_1 = \lambda_2 = \lambda_3 = -1$, $k_{1i} = k_{2i} = c_i =$

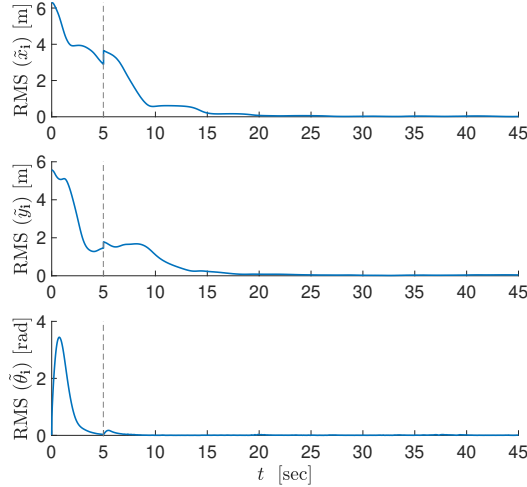


Figure 3.3: Convergence of the RMS formation errors of the ten follower vehicles in Example 1.

3, $\Delta_{xi} = \Delta_{\omega i} = 0.75$, $i = 1, \dots, 10$. To avoid excessive chattering, we used the hyperbolic tangent function $\tanh(\cdot/0.01)$ to approximate the discontinuous signum function $\text{sign}(\cdot)$.

Figure 3.2 illustrates the position trajectories of all agents at $t = 0$ s, $t = 25$ s, and $t = 45$ s. It is clear that the desired pentagram formation is achieved after the leader has traveled approximately 25 m in just over 25 seconds. Figure 3.3 shows the time history of the root mean square of all formation errors, which is of the form $\text{RMS}(\tilde{[\cdot]}_i) = \left(\frac{1}{n} \sum_{i=1}^n ([\cdot] - \bar{[\cdot]})_i^2 \right)^{1/2}$, demonstrating formation converging after 25s. It can also be seen that the breakage of communication at $t = 5$ s temporarily increases the overall formation errors but the asymptotic convergence continues after a short interruption.

3.4.2 Example 2

Consider a network of six heterogeneous planar underactuated vehicles with the indices $i = 0, 1, \dots, 5$. Agent **0** is the leader and agents **1** to **5** are the followers with the communication topology graph as shown in Figure 3.1 (b). We set the weighting coefficients $w_{31} = w_{34} = 0.5$ while the remaining coefficients are all set to 1.

Agent **0** is a PVTOL aircraft, where the model parameters are given as $m_i = 1$, $I_i = 0.1$, $\epsilon_i = 0.2$, and $g = 9.81$. Agents **1** and **2** are wheeled mobile robots, where the model parameters are given as (3.38). Agents **3** to **5** are different surface vessels, where agent **3** is with linear hydrodynamic damping, and the model parameters are given as (3.36); agents **4** and **5** are with nonlinear hydrodynamic damping and the model parameters are given as (3.37). We use the scenario where all types of vehicles are involved in coordination in order

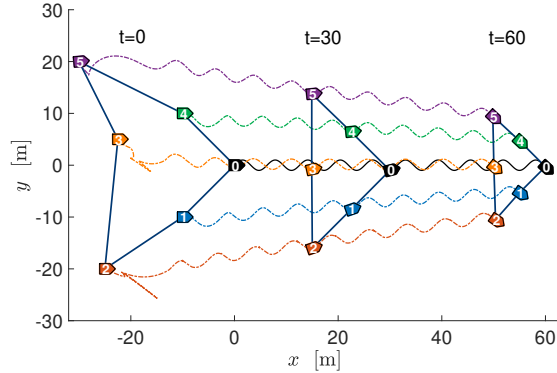


Figure 3.4: Illustration of the trajectories of the six planar vehicles in Example 2.

to show the versatility of the approach.

In this simulation, the leader is commanded to follow a sinusoidal path, i.e., $(x_d(t), y_d(t)) = (t, \sin(t))$. The geometric shape of the desired formation for the six vehicles is a time-varying isosceles right triangle, as shown in Figure 3.1(b). We set the length of the two congruent sides to $\sqrt{2}(20 - t/6)$. In other words, the position offsets are given as $(d_{40}^x, d_{40}^y) = (d_{54}^x, d_{54}^y) = (t/12 - 10, 10 - t/12)$, $(d_{10}^x, d_{10}^y) = (d_{21}^x, d_{21}^y) = (d_{34}^x, d_{34}^y) = (t/12 - 10, t/12 - 10)$. All vehicles start from rest at zero orientation, while their initial positions can be observed in Figure 3.4.

To demonstrate robustness, we applied disturbances $\delta_{xi}(t) = 0.25 \sin(t) + 0.5 \sin(20t)$ and $\delta_{\omega i}(t) = 0.4 \sin(t) + 0.5 \sin(10t)$. We use the super-twisting sliding mode approach proposed in Section 3.3.2. The control gains and disturbance bounds for all agents were selected as $\lambda_1 = \lambda_2 = \lambda_3 = -1$, $k_{1i} = k_{3i} = 5$, $k_{2i} = k_{4i} = 3$, $\Delta_{xi} = \Delta_{\omega i} = 0.75$, $i = 1, \dots, 5$. Figure 3.4 illustrates the position trajectories of all agents at $t = 0$ s, $t = 30$ s, and $t = 60$ s. It is clear that the desired triangle formation is achieved after the leader has traveled approximately 30 m in just over 30 seconds. Figure 3.5 shows the time history of the RMS formation errors demonstrating formation converging after about 30s.

3.5 Conclusion

In this chapter, we develop a distributed formation control framework for networks of *heterogeneous* planar *underactuated* vehicles *without requiring global position measurements*. A transformation is proposed to reduce the order of error dynamics and then two sliding mode control laws are employed to stabilize the error dynamics. While the sliding mode control approach is selected, other methods such as the backstepping technique can also be employed using the same error transformation introduced in this work. The proposed formation control laws guarantees UGAS of the closed-loop system subject to bounded uncertainties and

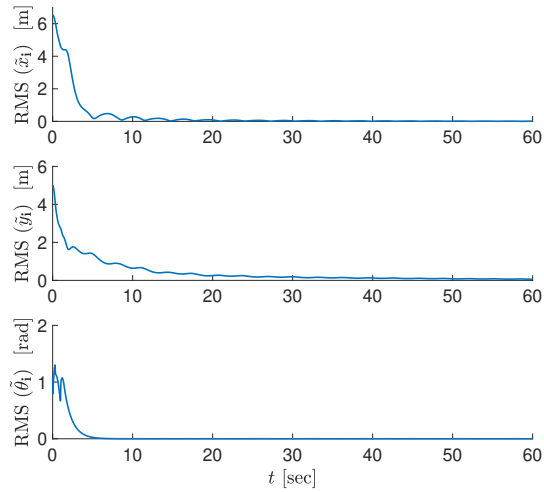


Figure 3.5: Convergence of the RMS formation errors of the six follower vehicles in Example 2.

disturbances. It is shown that the approach can be applied to networks of nonholonomic mobile robots, underactuated surface vessels with various modeling complexities, and planar air vehicles. Simulations are presented to demonstrate the effectiveness of the proposed control scheme.

Chapter 4

Formation Stabilization and Tracking Control for Planar Underactuated Vehicle Networks

4.1 Introduction

Because of the underactuation constraint, the formation stabilization and the formation tracking problems usually are studied as two distinct problems in the literature. Consequently, all agents must know the control problem in advance and switch between the two different types of controllers, i.e. formation stabilization controller and formation tracking controller. However, switching between controllers may be impractical when the vehicles operate in a fully autonomous mode [28]. Furthermore, in a distributed network, it is only the group leader that knows the group reference and the control objective, while no prior information on the group reference trajectory is available to all other agents [106]. Therefore, it is more practical if the two problems can be solved using a single control architecture.

The problem of *simultaneous stabilization and tracking* refers to finding a single control law that can solve both stabilization and tracking problems simultaneously without changing the controller structure [24]. For multi-agent systems, the problem of *formation stabilization and tracking* is a natural extension of the classical simultaneous stabilization and tracking problem.

In this chapter, we develop a new leader-follower formation control framework for a class of heterogeneous planar underactuated vehicle networks. Specifically,

- 1) We solve the simultaneous *formation stabilization and tracking* problem for planar underactuated vehicle systems using a single smooth time-varying control architecture. The control design is developed based on $u\delta$ -PE, and guarantees GAS for the origin of the closed-loop system.

- 2) We do not assume any particular structure of the internal dynamics of each vehicle but rather use a generic Euler-Lagrangian (EL) model, and the vehicles are allowed to have identical or non-identical dynamics. In other words, the formation is designed for *heterogeneous* planar underactuated vehicle networks, which include vehicles of different dynamic nature with different numbers of states (e.g., ground vehicles and surface vessels).
- 3) The proposed control law requires only neighbor-to-neighbor information exchange and does not require any global position measurements of the followers. Furthermore, the structure of the controller is relatively simple compared to the existing controllers in the literature.

4.2 Problem Formulation

Consider a network of $N+1$ heterogeneous planar underactuated vehicles, where the vehicles are numbered $\mathbf{i} = 0, 1, \dots, N$ with $\mathbf{0}$ representing the real group leader and $\mathbf{1}, \dots, \mathbf{N}$ the follower agents. The mathematical model of the planar underactuated vehicle \mathbf{i} can be written in the EL form [45, 87]

$$\dot{q}_{\mathbf{i}} = J(q_{\mathbf{i}})v_{\mathbf{i}}, \quad (4.1a)$$

$$M_{\mathbf{i}}\ddot{v}_{\mathbf{i}} + C_{\mathbf{i}}(v_{\mathbf{i}})v_{\mathbf{i}} + D_{\mathbf{i}}(v_{\mathbf{i}})v_{\mathbf{i}} = G_{\mathbf{i}}\tau_{\mathbf{i}}, \quad (4.1b)$$

where $q_{\mathbf{i}} = [x_{\mathbf{i}}, y_{\mathbf{i}}, \theta_{\mathbf{i}}]^{\top}$ is the configuration of the \mathbf{i} th vehicle; $v_{\mathbf{i}} = [v_{xi}, v_{yi}, \omega_{\mathbf{i}}]^{\top}$ is the generalized velocity vector consisting of the velocity of the center of mass (v_{xi}, v_{yi}) in the body-fixed frame $\{x_{bi}y_{bi}\}$ and its angular velocity $\omega_{\mathbf{i}}$; $\tau_{\mathbf{i}} = [\tau_{1i}, \tau_{2i}]^{\top}$ is the control input vector; $J(q_{\mathbf{i}})$ is the orthogonal kinematic transformation matrix; $M_{\mathbf{i}} = M_{\mathbf{i}}^{\top} > 0$ is the inertia matrix; $C_{\mathbf{i}}(v_{\mathbf{i}}) = -C_{\mathbf{i}}(v_{\mathbf{i}})^{\top}$ is the Coriolis and centrifugal matrix; $D_{\mathbf{i}}(v_{\mathbf{i}}) = D_{\mathbf{i}}(v_{\mathbf{i}})^{\top} \geq 0$ is the damping matrix; and $G_{\mathbf{i}}$ is the input matrix. All matrices above are assumed to be in appropriate dimensions.

Without loss generality, we make the following assumption.

Assumption 4.1. (i.) For each vehicle \mathbf{i} , assume that the inertia matrix $M_{\mathbf{i}}$ is diagonal, i.e., $M_{\mathbf{i}} = \text{diag}(m_{11,i}, m_{22,i}, m_{33,i})$. (ii.) Assume that the surge force and the yaw torque are two

independent control inputs. That is, the input matrix G_i may be written as¹

$$G_i = \begin{bmatrix} 1 & 0 \\ 0 & 0 \\ 0 & 1 \end{bmatrix}, \quad (4.2)$$

which implies that the underactuation is in the sway direction, i.e., v_{yi} -equation. (iii.) Assume that for each vehicle, the damping force in the sway direction satisfies $[D_i(v_i)]_{(2,2)} > 0$ for all $v_{yi} \neq 0$, and $v_{yi}/[D_i(v_i)]_{(2,2)} \rightarrow 0$ as $v_{yi} \rightarrow 0$, where $[D_i(v_i)]_{(2,2)}$ denotes the (2, 2)-element of $D_i(v_i)$.

Remark 4.1. The EL system (4.1a)-(4.1b) with Assumption 4.1 can model a wide class of planar underactuated vehicles in practical applications such as nonholonomic mobile robots [19, 88], underactuated ships [39, 45], underwater vehicles [44], etc. The assumption of damping force for the sway velocity is a mild one and has been adopted in the literature on the topic of underactuated ships [58]. Note that this assumption is automatically satisfied in the case of a linear damping model.

The network topology of the vehicles is defined by a directed graph $\mathcal{G} = (\mathcal{V}, \mathcal{E})$ where $\mathcal{V} = \{\mathbf{0}, \mathbf{1}, \dots, \mathbf{N}\}$ and $\mathcal{E} \subseteq \mathcal{V} \times \mathcal{V}$ represent its sets of vertices and edges, respectively. The set of neighboring nodes with edges connected to node i is denoted by $\mathcal{N}_i = \{\mathbf{j} \in \mathcal{V} : (\mathbf{i}, \mathbf{j}) \in \mathcal{E}\}$. The constant weighted adjacency matrix $\mathcal{A} = [a_{ij}]$ associated with \mathcal{G} is defined in accordance with the rule that $a_{ij} > 0$ in the case that $\mathbf{j} \in \mathcal{N}_i$ and $a_{ij} = 0$ otherwise. For the group leader, we have $a_{0j} \equiv 0$ for all $\mathbf{j} \in \mathcal{V}$, which implies that the leader $\mathbf{0}$ has no neighbors in the network. We also assume that $a_{ii} = 0$ for all $i \in \mathcal{V}$. The communication graph \mathcal{G} is assumed to contain a directed spanning tree.

We assume that the reference trajectory of the group leader is feasible and is generated by the following virtual vehicle

$$\dot{q}_d = J(q_d)v_d, \quad (4.3)$$

where $q_d = [x_d, y_d, \theta_d]^\top$ denotes the position and orientation of the virtual vehicle, and $v_d = [v_{xd}, v_{yd}, \omega_d]^\top$ denotes the linear and angular velocities of the virtual vehicle. We make the following assumption on the reference trajectory of the group leader.

Assumption 4.2. *The reference trajectory $(q_d(t), v_d(t))$ is only available to the group leader $\mathbf{0}$. Furthermore, the reference velocity $v_d(\cdot)$ is continuously differentiable and bounded with*

¹ G_i may be obtained in form (4.2) via a pre-input transformation. For instance, the actual control inputs for a mobile robot are torques τ_{Li} and τ_{Ri} applied to each wheel. However, one can easily obtain the input matrix of the form (4.2) via a linear transformation of the actual inputs. See [88] for more details.

bounded first derivative. Moreover, one of the following conditions holds.

A1) There exist T and $\mu_1 > 0$ such that

$$\int_t^{t+T} \omega_d(\tau)^2 d\tau \geq \mu_1, \quad \forall t \geq 0. \quad (4.4)$$

A2) There exist $\mu_2 > 0$ such that

$$\int_0^\infty |\omega_d(\tau)| d\tau \leq \mu_2. \quad (4.5)$$

The objective of *formation stabilization and tracking* is to design a distributed controller for each agent such that it coordinates its motion relative to one or more of its neighbors, and the network asymptotically converges to a predefined geometric pattern under Assumption 4.2. The geometric pattern of the vehicle network in terms of planar configuration is defined by a set of constant offset vectors $\{d_{ij} := (d_{ij}^x, d_{ij}^y, d_{ij}^\theta) \in \mathbb{R}^3 : i, j \in \mathcal{V}, i \neq j\}$. To be more specific, under Assumption 4.2, we will design a controller (τ_{1i}, τ_{2i}) for each agent without global position measurements such that: i.) all states in the closed-loop system are uniformly bounded; ii.) all the vehicles in the network maintain a prescribed formation in the sense that for all $i \in \mathcal{V}$

$$\lim_{t \rightarrow \infty} \sum_{j \in \mathcal{N}_i} |q_i(t) - q_j(t) - d_{ij}| = 0. \quad (4.6)$$

Denote the position reference trajectory for the vehicle i by

$$\bar{x}_i(t) := \frac{1}{\sum_{j \in \mathcal{N}_i} a_{ij}} \sum_{j \in \mathcal{N}_i} a_{ij} [x_j(t) + d_{ij}^x], \quad (4.7)$$

$$\bar{y}_i(t) := \frac{1}{\sum_{j \in \mathcal{N}_i} a_{ij}} \sum_{j \in \mathcal{N}_i} a_{ij} [y_j(t) + d_{ij}^y]. \quad (4.8)$$

Then, the feasible orientation trajectory $\bar{\theta}_i(t)$ is obtained from the feasible reference trajectory generation procedure given in Section 2.3. Let us denote $\bar{q}_i(t) := [\bar{x}_i(t), \bar{y}_i(t), \bar{\theta}_i(t)]^\top$, and $\bar{v}_i(t) := [\bar{v}_{xi}(t), \bar{v}_{yi}(t), \dot{\bar{\theta}}_i(t)]^\top$.

4.3 Formation Stabilization and Tracking Control Design

For the set-point stabilization problem of fully-actuated EL systems without kinematics equations

$$M_i \ddot{q}_i + C_i(\dot{q}_i) \dot{q}_i + D_i(\dot{q}_i) \dot{q}_i = \tau_i, \quad (4.9)$$

a fundamental result is achieving global asymptotic stabilization via energy shaping plus damping injection, where the controller always has a simple proportional-derivative (PD) form [87], i.e.,

$$\tau_i = -k_{pi}(q_i - \bar{q}_i) - k_{di}\dot{q}_i, \quad (4.10)$$

where k_{pi}, k_{di} are positive control gains. For the tracking control problem of fully-actuated EL systems (4.9), the PD+ controller originally introduced in [107] is a natural extension of the PD control law (4.10) and is given by

$$\tau_i = M\ddot{q}_i + C(\dot{q}_i)\dot{\bar{q}}_i + D(\dot{q}_i)\dot{\bar{q}}_i - k_{pi}(q_i - \bar{q}_i) - k_{di}(\dot{q}_i - \dot{\bar{q}}_i). \quad (4.11)$$

The PD+ controller was proved in [107] to achieve global asymptotic tracking using Matrosov's theorem. It is noted that the PD+ controller (4.11) reduces to the PD controller (4.10) when the reference velocity tends to zero. We will use a similar passivity-based technique in the simultaneous formation stabilization and tracking control design.

For the leader-follower tracking problem, we usually consider the problem for the follower i as tracking a reference leader similar to [19, 45, 59, 108, 109]. The basic idea is to calculate the dynamics of the tracking error $(q_i - \bar{q}_i, v_i - \bar{v}_i)$, and try to stabilize this error system. However, the error system often becomes very complex. Thus, instead of using \bar{v}_i , we define the new reference velocity in the body-fixed frame $\{x_{bi}y_{bi}\}$ as $\hat{v}_i := J(q_i)^\top \dot{\bar{q}}_i$. Correspondingly, for agent i , the error vectors in the body-fixed frame $\{x_{bi}y_{bi}\}$ are defined as $\tilde{q}_i^b = [\tilde{x}_i^b, \tilde{y}_i^b, \tilde{\theta}_i]^\top := J(q_i)^\top (q_i - \bar{q}_i)$, and $\tilde{v}_i = [\tilde{v}_{xi}, \tilde{v}_{yi}, \tilde{\omega}_i]^\top := (v_i - \hat{v}_i)$. Clearly, since $J(q_i)$ is invertible, stabilization of $(\tilde{q}_i^b, \tilde{v}_i)$ implies that $q_i(t) \rightarrow \bar{q}_i(t)$ and $\dot{q}_i(t) \rightarrow \dot{\bar{q}}_i(t)$ as $t \rightarrow \infty$ which solves formation control problem (8). Let us consider the following modified PD+ controller

$$\bar{\tau}_i = G_i^\dagger \left[M\dot{\hat{v}}_i + C(v_i)\hat{v}_i + D(v_i)\hat{v}_i - K_{pi}\tilde{q}_i^b - K_{di}\tilde{v}_i + u_i \right], \quad (4.12)$$

where $K_{pi} > 0$ and $K_{di} > 0$ are constant, diagonal control gain matrices; u_i is a new control input which will be designed later. We have the following result.

Proposition 4.1. *Consider the planar underactuated vehicle (4.1a)-(4.1b) satisfying Assumption 4.1. Then, under the modified PD+ control law (4.12) with $u_i \equiv 0$, the origin for the $(\tilde{x}_i^b, \tilde{\theta}_i, \tilde{v}_{xi}, \tilde{v}_{yi}, \tilde{\omega}_i)$ -subsystem is UGAS, and the solutions of the closed-loop system are UGB.*

Proof. Consider the function

$$V_i(\tilde{q}_i, \tilde{v}_i) = \frac{1}{2} \left[\tilde{v}_i^\top \left(G_i G_i^\dagger \right) M_i \tilde{v}_i + (\tilde{q}_i^b)^\top \left(G_i G_i^\dagger \right) K_{pi} \tilde{q}_i^b \right],$$

which is positive definite with respect to the error vector $(\tilde{x}_i^b, \tilde{\theta}_i, \tilde{v}_{xi}, \tilde{\omega}_i)$. Taking time derivative along the trajectories of the closed-loop system, we have

$$\begin{aligned}\dot{V}_i &= \tilde{v}_i^\top \left(G_i G_i^\dagger \right) M_i \tilde{v}_i + (\tilde{q}_i^b)^\top \left(G_i G_i^\dagger \right) K_{pi} \tilde{q}_i^b \\ &= \tilde{v}_i^\top \left(G_i G_i^\dagger \right) \left[G_i \tau_i - C_i(v_i) v_i - D_i(v_i) v_i - M_i \dot{\tilde{v}}_i \right] + (\tilde{q}_i^b)^\top \left(G_i G_i^\dagger \right) K_{pi} \tilde{q}_i^b \\ &= \tilde{v}_i^\top \left(G_i G_i^\dagger \right) \left[C(v_i) \hat{v}_i + D(v_i) \hat{v}_i - K_{pi} \tilde{q}_i^b - K_{di} \tilde{v}_i + u_i - C_i(v_i) v_i - D_i(v_i) v_i \right] \quad (4.13) \\ &\quad + (\tilde{q}_i^b)^\top \left(G_i G_i^\dagger \right) K_{pi} \tilde{q}_i^b\end{aligned}$$

$$\begin{aligned}&= -\tilde{v}_i^\top \text{sym} \left\{ \left(G_i G_i^\dagger \right) [D_i(v_i) + K_{di}] \right\} \tilde{v}_i + \tilde{v}_i^\top \left(G_i G_i^\dagger \right) u_i \\ &\leq \left[\left(G_i G_i^\dagger \right) \tilde{v}_i \right]^\top u_i, \quad (4.14)\end{aligned}$$

where the third equality is due to the fact that $G_i G_i^\dagger$ is idempotent, the fourth one is due to Property 2.1, and the last inequality is due to Property 2.2 and $K_{di} > 0$. It is clear that the input-output mapping $u_i \mapsto (G_i G_i^\dagger) \tilde{v}_i$ is passive. Consequently, if $u_i \equiv 0$, we have $(G_i G_i^\dagger) \tilde{v}_i \in L_2$, and the origin for the $(\tilde{x}_i^b, \tilde{\theta}_i, \tilde{v}_{xi}, \tilde{\omega}_i)$ -subsystem is UGS. It also follows from LaSalle-Yoshizawa theorem that $(\tilde{v}_{xi}, \tilde{\omega}_i) \rightarrow 0$ as $t \rightarrow \infty$. If we consider $\tilde{v}_{yi}(t)$ as a time-varying signal, then the origin of the $(\tilde{v}_{xi}, \tilde{\omega}_i)$ -subsystem is UGES. Then, the $(\tilde{v}_{xi}, \tilde{v}_{yi}, \tilde{\omega}_i)$ -subsystem is GES with respect to $(\tilde{v}_{xi}, \tilde{\omega}_i)$ uniformly in $\tilde{v}_{yi}(0)$ (i.e., partial-state stability with respect to $(\tilde{v}_{xi}, \tilde{\omega}_i)$). It also follows from the Assumption 4.1 item (iii.) that the origin of \tilde{v}_{yi} -dynamics is UGAS when $(\tilde{v}_{xi}, \tilde{\omega}_i) \equiv (0, 0)$ (i.e., 0-UGAS of \tilde{v}_{yi} -subsystem). Therefore, we conclude that the $(\tilde{v}_{xi}, \tilde{v}_{yi}, \tilde{\omega}_i)$ -subsystem is UGAS according to Theorem A.2. Moreover, the condition $v_{yi}/[D_i(v_i)]_{(2,2)} \rightarrow 0$ as $v_{yi} \rightarrow 0$ implies that $\tilde{v}_{yi} \in L_1$ and $\tilde{y}_i^b \in L_\infty$. Thus, we conclude that the solutions of the closed-loop system are UGB.

Next, consider the auxiliary function $W_i = (\tilde{q}_i^b)^\top (G_i G_i^\dagger) M_i \tilde{v}_i$ for the $(\tilde{x}_i^b, \tilde{\theta}_i, \tilde{v}_{xi}, \tilde{\omega}_i)$ -subsystem. Taking time derivative of W_i along trajectories of the closed-loop system, we have

$$\dot{W}_i = (\tilde{q}_i^b)^\top (G_i G_i^\dagger) M_i \tilde{v}_i + (\tilde{q}_i^b)^\top (G_i G_i^\dagger) M_i \dot{\tilde{v}}_i.$$

Then, evaluating \dot{W} on the set $\mathcal{M} := \{\tilde{v}_i = 0\}$ yields

$$\begin{aligned}\dot{W}_i|_{\mathcal{M}} &= -(\tilde{q}_i^b)^\top \text{sym} \left\{ \left(G_i G_i^\dagger \right) [C_i(v_i) + D_i(v_i) + K_{di}] \right\} \tilde{v}_i \\ &\quad - (\tilde{q}_i^b)^\top (G_i G_i^\dagger) K_{pi} \tilde{q}_i^b \\ &= -(\tilde{q}_i^b)^\top (G_i G_i^\dagger) K_{pi} \tilde{q}_i^b \leq 0.\end{aligned}$$

Thus, \dot{W}_i is non-zero definite on the set \mathcal{M} . It follows from the Matrosov's Theorem A.3 that the origin for the $(\tilde{x}_i^b, \tilde{\theta}_i, \tilde{v}_{xi}, \tilde{\omega}_i)$ -subsystem is UGAS. Therefore, we conclude that the origin of the $(\tilde{x}_i^b, \tilde{\theta}_i, \tilde{v}_{xi}, \tilde{v}_{yi}, \tilde{\omega}_i)$ -subsystem is UGAS by considering $\tilde{y}_i^b(t)$ as a bounded time-varying signal. \square

Under the modified passivity-based PD+ controller (4.12) with $u_i \equiv 0$, the velocity error vector $\tilde{v}_i(t) \rightarrow 0$, and the position error in the body-fixed frame $(\tilde{x}_i^b(t), \tilde{\theta}_i(t)) \rightarrow 0$ as $t \rightarrow \infty$. However, due to the underactuation, the position error $\tilde{y}_i^b(t)$ may converge only to a constant which is not necessarily zero. Denote the position error in the global frame by $(\tilde{x}_i, \tilde{y}_i) := (x_i - \bar{x}_i, y_i - \bar{y}_i)$. Although

$$\tilde{x}_i^b(t) = [\cos(\theta_i) \quad \sin(\theta_i)] [\tilde{x}_i(t) \quad \tilde{y}_i(t)]^\top \rightarrow 0 \quad (4.15)$$

does not imply that $(\tilde{x}_i(t), \tilde{y}_i(t)) \rightarrow 0$ because of the rank deficiency of $[\cos(\theta_i), \sin(\theta_i)]$, a persistently exciting $\theta_i(t)$ will guarantee that the position error $(\tilde{x}_i(t), \tilde{y}_i(t)) \rightarrow 0$ as $t \rightarrow \infty$.

Proposition 4.2. *Assume that the velocity error vector $\tilde{v}_i(t) \in L_1 \cap L_\infty$, and that $\omega_i(t)$ is persistently exciting ($\omega_i \in \text{PE}$), that is, there exist constants $T_i, \mu_i > 0$ such that*

$$\int_t^{t+T_i} \omega_i(\tau)^2 d\tau \geq \mu_i, \quad \forall t \geq 0. \quad (4.16)$$

Then, $\tilde{x}_i^b(t) \rightarrow 0$ as $t \rightarrow \infty$ implies that $(\tilde{x}_i(t), \tilde{y}_i(t)) \rightarrow 0$ as $t \rightarrow \infty$.

Proof. Note that $J(q_i)$ is an orthogonal matrix, and $\tilde{v}_i(t) \in L_1 \cap L_\infty$ implies that $(\dot{q}_i(t) - \dot{\bar{q}}_i(t)) \in L_1 \cap L_\infty$. Also, $\tilde{v}_i(t) \rightarrow 0$ implies that $(\dot{q}_i(t) - \dot{\bar{q}}_i(t)) \rightarrow 0$ as $t \rightarrow \infty$. Thus, by integrating both sides, we conclude that $(\tilde{x}_i(t), \tilde{y}_i(t)) \rightarrow \text{const}$. Now, consider the following equation

$$c_1 \cos(\theta_i) + c_2 \sin(\theta_i) = 0, \quad (4.17)$$

where c_1, c_2 are constants. If one of c_1 and c_2 is non-zero, then the equation (4.17) has only isolate solutions $\theta_i = \text{const}$. On the other hand, by the filter property of persistently exciting signals, $\omega_i \in \text{PE}$ implies that θ_i does not converge to a constant as $t \rightarrow \infty$. Thus, by contradiction and the continuity of (4.15), we conclude that the position error $(\tilde{x}_i(t), \tilde{y}_i(t)) \rightarrow 0$ as $t \rightarrow \infty$. \square

It follows from Propositions 4.1 and 4.2 that if the angular velocity of the vehicle i is PE, then the modified PD+ controller (4.12) with $u_i \equiv 0$ can be used to solve the formation tracking problem. However, in the cases of formation stabilization and formation tracking

of a straight line, the angular velocity of the vehicle \mathbf{i} converges to zero and thus the PE property is lost. In this case, we will use $u_{\mathbf{i}}$ as a “PE perturbation” on the angular motion to prevent $(\tilde{x}_{\mathbf{i}}(t), \tilde{y}_{\mathbf{i}}(t))$ converging to a non-zero constant. The new control input $u_{\mathbf{i}}$ is defined as

$$u_{\mathbf{i}} = \begin{bmatrix} 0 & 0 & \alpha_{\mathbf{i}}(t, \tilde{y}_{\mathbf{i}}^b) \end{bmatrix}^\top, \quad (4.18)$$

where $\alpha_{\mathbf{i}}(t, \tilde{y}_{\mathbf{i}}^b) = k_{\rho_{\mathbf{i}}} \rho_{\mathbf{i}}(t) \tilde{y}_{\mathbf{i}}^b(t)$, $k_{\rho_{\mathbf{i}}} > 0$ is a constant, and the time-varying signal $\rho_{\mathbf{i}}(t)$ is PE, continuously differentiable, and bounded with bounded first derivative. Note that the excitation property of $\alpha_{\mathbf{i}}$ is reminiscent of $u\delta$ -PE with respect to $\tilde{y}_{\mathbf{i}}^b$ [110], i.e., for each $\delta > 0$ there exist $T, \mu > 0$ such that

$$|\tilde{y}_{\mathbf{i}}^b(t)| > \delta \Rightarrow \int_t^{t+T} \alpha_{\mathbf{i}}(\tau, \tilde{y}_{\mathbf{i}}^b)^2 d\tau > \mu, \quad \forall t \geq 0. \quad (4.19)$$

The illustration of the modified PD+ controller (4.12) with $u\delta$ -PE “perturbation” (4.18) in a closed loop is shown in Figure 4.1. It is noted that $\theta_{\mathbf{i}}(t)$ and $\omega_{\mathbf{i}}(t)$ should be considered as perturbation signals in the linear motion error dynamics and for any $(\theta_{\mathbf{i}}, \omega_{\mathbf{i}}) \in L_\infty$, the linear motion error dynamics are globally asymptotically stable with respect to $(\tilde{x}_{\mathbf{i}}^b, \tilde{v}_{x\mathbf{i}}, \tilde{v}_{y\mathbf{i}})$ uniformly in $\tilde{y}_{\mathbf{i}}^b(0)$.

Proposition 4.3. *Consider the planar underactuated vehicle (4.1a)-(4.1b) satisfying Assumption 4.1. Then, under the modified PD+ control law (4.12) and (4.18), the origin for the $(\tilde{x}_{\mathbf{i}}^b, \tilde{y}_{\mathbf{i}}^b, \tilde{\theta}_{\mathbf{i}}, \tilde{v}_{x\mathbf{i}}, \tilde{v}_{y\mathbf{i}}, \tilde{\omega}_{\mathbf{i}})$ -dynamics is GAS.*

Proof. It follows from Proposition 4.1 that if $\alpha_{\mathbf{i}}(t, \tilde{y}_{\mathbf{i}}^b) = 0$, the $(\tilde{x}_{\mathbf{i}}^b, \tilde{\theta}_{\mathbf{i}}, \tilde{v}_{x\mathbf{i}}, \tilde{v}_{y\mathbf{i}}, \tilde{\omega}_{\mathbf{i}})$ -subsystem is UGAS to its origin. Furthermore, due to the damping term $K_{d\mathbf{i}}$ in the PD+ control law (4.12), the angular motion dynamics is input-to-state stable (ISS) by considering $\alpha_{\mathbf{i}}(t, \tilde{y}_{\mathbf{i}}^b)$ as an input, as shown in Figure 4.1. It also follows from the proof in Proposition 4.2 that $\tilde{y}_{\mathbf{i}}^b(t)$ converges to a constant as $t \rightarrow \infty$. Now, assume that $\tilde{y}_{\mathbf{i}}^b(t)$ converges to a non-zero constant. Then, (4.19) implies $\alpha_{\mathbf{i}} \in \text{PE}$, and from the filter property we have $\omega_{\mathbf{i}}(t) \in \text{PE}$. Then, it follows from Proposition 4.2 that $(\tilde{x}_{\mathbf{i}}(t), \tilde{y}_{\mathbf{i}}(t)) \rightarrow 0$ as $t \rightarrow \infty$, which contradicts the assumption that $\tilde{y}_{\mathbf{i}}^b(t)$ converges to a non-zero constant. Thus, we conclude that $\tilde{y}_{\mathbf{i}}^b(t) \rightarrow 0$ as $t \rightarrow \infty$ by contradiction. The GAS of the origin comes from the ISS property when $\alpha_{\mathbf{i}}(t, \tilde{y}_{\mathbf{i}}^b) \rightarrow 0$ as $t \rightarrow \infty$, which completes the proof. \square

Our main result comes from the previous rationale.

Theorem 4.1. *Consider a network of heterogeneous planar underactuated vehicles. Then, the formation is achieved under the modified PD+ control law (4.12) and (4.18) if the directed communication graph \mathcal{G} contains a spanning tree.*

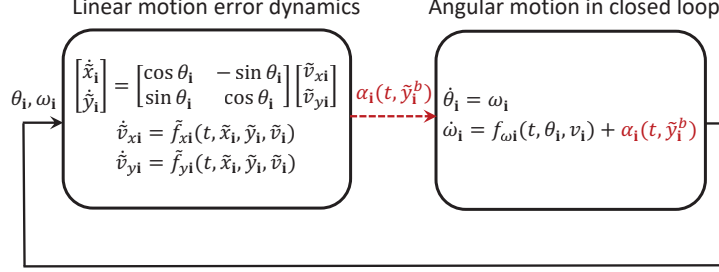


Figure 4.1: Illustration of the modified PD+ controller (4.12) in closed loop with $u\delta$ -PE ‘perturbation’ (4.18).

Proof. By the assumption of the spanning tree topology in the communication graph and using Proposition 4.3, an immediate consequence of the claim is that for each vehicle i in the group, the origin for the $(\tilde{x}_i^b, \tilde{y}_i^b, \dot{\theta}_i, \tilde{v}_{xi}, \tilde{v}_{yi}, \tilde{\omega}_i)$ -dynamics is GAS. It follows from the converse Lyapunov theorem that there exists a continuously differentiable function $\mathbf{V}_i : \mathbb{R} \times \mathbb{R}^6 \rightarrow \mathbb{R}_{\geq 0}$, $\varphi_{1i}, \varphi_{2i} \in \mathcal{K}_\infty$, and a positive definite function \mathbf{W}_i such that

$$\begin{aligned} \varphi_{1i}(|(\tilde{q}_i^b, \tilde{v}_i)|) &\leq \mathbf{V}_i(t, \tilde{q}_i^b, \tilde{v}_i) \leq \varphi_{2i}(|(\tilde{q}_i^b, \tilde{v}_i)|), \\ \dot{\mathbf{V}}_i &\leq -\mathbf{W}_i((\tilde{q}_i^b, \tilde{v}_i)). \end{aligned}$$

Then, define the Lyapunov candidate

$$\mathbf{V} := \sum_{i \in \mathcal{V}} \sum_{j \in \mathcal{N}_i} a_{ij} \mathbf{V}_i. \quad (4.20)$$

It follows from Lemmas 2.4 and 2.6 in [2] that if the communication graph contains a spanning tree, the Laplacian matrix has exactly one zero eigenvalue with an associated eigenvector $\mathbf{1}_n$. Then the Lyapunov candidate \mathbf{V} covers all the agents in the network. Taking the time derivative along the trajectories of the closed-loop system, we have that

$$\dot{\mathbf{V}} \leq - \sum_{i \in \mathcal{V}} \sum_{j \in \mathcal{N}_i} a_{ij} \mathbf{W}_i((\tilde{q}_i^b, \tilde{v}_i)). \quad (4.21)$$

Thus, the formation error converges to zero as $t \rightarrow \infty$, and we conclude that the formation is achieved if the communication graph contains a spanning tree. \square

4.4 Applications and Simulation Results

In this section, we present specific forms of the general EL model (4.1a)-(4.1b) for various vehicles, and present numerical simulations to illustrate the effectiveness of the proposed formation control law. The vehicles chosen are underactuated surface vessels and ground mobile robots. The above combination of vehicles can be used in robotic manipulators installed on boards of surface vessels and ground vehicles for coordinated load carrying in canals, for surveillance operations where coordination between the units on bodies of water (particularly rivers) and on the ground is needed, and for military operations to increase the striking force from multiple sources in the sea and on the ground, to name a few examples.

4.4.1 Applications

Underactuated Surface Vessels. The EL equations for an underactuated surface vessel model with nonlinear hydrodynamic damping are given by (4.1a)-(4.1b) with

$$M = \begin{bmatrix} m_{11} & 0 & 0 \\ 0 & m_{22} & 0 \\ 0 & 0 & m_{33} \end{bmatrix}, C(v) = \begin{bmatrix} 0 & 0 & -m_{22}v_y \\ 0 & 0 & m_{11}v_x \\ m_{22}v_y & -m_{11}v_x & 0 \end{bmatrix},$$

$$D(v) = \begin{bmatrix} d_{11}|v_x|^{\alpha_{11}} & 0 & 0 \\ 0 & d_{22}|v_y|^{\alpha_{22}} & 0 \\ 0 & 0 & d_{33}|\omega|^{\alpha_{33}} \end{bmatrix}, G = \begin{bmatrix} 1 & 0 \\ 0 & 0 \\ 0 & 1 \end{bmatrix},$$

where $m_{ii} > 0$; $d_{ii} > 0$ and $0 \leq \alpha_{ii} < 1$ for $i = 1, 2, 3$ [45, 58]. This model is also applicable to linear hydrodynamic damping with $\alpha_{ii} = 0$, which is the model used in [39, 42–44]. Note that the conditions in Assumption 4.1 can be verified directly and are satisfied for this model.

Wheeled Mobile Robots. Due to the nonholonomic constraints, the dimensions of the tangent (velocity) space are reduced. The EL equations for a nonholonomic mobile robot model are given by (4.1a)-(4.1b) with

$$M = \begin{bmatrix} \tilde{m} & 0 \\ 0 & \tilde{I} \end{bmatrix}, C(v) = \begin{bmatrix} 0 & -md\omega \\ md\omega & 0 \end{bmatrix}, D(v) = 0, G = \begin{bmatrix} \frac{1}{r} & 0 \\ 0 & \frac{a}{r} \end{bmatrix},$$

where $\tilde{m} = m + 2J/r^2$, $\tilde{I} = I + md^2 + a^2J/r^2$, and $m, d, I, J, a, r > 0$ are constants [28, 57, 59]. Although there is no v_y -dynamics in the model and the damping matrix $D(v)$ is zero, the nonholonomic constraint $v_y = d\omega$ suggests that the damping term introduced by the control law K_{di} makes the output of the dynamic equations strictly passive. Thus, the modified

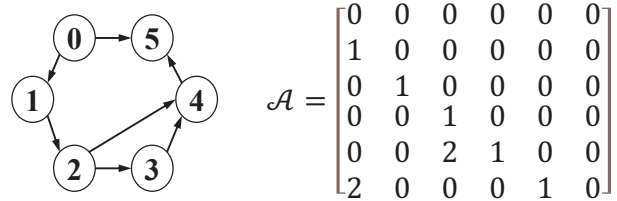


Figure 4.2: *Directed communication topology and the weighted adjacency matrix used in the simulations.*

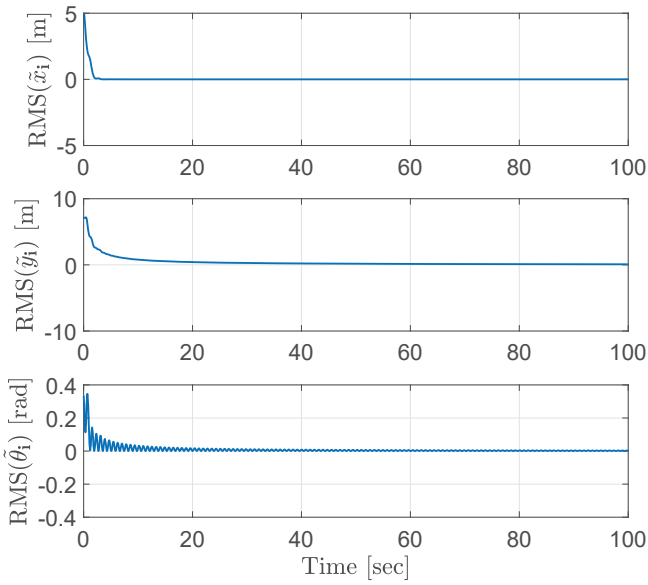


Figure 4.3: *Time history of the RMS errors of the formation stabilization.*

PD+ control law (4.12), (4.18) can be applied to this model directly, and the UGAS for the v_y -subsystem comes directly from the linear relationship between the ω -dynamics and the v_y -dynamics.

4.4.2 Numerical Simulations

Let us consider a group of six planar underactuated vehicles with the indices **0 – 5**. Agent **0** is the leader and agents **1 – 5** are the followers with the communication topology graph and the weighted adjacency matrix as shown in Figure 4.2. Note that we assume that the communication from agent **0** to agent **5**, and the communication from agent **2** to agent **4** are twice as important as the other communication links. We assume that agents **0, 1** are surface

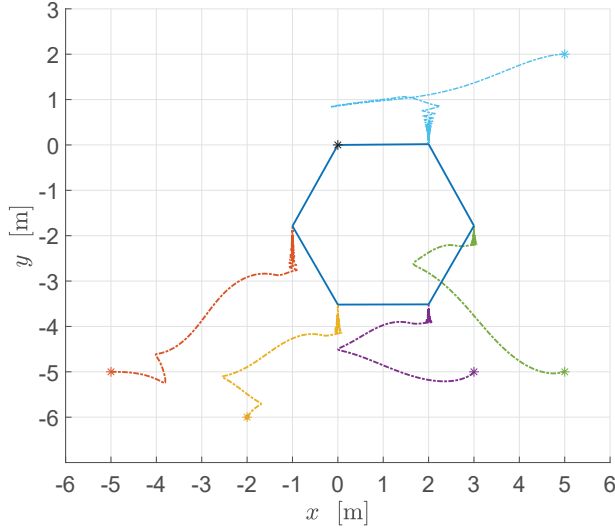


Figure 4.4: Position paths in the $\{XY\}$ frame of the formation stabilization.

vessels with linear hydrodynamic damping whose parameters are given as

$$\begin{aligned} m_{11,i} &= 1.412, & m_{22,i} &= 1.982, & m_{33,i} &= 0.354, \\ d_{11,i} &= 3.436, & d_{22,i} &= 12.99, & d_{33,i} &= 0.864; \end{aligned}$$

agents **2, 3** are surface vessels with nonlinear hydrodynamic damping whose parameters are given as

$$\begin{aligned} m_{11,i} &= 1.317, & m_{22,i} &= 3.832, & m_{33,i} &= 0.926, \\ d_{11,i} &= 5.252, & d_{22,i} &= 14.14, & d_{33,i} &= 2.262, \\ \alpha_{11,i} &= 0.510, & \alpha_{22,i} &= 0.747, & \alpha_{33,i} &= 1.592; \end{aligned}$$

agents **4, 5** are nonholonomic mobile robots whose parameters are given as

$$\begin{aligned} m_i &= 3.0, & I_i &= 0.025, & J_i &= 6 \times 10^{-6}, \\ a_i &= 0.33, & d_i &= 0.08, & r_i &= 0.05. \end{aligned}$$

All the parameters are given in SI units. The desired geometric pattern in formation is assumed to be a regular hexagon with the side length $h = 2$, i.e., $(d_{10}^x, d_{10}^y) = (-1, -\sqrt{3})$, $(d_{21}^x, d_{21}^y) = (1, -\sqrt{3})$, $(d_{32}^x, d_{32}^y) = (0, 2)$, $(d_{43}^x, d_{43}^y) = (1, \sqrt{3})$, $(d_{54}^x, d_{54}^y) = (-1, \sqrt{3})$. The vehicles are assumed to be initially stationary at the coordinates

$$\begin{aligned} q_0(0) &= (0, 0, 0), & q_1(0) &= (-5, -5, 0), & q_2(0) &= (-2, -6, 1), \\ q_3(0) &= (3, -5, 1), & q_4(0) &= (5, -5, 1), & q_5(0) &= (5, 2, 0). \end{aligned}$$

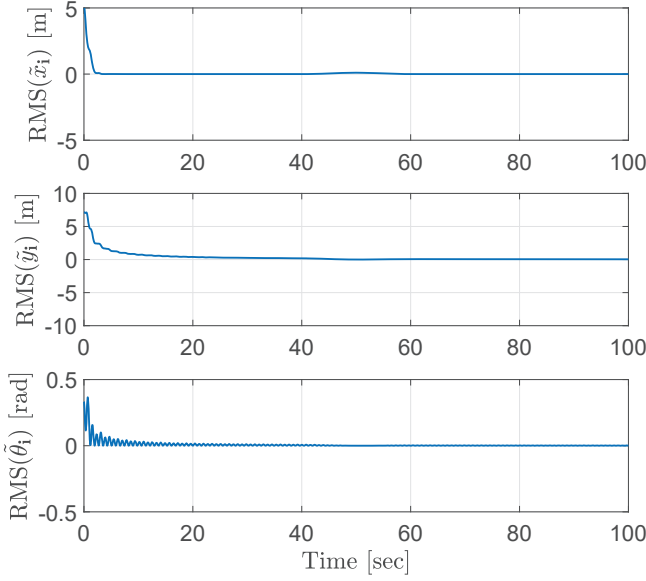


Figure 4.5: Time history of the RMS errors of the formation tracking.

Formation Stabilization. In the first simulation, we assume that the desired configuration for the group leader **0** is at the origin for all times $t \geq 0$. The control parameters are selected as $K_{pi} = \text{diag}\{5, 5, 5\}$, $K_{di} = \text{diag}\{4, 4, 4\}$, $k_{\rho i} = 2$ and $\rho_i(t) = \sin(2t)$ for all $i \in \mathcal{V}$.

The simulation results are shown in Figures 4.3-4.4, where the root mean square (RMS) error shown in Figure 4.3 is of the form $\text{RMS}([\cdot]_i) = (\frac{1}{n} \sum_{i=1}^n [\cdot]_i^2)^{1/2}$. It can be seen from the figures that the formation errors approach zero after 40 seconds. As shown in Figures 4.3-4.4, firstly, each vehicle converges to a small neighborhood of the desired formation position very fast. Then, it converges to the desired formation position with oscillation, and this convergence phase is slow. This oscillation is due to the $u\delta$ -PE term α_i introduced in the control law, and it is a common phenomenon in the stabilization of nonholonomic and underactuated systems via smooth time-varying feedbacks.

Formation Tracking. In the second simulation, we assume that the desired path for the group leader **0** is a U-shape function, i.e.,

$$(x_d(t), y_d(t)) = \begin{cases} (0.5t, 0), & 0 \leq t < 40, \\ (20 + 5 \sin(\frac{\pi t}{20}), 5 - 5 \cos(\frac{\pi t}{20})), & 40 \leq t < 60, \\ (20 - 0.5(t - 60), 10), & 60 \leq t. \end{cases}$$

The control parameters are selected as $K_{pi} = \text{diag}\{8, 8, 8\}$, $K_{di} = \text{diag}\{4, 4, 4\}$, $k_{\rho i} = 4$ and $\rho_i(t) = \sin(4t)$ for all $i \in \mathcal{V}$.

The simulation results are shown in Figures 4.5-4.6. It can be seen from the figures that

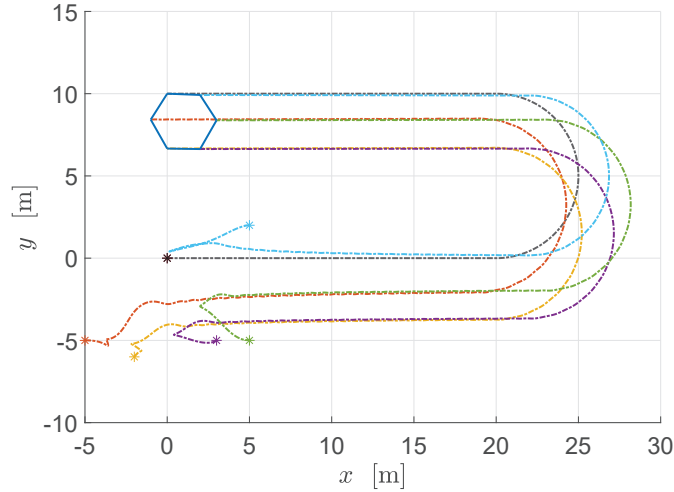


Figure 4.6: Position paths in the $\{XY\}$ frame of the formation tracking.

all formation tracking errors approach zero with satisfactory performance. It is noted that the proposed control law is essentially a PD-type controller. Thus, it is reasonable to expect better performance and robustness with high control gains. Based on the above simulations, the effectiveness of the proposed formation control scheme is verified.

4.5 Concluding Remarks

In this chapter, we presented a distributed control framework to *simultaneously* address the formation stabilization and tracking control problem for heterogeneous planar underactuated vehicle networks without global position measurements. The vehicles in the network are modeled as generic EL systems and are allowed to have identical or non-identical dynamics. The control design is developed based on partial stability theory, Matrosov's theorem, and $u\delta$ -PE, and guarantees GAS for the origin of the closed-loop system. The proposed controller has a PD+ form and is relatively simple compared to existing controllers in the literature that, in addition, solve the stabilization and tracking problems *separately*. Thus, it is practical and easy to implement. One possible disadvantage of the proposed controller is that it may be difficult for large-scale vehicles to implement the PE-based controllers since they cannot move with high frequency.

Chapter 5

Source Seeking for Planar Underactuated Vehicles

5.1 Introduction

Extremum seeking (ES) is a real-time model-free optimization approach that is applicable not only to static maps but also, somewhat uniquely, to dynamical systems [111]. Following the development of the ES convergence guarantees by [112], and their semi-global extension by [113], ES has been a flourishing research area, especially in the domain of autonomous vehicle control for finding sources of signals (electromagnetic, optical, chemical, etc.), distance-based localization, distance-based formation control, etc. The motivation for source seeking algorithms by and large comes from the fact that Global Positioning System (GPS) signals are not available in unstructured environments. Besides, the cost, weight, and complexity of onboard inertial navigation systems (INS) that do not drift over longer periods of time are prohibitive. Hence, autonomous vehicles that operate without GPS or INS benefit from source seeking capabilities.

There are several different models to describe the motion of a vehicle. The simplest is probably that of a kinematic point mass. For this particular model, the problem of source seeking is studied in [114, 115]. A more realistic description of a vehicle is given by the kinematic unicycle model. For this model, control laws for the source seeking problem can be found, for example, in [116–118]. In practice, however, a vehicle is steered by the forces of an engine. It is therefore of interest to consider models in which the acceleration is controlled. Source seeking control laws for force-actuated point masses are presented in [114], and source seeking control laws for force-actuated unicycles are presented in [119, 120]. In addition to the applications on ground vehicles, source seeking algorithms are extremely useful in the marine and aerial industry and military and expect to apply to marine surface vessels, aircraft, and

underwater vehicles. Thus, it is practical to consider the source seeking problems for a generic force-controlled Euler-Lagrangian vehicle model.

Most real vehicles are *underactuated*, where by underactuated it is commonly meant that the number of independent actuators of a vehicle is strictly lower than the number of its DOF, as defined by the dimension of the configuration space [86]. As a consequence of the underactuation, the control design for these vehicles is much more difficult than for fully-actuated vehicles [121]. Specifically, fully-actuated *mechanical system* models (comprising the kinematic and dynamic equations) can be feedback linearized into double-integrator dynamics. This is not possible for underactuated vehicles. Furthermore, unlike (first-order) nonholonomic systems, where nonintegrable constraints are imposed on system velocities (such as in the unicycle), underactuated dynamic vehicle models describe the motions constrained by nonintegrable acceleration constraints, and thus, ES algorithms developed for first-order systems cannot be directly applied to underactuated vehicles.

In this chapter, we develop a novel source seeking strategy for generic force-controlled planar underactuated vehicles. The main contributions are summarized as follows:

- 1) We provide a theoretical foundation for ES algorithms based on symmetric product approximations. We prove that the trajectories of a class of underactuated mechanical systems can be approximated by the trajectories of corresponding *symmetric product systems*. By incorporating symmetric product approximation, averaging, passivity, and partial-state stability theory, we show that the P-SPUAS of a class of underactuated mechanical systems follows from P-UGAS of the corresponding symmetric product system.
- 2) We consider the dynamic model of planar vehicles, instead of considering only the kinematic model such as in [116, 117, 122, 123]. Furthermore, unlike the strategies presented in [114, 124–127] for fully-actuated vehicles, the proposed approach applies to strictly dissipative *underactuated* vehicles, including boats/ships, planar underwater vehicles, etc. and allows the vehicle to start from rest if desired.
- 3) The presented seeking scheme does not require any position or velocity measurements. It requires only real-time measurements of the source signal at the current position of the vehicle and ensures SPUAS with respect to the linear motion coordinates for the closed-loop systems. The structure of the proposed controller is exceptionally simple and easy to implement: the measured output is multiplied by a periodic signal and fed into the surge force.

5.2 Problem Statement

5.2.1 Control/Optimization Objective

Consider the planar underactuated vehicle system

$$\dot{q} = J(q)v, \quad (5.1a)$$

$$M\dot{v} + C(v)v + Dv = Gu, \quad (5.1b)$$

where $q = [x, y, \theta]^\top \in \mathbb{R}^3$ is the configuration of the vehicle; $v = [v_x, v_y, \omega]^\top \in \mathbb{R}^3$ is the generalized velocity vector consisting of the linear velocity (v_x, v_y) in the body-fixed frame and the angular velocity ω ; $u = [u_1, u_2]^\top \in \mathbb{R}^2$ is the control input vector; $J(q)$ is the kinematic transformation matrix; $M = \text{diag}\{m_{11}, m_{22}, m_{33}\} > 0$ is the inertia matrix; $C(v) = -C(v)^\top$ is the Coriolis matrix. The components of vector $C(v)v$ are homogeneous polynomials in $\{v_x, v_y, \omega\}$ of degree 2 [86]. We assume that the damping matrix D is positive definite and constant, which implies that the damping force is proportional to the velocity.

Assume that the position-dependent nonlinear cost function $\rho : \mathbb{R}^2 \rightarrow \mathbb{R}_{\geq 0}$ is smooth and has a global extremum, i.e., there exists a unique $(x^*, y^*) \in \mathbb{R}^2$ such that

$$\nabla\rho(x^*, y^*) = 0 \text{ and } \nabla\rho(x, y) \neq 0, \forall (x, y) \neq (x^*, y^*). \quad (5.2)$$

In applications, $\rho(\cdot)$ may represent the distance between the vehicle and a source, the strength of a certain (electromagnetic, optical, etc.) signal, or the concentration of chemical materials. Without loss of generality, we assume that (x^*, y^*) is the minimum of the function ρ and the vehicle can measure the value of $\rho(x(t), y(t))$ in real-time, as shown in Figure 5.1. Note that both the extremum (x^*, y^*) and the gradient $\nabla\rho$ are unknown. Given any constant $\varepsilon > 0$, the objective is to develop a feedback controller to steer the vehicle without position and velocity measurements such that

$$\lim_{t \rightarrow \infty} |(x(t), y(t)) - (x^*, y^*)| \leq \varepsilon. \quad (5.3)$$

5.2.2 Shifted Passivity

In the existing literature, there are generally two types of source seeking schemes for vehicle systems: 1) tuning the forward motion of the vehicle by the ES loop while keeping the angular speed constant (e.g., [116, 118, 119]), and 2) tuning the angular motion of the vehicle by the ES loop while keeping the forward velocity constant (e.g., [117, 123, 128]). In either case, the

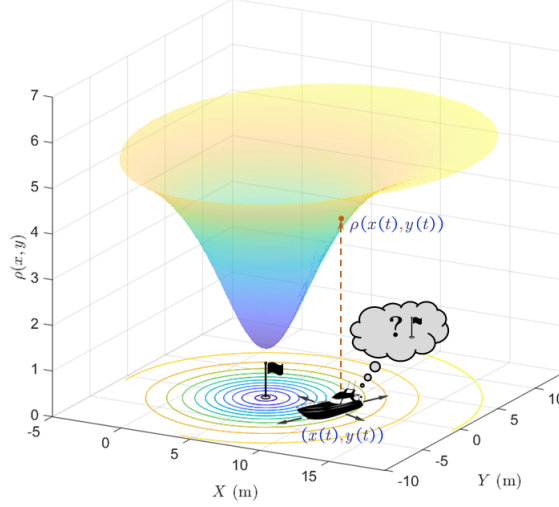


Figure 5.1: Illustration of source seeking problem for planar vehicles.

desired (linear/angular) velocity component is not zero, but instead has a steady-state value corresponding to a non-zero constant input. We formulate this property from the viewpoint of *shifted passivity* [129].

Consider the system (5.1a)-(5.1b) with the output $\eta := G^\top v$. Define the steady-state set

$$\mathcal{E} := \{(v, u) \in \mathbb{R}^3 \times \mathbb{R}^2 : C(v)v + Dv - Gu = 0\}. \quad (5.4)$$

Fix $(v^*, u^*) \in \mathcal{E}$ and the steady-state output $\eta^* := G^\top v^*$.

Definition 5.1 (Shifted passivity). The system (5.1a)-(5.1b) is said to be *shifted passive* if the input-output mapping $(u - u^*) \mapsto (\eta - \eta^*)$ is passive, i.e., there exists a storage function $\mathcal{H} : \mathbb{R}^3 \rightarrow \mathbb{R}_{\geq 0}$ such that for all $(v, u) \in \mathbb{R}^3 \times \mathbb{R}^2$,

$$\dot{\mathcal{H}} := (\nabla \mathcal{H}(v))^\top \dot{v} \leqslant (u - u^*)^\top (\eta - \eta^*). \quad (5.5)$$

Proposition 5.1. Consider the system (5.1a)-(5.1b) with the steady-state input $u^* = [0, c]^\top$, where $c > 0$ is a constant. Then, there exists $\hat{c} > 0$ such that for all $c \in (0, \hat{c})$, the system (5.1a)-(5.1b) is shifted passive.

Proof. Fix the input $u^* = [0, c]^\top$, and the corresponding steady-state velocity and output are $v^* = [0, 0, \omega^*]^\top$ and $\eta^* = [0, \omega^*]^\top$, respectively. Let the storage function be $\mathcal{H}(v) = \frac{1}{2}(v - v^*)^\top M(v - v^*)$. Then, the time derivative of $\mathcal{H}(v)$ along the trajectories of (5.1a)-

(5.1b) is given by

$$\begin{aligned}
\dot{\mathcal{H}} &= (v - v^*)^\top [G(u - u^*) - C(v)v - Dv + Gu^*] \\
&= (\eta - \eta^*)^\top (u - u^*) - (v - v^*)^\top [C(v)v + Dv - Gu^*] \\
&= (\eta - \eta^*)^\top (u - u^*) - (v - v^*)^\top D(v - v^*) \\
&\quad - (v - v^*)^\top [C(v) - C(v^*)] v^*, \tag{5.6}
\end{aligned}$$

where we used (5.1b), and added and subtracted the term Gu^* in the first identity, added and subtracted the term $(C(v) + D)v^*$ in the second identity, and used $Gu^* = C(v^*)v^* + Dv^*$ in the third identity. Let us denote $\mathcal{J}(v) := C(v)v^* + Dv$. From (5.6) we have

$$\dot{\mathcal{H}} = (\eta - \eta^*)^\top (u - u^*) - (v - v^*)^\top [\mathcal{J}(v) - \mathcal{J}(v^*)]. \tag{5.7}$$

It follows from the homogeneity of $C(v)v$ that for all $v \in \mathbb{R}^3$, $\|\partial[C(v)e_3]/\partial v\|$ is bounded, where $e_3 = [0, 0, 1]^\top$. Thus, we can always choose ω^* small enough such that $\partial[C(v)v^*]/\partial v + [\partial[C(v)v^*]/\partial v]^\top \leq 2D$, which implies that $(\partial\mathcal{J}(v)/\partial v) + (\partial\mathcal{J}(v)/\partial v)^\top \geq 0$ for all $v \in \mathbb{R}^3$. Therefore, the map $\mathcal{J}(\cdot)$ is monotone, and correspondingly, $(v - v^*)^\top [\mathcal{J}(v) - \mathcal{J}(v^*)] \geq 0$, which completes the proof. \square

5.3 Symmetric Product Approximations

5.3.1 Motivational Example

The classical averaging technique [114, 116] and the Lie bracket averaging approach [118] cannot be directly applied to system (5.1a)-(5.1b). The classical averaging technique applies to systems in the form

$$\dot{\xi} = \varepsilon f(t, \xi, \varepsilon), \tag{5.8}$$

where $\varepsilon > 0$ is a small parameter and f is (almost) periodic in t . However, it is not possible to find a transformation for rewriting system (5.1a)-(5.1b) into the form (5.8) in general [93]. The Lie bracket averaging approach applies to input-affine systems in the form [118, 130]

$$\dot{\xi} = b_0(t, \xi) + \sum_{i=1}^m b_i(t, \xi) \sqrt{\omega} u_i(t, \omega t), \tag{5.9}$$

where $\omega \in (0, \infty)$, m is a positive integer, and the corresponding Lie bracket system is given by

$$\dot{\zeta} = b_0(t, \zeta) + \sum_{\substack{i=1 \\ j=i+1}}^m [b_i, b_j](t, \zeta) w_{ji}(t), \quad (5.10)$$

where $w_{ji}(t) = \frac{1}{T} \int_0^T u_j(t, s) \int_0^s u_i(t, \tau) d\tau ds$. For illustration, let us consider a damped double-integrator system

$$\begin{bmatrix} \dot{\xi}_1 \\ \dot{\xi}_2 \end{bmatrix} = \underbrace{\begin{bmatrix} \xi_2 \\ -\xi_2 \end{bmatrix}}_{b_0(\xi_2)} + \sum_{i=1}^m \underbrace{\begin{bmatrix} 0 \\ k_i(\xi_1) \end{bmatrix}}_{b_i(\xi_1)} u_i(t). \quad (5.11)$$

where $\xi_1, \xi_2, u_i \in \mathbb{R}$, $\xi = [\xi_1, \xi_2]^\top$, and $k_i(\cdot)$'s represent arbitrary ξ_1 (position)-dependent functions. A simple calculation shows that the Lie brackets between any two input vector fields are zero, i.e., $[b_i, b_j] \equiv 0$ for any $i, j = 1, \dots, m$, and thus, the Lie bracket approximations cannot be applied to the double-integrator system (5.11), let alone the system (5.1a)-(5.1b).

Next, we will show that the symmetric product approximations can be used to solve the ES problem for (5.1a)-(5.1b). To illustrate the main idea, consider (5.11) again. We first change the time scale by setting $\tau = t/\varepsilon$, and let $u_i(t) = (1/\varepsilon)v_i(t/\varepsilon)$. Then, (5.11) becomes

$$\frac{d}{d\tau}\xi = \varepsilon f(\xi) + g(\tau, \xi), \quad (5.12)$$

where $f(\xi) = b_0(\xi_2)$ and $g(\tau, \xi) = \sum_{i=1}^m b_i(\xi_1)v_i(\tau)$. According to the variation of constants formula given in Appendix A.3, the corresponding *pull back system* is given by

$$\frac{d}{d\tau}z = \varepsilon F(\tau, z), \quad z(0) = \xi(0), \quad (5.13)$$

where $z = [z_1, z_2]^\top$ and

$$F(\tau, z) = f(z) + \sum_{k=1}^{\infty} \int_0^{\tau} \cdots \int_0^{s_{k-1}} (\text{ad}_{g(s_k, z)} \cdots \text{ad}_{g(s_1, z)} f(z)) ds_k \cdots ds_1.$$

By direct calculations, we have

$$\text{ad}_{g(s_1, z)} f(z) = - \sum_{i=1}^m v_i(s_1) \begin{bmatrix} -k_i(z_1) \\ k_i(z_1) + k'_i(z_1)z_2 \end{bmatrix}, \quad (5.14)$$

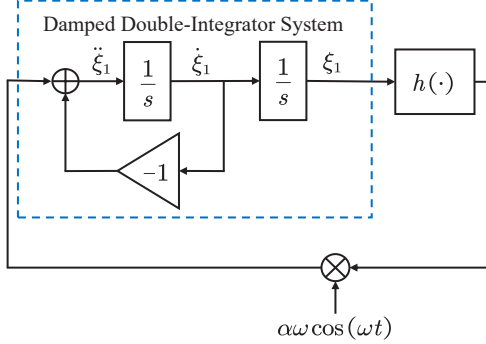


Figure 5.2: Extremum seeking scheme for the damped double-integrator system.

and

$$\text{ad}_{g(s_2,z)} \text{ad}_{g(s_1,z)} f(z) = - \sum_{i,j=1}^m v_i(s_1) v_j(s_2) \begin{bmatrix} 0 \\ (k_i(z_1) k_j(z_1))' \end{bmatrix}. \quad (5.15)$$

Note that the structural property of the system (5.11) guarantees that the higher order terms $\text{ad}_{g(s_k,z)} \dots \text{ad}_{g(s_1,z)} f(z) \equiv 0$ for all $k \geq 3$. Thus, the pull-back vector field F can be written as

$$F(\tau, z) = f(z) - \sum_{i=1}^m \begin{bmatrix} -k_i(z_1) \\ k_i(z_1) + k'_i(z_1) z_2 \end{bmatrix} \int_0^\tau v_i(s_1) ds_1 - \sum_{i,j=1}^m \begin{bmatrix} 0 \\ (k_i(z_1) k_j(z_1))' \end{bmatrix} \int_0^\tau \int_0^{s_1} v_i(s_1) v_j(s_2) ds_2 ds_1.$$

Denote the solution of the pull-back system (5.13) by $z(t)$. Then, it follows from the variation of constants formula in Appendix A.3 that the solution of the system (5.12) is given by the initial value problem

$$\frac{d}{d\tau} \begin{bmatrix} \xi_1 \\ \xi_2 \end{bmatrix} = \sum_{i=1}^m \begin{bmatrix} 0 \\ k_i(\xi_1) \end{bmatrix} v_i(\tau), \quad \xi(0) = z(\tau). \quad (5.16)$$

We change the time scale back to $t = \varepsilon\tau$, and it follows from (5.16) that $\dot{\xi}_1 \equiv 0$, which implies that $\xi_1(t) \equiv \xi_1(0) \equiv z_1(t)$. That is, the position trajectory of the double-integrator system (5.11) is the z_1 -trajectory of the pull-back system (5.13).

The basic ES scheme for the double-integrator system (5.11) is illustrated in Fig. 5.2.

The closed-loop system can be written as

$$\begin{bmatrix} \dot{\xi}_1 \\ \dot{\xi}_2 \end{bmatrix} = \begin{bmatrix} \xi_2 \\ -\xi_2 \end{bmatrix} + \begin{bmatrix} 0 \\ h(\xi_1) \end{bmatrix} \alpha \omega \cos(\omega t), \quad (5.17)$$

where $h(\cdot)$ is the cost function and $\alpha \in \mathbb{R}$ is a constant. The pull back system in time scale $\tau = t/\varepsilon = \omega t$ is given by

$$\frac{dz}{d\tau} = \varepsilon \left\{ f(z) - \alpha \begin{bmatrix} -h(z_1) \\ h(z_1) + h'(z_1)z_2 \end{bmatrix} \sin(\tau) - \frac{\alpha^2}{2} \begin{bmatrix} 0 \\ (h^2(z_1))' \end{bmatrix} \sin^2(\tau) \right\}.$$

The pull back system is in the form of (5.8), and the averaged pull back system in time scale t is given by [93, Section 10.4]

$$\begin{bmatrix} \dot{\bar{z}}_1 \\ \dot{\bar{z}}_2 \end{bmatrix} = \begin{bmatrix} \bar{z}_2 \\ -\bar{z}_2 \end{bmatrix} - \frac{\alpha^2}{4} \begin{bmatrix} 0 \\ 2h(\bar{z}_1)\nabla h(\bar{z}_1) \end{bmatrix}. \quad (5.18)$$

Letting $V(\bar{z}_1, \bar{z}_2) = \frac{\alpha^2}{4}h^2(\bar{z}_1) + \frac{1}{2}\bar{z}_2^2$ and taking the time derivative along trajectories of (5.18), we have $\dot{V} = -\bar{z}_2^2 \leq 0$. If the cost function $h(\cdot)$ has a global minimum $h(\xi_1^*) \geq 0$, then it follows from the Krasovskii-LaSalle principle that the global minimum is GAS. Finally, using the averaging theorem in [131] and the conclusion that $\xi_1(t) \equiv z_1(t)$, the global minimum is SPUAS for the closed-loop system (5.17), i.e., the position trajectory $\xi_1(t)$ converges to an $O(\varepsilon)$ -neighborhood of the global minimum point ξ_1^* as $t \rightarrow \infty$. We will now generalize this idea to system (5.1a)-(5.1b).

5.3.2 Symmetric Product Approximations

Consider the system (5.1a)-(5.1b). Let the input vector be

$$u = b_0 + \frac{1}{\varepsilon} \sum_{i=1}^m b_i(q) w_i \left(\frac{t}{\varepsilon} \right), \quad (5.19)$$

where ε is a positive constant, m is a positive integer, $b_0 = [b_{10}, b_{20}]^\top$ is a constant vector, $b_i(q) = [b_{1i}(q), b_{2i}(q)]^\top$, and $\{w_i(t)\}$ are T -periodic functions satisfying

$$\int_0^T w_i(s_1) ds_1 = 0, \quad i = 1, \dots, m, \quad (5.20)$$

$$\int_0^T \int_0^{s_2} w_i(s_1) ds_1 ds_2 = 0, \quad i = 1, \dots, m. \quad (5.21)$$

Then, (5.1a)-(5.1b) with the input vector (5.19) in time scale $\tau = t/\varepsilon$ can be written as

$$\frac{d}{d\tau} \begin{bmatrix} q \\ v \end{bmatrix} = \varepsilon \underbrace{\begin{bmatrix} J(q)v \\ -M^{-1}[C(v)v + Dv - B_0] \end{bmatrix}}_{\mathbf{f}(q,v)} + \underbrace{\begin{bmatrix} 0 \\ \sum_{i=1}^m B_i w_i(\tau) \end{bmatrix}}_{\mathbf{g}(\tau,q)}, \quad (5.22)$$

where $B_0 = Gb_0$ and $B_i(q) = M^{-1}Gb_i(q)$ for $i = 1, \dots, m$. Denote $\mathbf{f}_2(v) = -M^{-1}[C(v)v + Dv - B_0]$. The *symmetric product* of two vector fields $X, Y : \mathbb{R}^3 \rightarrow \mathbb{R}^3$ corresponding to system (5.1a)-(5.1b) is defined as

$$\langle X : Y \rangle = \frac{\partial X}{\partial q} J(q) Y + \frac{\partial Y}{\partial q} J(q) X - \left(\frac{\partial}{\partial v} \left(\frac{\partial \mathbf{f}_2}{\partial v} X \right) \right) Y. \quad (5.23)$$

The symmetric product $\langle \cdot : \cdot \rangle$ satisfies $\langle X : Y \rangle = \langle Y : X \rangle$.

In the next theorem, we show that system (5.1a)-(5.1b) with input (5.19) can be approximated by the *symmetric product system*

$$\dot{\bar{q}} = J(\bar{q})\bar{v}, \quad (5.24a)$$

$$M\dot{\bar{v}} + C(\bar{v})\bar{v} + D\bar{v} = B_0 - M \sum_{i,j=1}^m \Lambda_{ij} \langle B_i : B_j \rangle(\bar{q}), \quad (5.24b)$$

where

$$\Lambda_{ij} = \frac{1}{2T} \int_0^T \left(\int_0^{s_1} w_i(s_2) ds_2 \right) \left(\int_0^{s_1} w_j(s_2) ds_2 \right) ds_1. \quad (5.25)$$

Define the time-varying vector field as

$$\Xi(t, q) := \sum_{i=1}^m \left(\int_0^t w_i(s) ds \right) B_i(q). \quad (5.26)$$

Theorem 5.1. Consider the system (5.1a)-(5.1b) with input vector (5.19) and the symmetric product system (5.24a)-(5.24b). Assume that the initial conditions of the two systems are the same. Denote the solutions of (5.1a)-(5.1b) and (5.24a)-(5.24b) as $(q(t), v(t))$ and $(\bar{q}(t), \bar{v}(t))$ for $t \geq 0$, respectively. If the system (5.24a)-(5.24b) is GAS with respect to $(\bar{x}, \bar{y}, \bar{v}_x, \bar{v}_y)$ uniformly in $(\bar{\theta}(0), \bar{\omega}(0))$, then the system (5.1a)-(5.1b) is SPAS with respect to (x, y, v_x, v_y) uniformly in $(\theta(0), \omega(0))$.

Proof. By the variation of constants formula in Appendix A.3, the corresponding pull back system of (5.22) is given by

$$\frac{d}{d\tau} \begin{bmatrix} \hat{q} \\ \hat{v} \end{bmatrix} = \varepsilon \mathsf{F}(\tau, \hat{q}, \hat{v}), \quad (5.27)$$

where $(\hat{q}(0), \hat{v}(0)) = (q(0), v(0))$ and

$$\mathsf{F}(\tau, q, v) = \mathbf{f}(q, v) + \sum_{k=1}^{\infty} \int_0^\tau \cdots \int_0^{s_{k-1}} (\text{ad}_{g(s_k, q)} \cdots \text{ad}_{g(s_1, q)} \mathbf{f}(q, v)) ds_k \cdots ds_1.$$

By direct calculations, we have

$$\text{ad}_{g(s_1, z)} \mathbf{f}(q, v) = \sum_{i=1}^m w_i(s_1) \left[\left(\frac{\partial \mathbf{f}_2}{\partial v} \right) B_i - \left(\frac{\partial B_i}{\partial q} \right) J(q)v \right],$$

and

$$\text{ad}_{g(s_2, q)} \text{ad}_{g(s_1, q)} \mathbf{f}(q, v) = - \sum_{i,j=1}^m w_i(s_1) w_j(s_2) \begin{bmatrix} 0 \\ \langle B_i : B_j \rangle \end{bmatrix}.$$

Note that the symmetric product $\langle B_i : B_j \rangle$ is a vector field depending only on q . Thus, the higher order terms $\text{ad}_{g(s_k, q)} \cdots \text{ad}_{g(s_1, q)} \mathbf{f}(q, v) \equiv 0$ for all $k \geq 3$. The pull back vector field F is given by

$$\begin{aligned} \mathsf{F} &= \mathbf{f} + \sum_{i=1}^m \left[\left(\frac{\partial \mathbf{f}_2}{\partial v} \right) B_i - \left(\frac{\partial B_i}{\partial q} \right) J(q)v \right] \int_0^\tau w_i(s_1) ds_1 \\ &\quad - \sum_{i,j=1}^m \begin{bmatrix} 0 \\ \langle B_i : B_j \rangle \end{bmatrix} \int_0^\tau \int_0^{s_1} w_i(s_1) w_j(s_2) ds_2 ds_1. \end{aligned} \quad (5.28)$$

Denote the solution of the pull back system (5.27) by $(\hat{q}(\tau), \hat{v}(\tau))$. Then, it follows from Theorem A.4 that the solution of (5.22) is given by the initial value problem

$$\frac{d}{d\tau} \begin{bmatrix} q \\ v \end{bmatrix} = \begin{bmatrix} 0 \\ \sum_{i=1}^m B_i(q) w_i(\tau) \end{bmatrix}, \quad \begin{bmatrix} q(0) \\ v(0) \end{bmatrix} = \begin{bmatrix} \hat{q}(\tau) \\ \hat{v}(\tau) \end{bmatrix}. \quad (5.29)$$

Therefore, we have

$$q(\tau) = q(0) = \hat{q}(\tau), \quad (5.30)$$

$$v(\tau) = \hat{v}(\tau) + \Xi(\tau, q(\tau)). \quad (5.31)$$

The pull back system (5.27) is in the classical averaging form [93, Section 10.4]. Consider the average system

$$\frac{d}{d\tau} \begin{bmatrix} \bar{q} \\ \bar{v} \end{bmatrix} = \frac{\varepsilon}{T} \int_0^T \mathsf{F}(\tau, \bar{q}, \bar{v}) d\tau, \quad (5.32)$$

and denote the solution by $(\bar{q}(t), \bar{v}(t))$. It follows from (5.21), the symmetry of the symmetric product, and integration by parts, that the averaged system (5.32) in time scale $t = \varepsilon\tau$ is the symmetric product system (5.24a)-(5.24b).

According to the averaging theorem [93, Theorem 10.4], there exists $\varepsilon^* > 0$ such that for all $0 < \varepsilon < \varepsilon^*$,

$$|\hat{q}(t) - \bar{q}(t)| = O(\varepsilon), \quad \text{and} \quad |\hat{v}(t) - \bar{v}(t)| = O(\varepsilon) \quad (5.33)$$

as $\varepsilon \rightarrow 0$ on time scale 1. We recover the partial converging trajectories property by substituting (5.30)-(5.31) into (5.33). Finally, it follows directly from Proposition A.1 that the system (5.1a)-(5.1b) is SPAS with respect to (x, y, v_x, v_y) uniformly in $(\theta(0), \omega(0))$, which completes the proof. \square

Remark 5.1. In Theorem 5.1, instead of requiring UGAS of the symmetric product system (5.24a)-(5.24b) as in classical averaging theory [131], we only assume (5.24a)-(5.24b) to be P-UGAS with respect to $(\bar{x}, \bar{y}, \bar{v}_x, \bar{v}_y)$, while the remaining part of the state $(\bar{\theta}(t), \bar{\omega}(t))$ does not necessarily converge to $(0, 0)$. Correspondingly, in the source seeking design in the next section, the approximation in the linear motion $|(x, y, v_x, v_y) - (x^*, y^*, 0, 0)| = O(\varepsilon)$ is valid for all $t \geq 0$, while the angular motion of the vehicle can be persistently exciting.

Remark 5.2. The total energy of the planar vehicle is $E = \frac{1}{2}v^\top Mv$. If the vector fields $B_i(q)$ are integrable, they can be written as $B_i(q) = \nabla\varphi_i(q)$ for some scalar functions $\varphi_i(q)$, where $i = 1, \dots, m$. It follows from [132] that if we define *symmetric product for two scalar functions* (Beltrami bracket) according to $\langle \varphi_i : \varphi_j \rangle := (\nabla\varphi_i)^\top \nabla\varphi_j$, then we have $\nabla\langle \varphi_i : \varphi_j \rangle(q) = \langle \nabla\varphi_i : \nabla\varphi_j \rangle(q) = \langle B_i : B_j \rangle(q)$. Correspondingly, the total energy of the symmetric product system (5.24a)-(5.24b) is $E_{av} = \frac{1}{2}\bar{v}^\top M\bar{v} + \sum_{i,j=1}^m \Lambda_{ij} \langle \varphi_i : \varphi_j \rangle(\bar{q})$. The term $\sum_{i,j=1}^m \Lambda_{ij} \langle \varphi_i : \varphi_j \rangle(\bar{q})$, introduced by the “high magnitude high-frequency forces”, is called the *averaged potential* [133]. Thus, the control law (5.19) can be viewed as a “potential energy shaping” technique, where the desired potential energy function can be injected by designing appropriate input

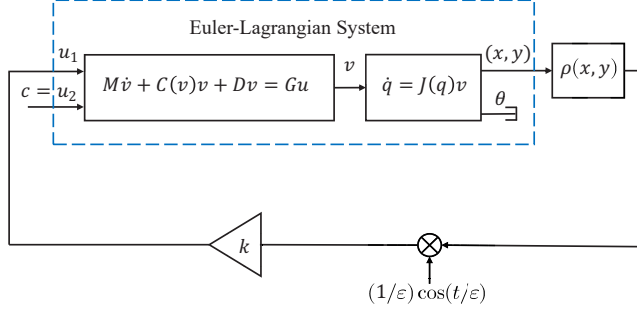


Figure 5.3: Source seeking scheme for planar vehicle system (5.1a)-(5.1b).

vectors $B_i(q)$. This viewpoint shows that besides the classical averaging approach in [112] and the Lie bracket averaging approach in [118], the symmetric product approximation can also be used to obtain gradient information, which will be used in the source seeking design.

5.4 Source Seeking for Underactuated Vehicles

5.4.1 Source Seeking Scheme

We propose a source seeking scheme for the planar vehicle system (5.1a)-(5.1b) as it is depicted in Fig. 5.3. In the proposed scheme, the surge force of the vehicle is tuned by the ES loop, while the yaw torque keeps a certain constant value. The proposed surge force tuning-based source seeking scheme is similar to the methods in [116, 118, 120], but will be analyzed in the symmetric product approximation framework.

The control law in Fig. 5.3 is given by

$$u_1 = \frac{k}{\varepsilon} \cos\left(\frac{t}{\varepsilon}\right) \rho(x, y), \quad (5.34)$$

$$u_2 = c, \quad (5.35)$$

where ε , k , and c are positive parameters. The gain k is used to tune the transient performance. The small parameter ε introduces the “high-magnitude high-frequency force”, which leads to the symmetric product approximation. The constant torque c maintains a persistently exciting angular motion of the vehicle, which is necessary to establish convergence for underactuated vehicle systems.

5.4.2 Stability Analysis

Theorem 5.2. Consider the system (5.1a)-(5.1b) with inputs (5.34)-(5.35). Suppose that the cost function $\rho(x, y) \geq 0$ satisfies (5.2). Then, there exists $\hat{c} > 0$ and for any $c \in (0, \hat{c})$, there exists $\hat{\varepsilon} > 0$ such that for the given c and any $\varepsilon \in (0, \hat{\varepsilon})$ and $k > 0$, the closed-loop system is SPAS with respect to $(x - x^*, y - y^*, v_x, v_y)$ uniformly in $(\theta(0), \omega(0))$.

Proof. Note that the control law (5.34)-(5.35) is in the form of (5.19), where $m = 1$, $b_0 = [0, c]^\top$, $b_1(q) = [k\rho(x, y), 0]^\top$, and $w_1(t) = \cos(t)$. It can be verified that conditions (5.20)-(5.21) hold for $T = 2\pi$. Thus, it follows from Theorem 5.1 that the closed-loop system is SPAS with respect to $(x - x^*, y - y^*, v_x, v_y)$ uniformly in $(\theta(0), \omega(0))$ if the corresponding symmetric product system (5.24a)-(5.24b) is GAS with respect to $(\bar{x} - x^*, \bar{y} - y^*, \bar{v}_x, \bar{v}_y)$ uniformly in $(\theta(0), \omega(0))$. Next, we show that it is indeed the case.

By direct calculations, we have $\Lambda_{11} = 1/4$, and the symmetric product is given by $\langle B_1 : B_1 \rangle(\bar{q}) = 2(m_{11}^{-1}k)^2\rho(\bar{x}, \bar{y})[\rho'_x(\bar{x}, \bar{y})\cos(\bar{\theta}) + \rho'_y(\bar{x}, \bar{y})\sin(\bar{\theta}), 0, 0]^\top$, where $\rho'_x(x, y) := \partial\rho(x, y)/\partial x$ and $\rho'_y(x, y) := \partial\rho(x, y)/\partial y$. The constant torque c is selected such that Proposition 5.1 holds, and then, the system (5.24a)-(5.24b) is shifted passive under the steady-state input $u^* = b_0$. Denote $\alpha = (m_{11}^{-1}k)^2/2$ and $C_i(\cdot)$ the i -th component of the vector $-M^{-1}C(\bar{v})\bar{v}$. The symmetric product system can be viewed as a feedback interconnection of two subsystems, as shown in Fig. 5.4.

When the input $\bar{v}_y \equiv 0$, the nominal system of the upper subsystem is exactly the unicycle model under passive feedback. We first prove the nominal system of the upper subsystem (i.e., $\bar{v}_y \equiv 0$) is P-UGAS. Let $V_1(\bar{x}, \bar{y}, \bar{v}_x) = \frac{1}{2}\bar{v}_x^2 + \frac{\alpha}{2}\rho(\bar{x}, \bar{y})^2$, and along trajectories of the nominal system, we have $\dot{V}_1|_{\text{nominal}} = -\frac{d_{11}}{m_{11}}\bar{v}_x^2 \leq 0$, which, according to Theorem A.1, shows that the nominal system is US and UGB with respect to $(\bar{x} - x^*, \bar{y} - y^*, \bar{v}_x)$ uniformly in $(\bar{\theta}(0), \bar{\omega}(0))$. Then, consider the auxiliary function $V_2 = \bar{v}_x\rho(\bar{x}, \bar{y})(\rho'_x\cos(\bar{\theta}) + \rho'_y\sin(\bar{\theta}))$. Evaluating the time derivative of V_2 along trajectories of the nominal system on the set $\{\bar{v}_x = 0\}$, we have $\dot{V}_2|_{\text{nominal}, \bar{v}_x=0} = -\alpha\rho^2(\rho'_x\cos(\bar{\theta}) + \rho'_y\sin(\bar{\theta}))^2$, which is non-zero definite. It follows from Matrosov's theorem [121, 134] that the nominal system is UGAS with respect to $(\bar{x} - x^*, \bar{y} - y^*, \bar{v}_x)$ uniformly in $(\bar{\theta}(0), \bar{\omega}(0))$.

Second, we prove that the upper subsystem is input-to-output stable (IOS) by viewing \bar{v}_y as input and $(\bar{v}_x, \bar{\omega})$ as output. Because the nominal part of the upper subsystem is P-UGAS, for each $r > 0$, there exists a constant $\delta_r > 0$ such that for all initial conditions starting in the ball centering at the equilibrium with radius r , we have $\max\{|\rho'_x\cos(\bar{\theta}) + \rho'_y\sin(\bar{\theta})|, |\rho'_x\cos(\bar{\theta}) + \rho'_y\sin(\bar{\theta})|^2, |c\rho(\rho'_x\sin(\bar{\theta}) - \rho'_y\cos(\bar{\theta}))|/d_{33}, |\rho(\rho''_{xx}\cos(\bar{\theta})^2 + 2\rho''_{xy}\sin(\bar{\theta}))\cos(\bar{\theta})|\} < \delta_r$. Let $\mathcal{V}_r = \beta_r V_1 + V_2$, where $\beta_r > 0$ is a constant to be determined. It follows from Young's inequality $ab \leq a^2/(2\epsilon) + (\epsilon b^2)/2$ that $\mathcal{V}_r > 0$ and $\dot{\mathcal{V}}_r|_{\text{nominal}} \leq -\bar{v}_x^2 - \frac{\alpha}{2}\rho^2(\rho'_x\cos(\bar{\theta}) + \rho'_y\sin(\bar{\theta}))^2 + \bar{v}_x\delta_r$ by

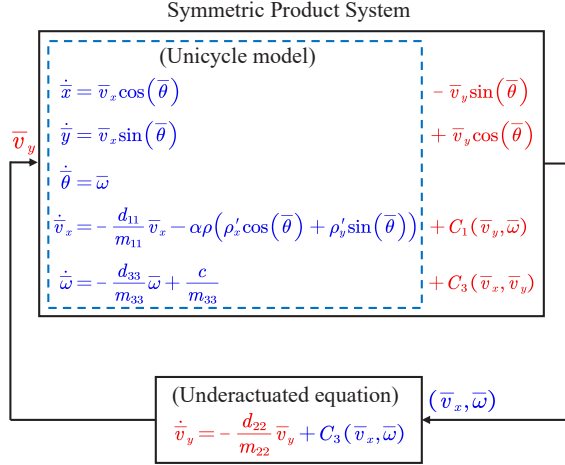


Figure 5.4: Feedback interconnection of the symmetric product system (5.24a)-(5.24b).

selecting $\beta_r > \max \{ \delta_r^2 / \alpha, 1 + 2m_{11}\delta_r/d_{11} + d_{11}/(2\alpha m_{11}) \}$. Then, taking the time derivative of \mathcal{V}_r along trajectories of the upper subsystem, and noting that the quadratic terms $-\bar{v}_x^2 - \frac{\alpha}{2}\rho^2(\rho'_x \cos(\bar{\theta}) + \rho'_y \sin(\bar{\theta}))^2$ dominate $\dot{\mathcal{V}}_r|_{\text{upper}}$ when $|(\bar{v}_x, \rho(\rho'_x \cos(\bar{\theta}) + \rho'_y \sin(\bar{\theta})))|$ are large, we conclude that the upper subsystem is IOS with input \bar{v}_y and output $(\bar{v}_x, \bar{\omega})$.

Due to the fact that the lower subsystem in Fig. 5.4 is a stable linear system, it is also IOS by viewing $(\bar{v}_x, \bar{\omega})$ as the input and \bar{v}_y as the output, and the IOS-gain can be rendered arbitrarily small by selecting c small enough. Therefore, the symmetric product system (5.24a)-(5.24b) is a feedback interconnection of two IOS subsystems, where the zero-state detectability can be easily verified. It follows from the small-gain theorem [135] that, there exists $\hat{c} > 0$ such that the symmetric product system (5.24a)-(5.24b) is GAS with respect to $(\bar{x} - x^*, \bar{y} - y^*, \bar{v}_x, \bar{v}_y)$ uniformly in $(\theta(0), \omega(0))$ for all $c \in (0, \hat{c})$. Finally, we conclude that the closed-loop system is SPAS with respect to $(x - x^*, y - y^*, v_x, v_y)$ uniformly in $(\theta(0), \omega(0))$ by invoking Theorem 5.1. \square

Remark 5.3. Compared with the surge force tuning-based source seeking schemes in [116, 118], the presented scheme does not require an additive periodic perturbation. The additive periodic perturbation is necessary in the Lie bracket averaging-based algorithm [118] since it is used to introduce the back-and-forth motion of a vehicle. However, as shown in Section 5.3, only with a multiplicative periodic perturbation, the pull back system still involves an operation that is calculating Lie bracket with the vector \mathbf{g} , i.e., $[\mathbf{g}(s_2, q), [\mathbf{g}(s_1, q), \mathbf{f}(q, v)]]$.

Remark 5.4. In Theorem 5.2, it is assumed that the constant torque c must be selected small enough. The reason is, as shown in Proposition 5.1, with a small c , the natural damping stabilizes the underactuated equation and the symmetric product system keeps shifted passive.

In other words, a large torque can destabilize a lightly damped system. This is why c must be small and relative to damping.

5.5 Simulations

Consider a boat with linear hydrodynamic damping [121], where the equations are given by (5.1a)-(5.1b) with

$$C(v) = \begin{bmatrix} 0 & 0 & -m_{22}v_y \\ 0 & 0 & m_{11}v_x \\ m_{22}v_y & -m_{11}v_x & 0 \end{bmatrix}$$

and $D = \text{diag}\{d_{11}, d_{22}, d_{33}\}$, where

$$\begin{aligned} m_{11} &= 1.412, & m_{22} &= 1.982, & m_{33} &= 0.354, \\ d_{11} &= 3.436, & d_{22} &= 12.99, & d_{33} &= 0.864. \end{aligned}$$

The boat is assumed to rest at the origin initially, i.e., $(q(0), v(0)) = (0, 0)$. Assume that the cost function is $\rho(x, y) = (x - 2)^2 + 0.5(y - 3)^2 + 1$.

It follows from (5.1a)-(5.1b) that the constant input $(u_1^*, u_2^*) = (0, c)$ leads to the steady-state velocity $v^* = (v_x^*, v_y^*, \omega^*) = (0, 0, c/d_{33})$. Then, the constant c is chosen such that $\partial[C(v)v^*]/\partial v + [\partial[C(v)v^*]/\partial v]^\top \leq 2D$ holds. By direct calculation, we have $4d_{11}d_{22} - (\omega^*)^2(m_{11} - m_{22})^2 \geq 0$, which implies that $c \leq 2\sqrt{d_{11}d_{22}}d_{33}/(m_{22} - m_{11}) = 20.25$. That is, with the steady-state input $u^* = [0, c]^\top$ with $c \leq 20.25$, the system is shifted passive.

In the first example, we select the control parameters in (5.34)-(5.35) to be $c = 1$, $k = 1$. The simulation results are shown in Fig. 5.5 for $\varepsilon = 0.1$ and $\varepsilon = 0.05$. In the second example, we increase the constant torque to $c = 3$. The simulation results of the second example are shown in Fig. 5.6 for $\varepsilon = 0.1$ and $\varepsilon = 0.02$. It can be seen from both examples that the position trajectory of the underactuated boat converges to the $O(\varepsilon)$ -neighborhood of the desired position $(x^*, y^*) = (2, 3)$. Furthermore, as $\varepsilon \rightarrow 0$, the trajectories of the boat converge to the trajectory of the symmetric product system which represents the ideal solution. In general, a smaller ε leads to a smoother trajectory. The only limitation on the value of ε is the value of the control input (5.34) which increases as ε decreases.

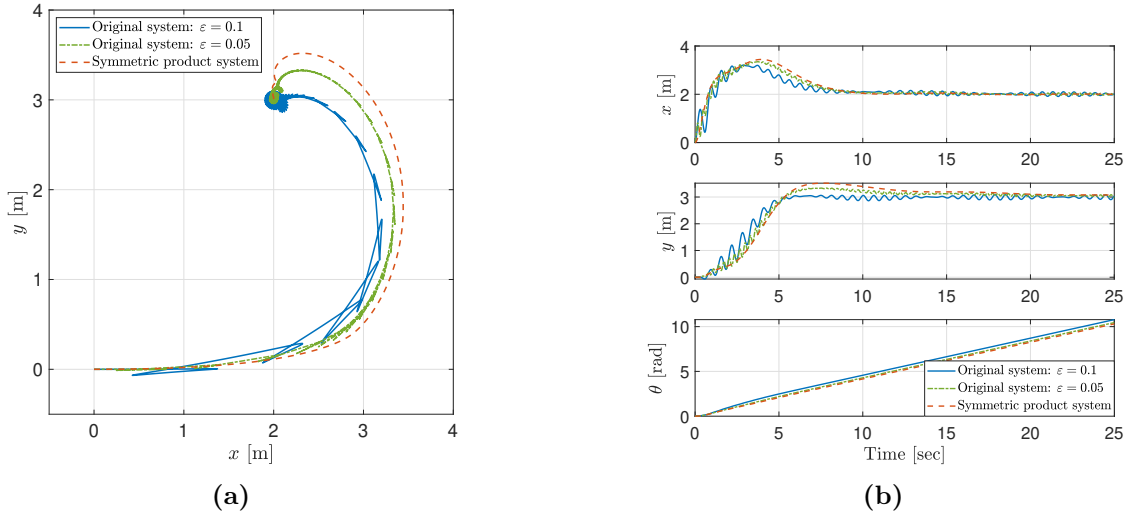


Figure 5.5: Paths and configuration trajectories of the underactuated boat in source seeking ($c = 1$).

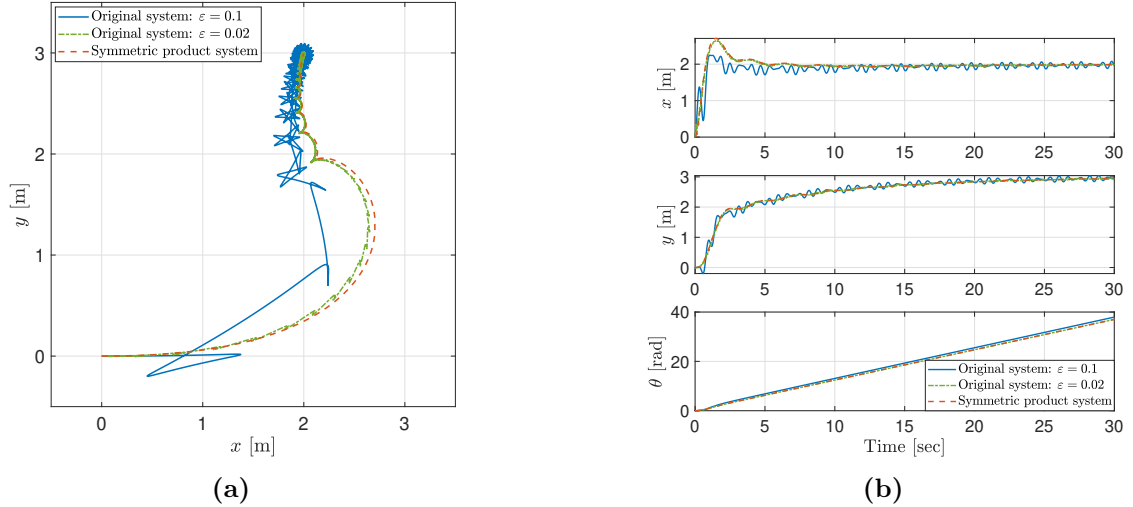


Figure 5.6: Paths and configuration trajectories of the underactuated boat in source seeking ($c = 3$).

5.6 Experimental Results

To illustrate the algorithm's practicality and performance in the real world, experiments were performed with a small boat in the laboratory environment. The boat components include electronic speed control motors and propellers, a Raspberry Pi 3, a PWM driver, and a 3000 mAh lithium polymer battery. The boat operates in a pool equipped with the Vicon motion capture system, as shown in Fig. 5.7. The Vicon camera system captures infrared LED balls located on the boat and provides relative distance between the feature point (source) and the boat to the control software implemented in MATLAB/Simulink. The control signals are

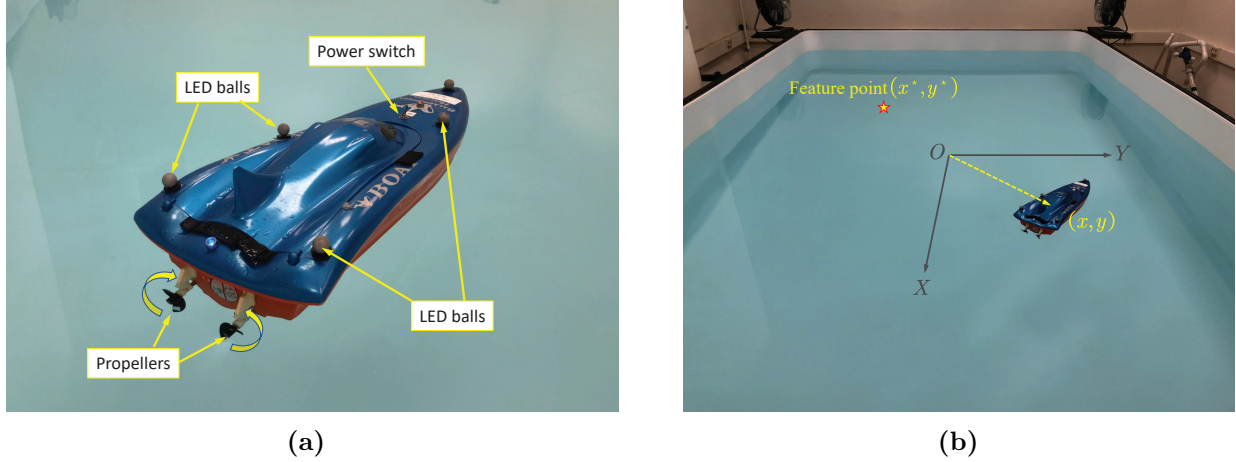


Figure 5.7: The experimental boat in the water tank.

sent to the Raspberry Pi via a Wi-Fi router.

In the experiments, we put the feature point at the position $(x^*, y^*) = (-0.5, -0.5)$ m and the boat starts from rest. In the first case, we selected the control parameters as $c = 2.2 \times 10^{-3}$, $\varepsilon = 0.5$, and $k = 0.08$. Figure 5.8 shows the boat's path and pose time history and demonstrates that the boat successfully finds the source. Figure 5.8c shows the boat's velocity and surge force time history. In the second case, we increased the torque and frequency by letting $c = 5.5 \times 10^{-3}$ and $\varepsilon = 0.2$, and kept $k = 0.08$. Figure 5.9 shows that the boat speeds up and goes through a higher frequency motion. As a result, the control effort is much higher to travel a larger distance without any improvement in convergence speed. Figure 5.9c shows the boat's velocity and surge force time history in the second case. In the third case, we kept the higher torque value $c = 5.5 \times 10^{-3}$ but increased $\varepsilon = 1$ and $k = 0.33$. It can be seen from Fig. 5.10 that increasing the gain k may improve convergence speed, but on the other hand, the path becomes less predictable. Figure 5.10c shows the boat's velocity and surge force time history in the third case. It can be observed from Figs. 5.8c, 5.9c, and 5.10c that the boat was driven by surge force that fluctuates around zero. However, the surge velocity does not necessarily fluctuate around zero because the backward motion of the boat has a larger damping force compared with the forward motion.

5.7 Conclusions

The ES design for force-controlled underactuated mechanical systems without position or velocity measurements was previously an open problem. In this work, we developed a source seeking scheme for generic force-controlled planar underactuated vehicles by surge force tun-

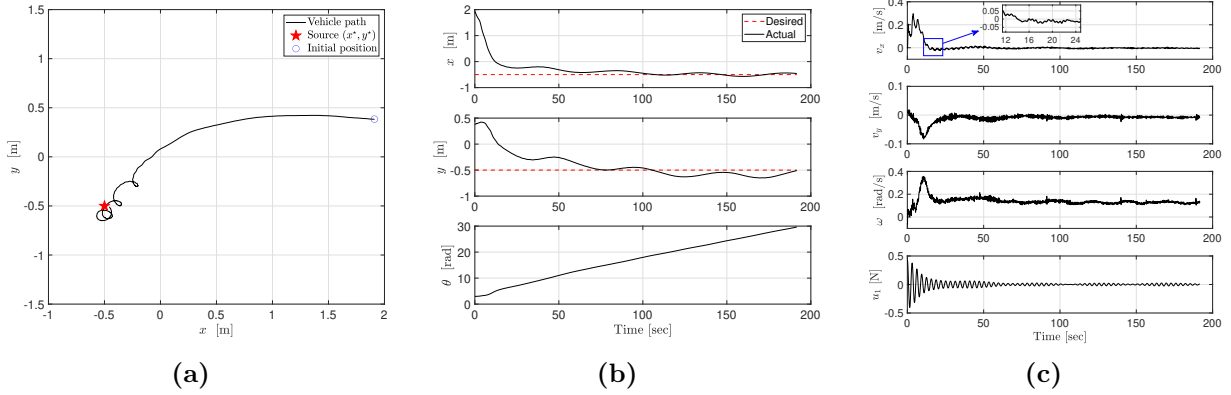


Figure 5.8: Experimental path, configuration, velocity trajectories and the surge force of the underactuated boat in source seeking (Case 1: $c = 2.2 \times 10^{-3}$, $\varepsilon = 0.5$, $k = 0.08$).

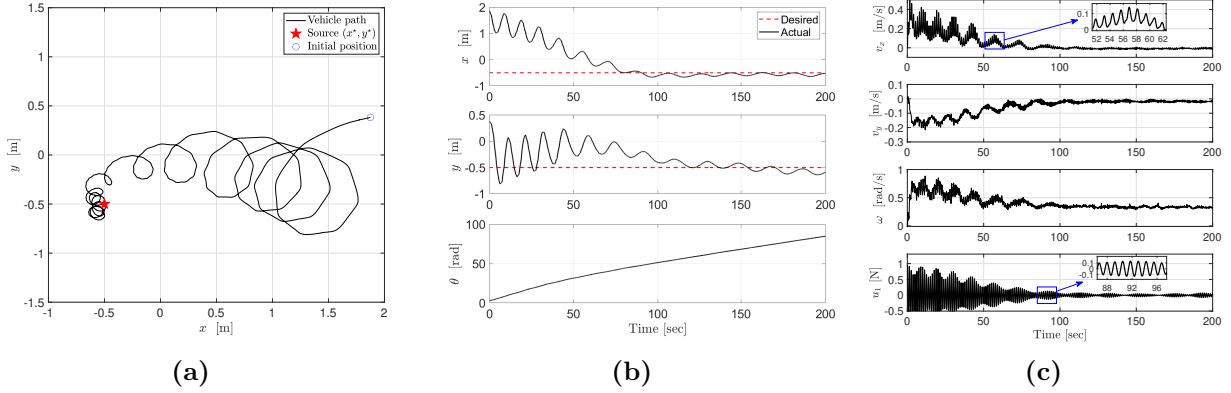


Figure 5.9: Experimental path, configuration, velocity trajectories and the surge force of the underactuated boat in source seeking (Case 2: $c = 5.5 \times 10^{-3}$, $\varepsilon = 0.2$, $k = 0.08$).

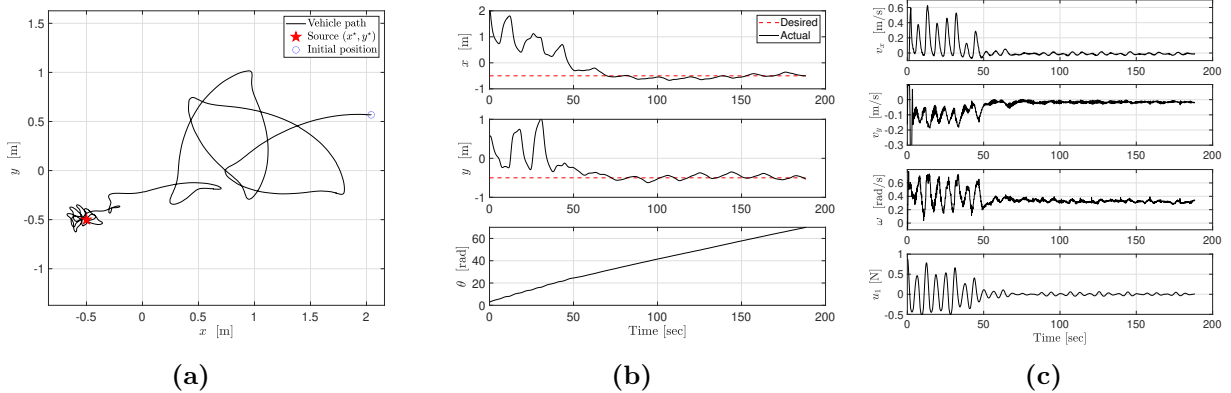


Figure 5.10: Experimental path, configuration, velocity trajectories and the surge force of the underactuated boat in source seeking (Case 3: $c = 5.5 \times 10^{-3}$, $\varepsilon = 1$, $k = 0.33$).

ing. The control design is based on symmetric product approximations, averaging, passivity, and partial-state stability theory. The controller does not require any position or velocity measurements but only real-time measurements of the source signal at the current position. The P-SPUAS is proven for the closed-loop source seeking system. Both numerical simulations and experimental results of an underactuated boat are presented to illustrate the performance of the proposed source seeker. It should be noted that the proposed source seeking algorithm guarantees only practical asymptotic convergence. The convergence rate is neither chosen by the user nor given by the analysis. In order to determine the settling time, finite-time or prescribed-time design may be considered in the future.

The averaging technique of symmetric product approximation extends the earlier results of classical averaging and Lie bracket averaging and is the basis of vibrational control for mechanical systems. Recently, symmetric product approximation has been applied to the extremum seeking problems for acceleration-controlled unicycles [120] and fully-actuated mechanical systems [127]. This chapter is devoted to an in-depth study and extends the results in [127] to a class of *underactuated* mechanical systems. Other concrete open questions include:

- 1) Design of symmetric product approximation-based source seeking algorithms for planar underactuated vehicles using angular torque tuning.
- 2) Extension of the asymptotic convergence results of the symmetric product approximation-based extremum seeking to finite-time and/or prescribed-time convergence.
- 3) Extension of the periodic averaging to stochastic averaging for the symmetric product approximation-based extremum seeking algorithms.
- 4) Generalization of the results in this chapter to more generic vehicle models including quadcopters, underactuated underwater vehicles, etc. for 3D source seeking.

Chapter 6

Range Observer-Based Formation Control for Spatial Underactuated Vehicle Networks

6.1 Introduction

An important theme in multi-agent control systems is *decentralization*, namely, *distributed algorithms* where each agent senses the *relative* configuration variables of its neighbors with respect to its *local* coordinate system [5]. In other words, distributed control schemes do not require a global coordinator where measurements are performed by onboard sensors and are significantly more scalable and robust compared to the centralized ones, which is extremely useful in the Global Positioning System (GPS)-denied environments. For these controllers, cameras and inertial measurement units (IMUs) are usually the preferred onboard sensors compared to LiDARs due to lower weight and cost. These sensors can measure bearing angles, postures, velocities, and accelerations, while the range between vehicles cannot be directly measured by these sensors. Hence, the range or relative position must be estimated. Another requirement for distributed cooperative control of multi-agent systems is communication [66]. Switching communication topologies and communication delays are common in a communication network, and thus, they should be considered when designing a controller.

In this chapter, we focus on the distributed formation control problem for heterogeneous networks of *spatial* underactuated vehicles with two degrees of underactuation. The main contributions of this chapter are summarized as follows:

- 1) We solve the distributed formation control problem for a class of *heterogeneous* spatial underactuated vehicle networks with a directed communication graph. We consider a generic spatial vehicle model with two degrees of underactuation, which includes underwater and aerial vehicles with one translational actuator and three rotational actuators, without any simplification. For each vehicle, the dynamics are decoupled into two parts: the attitude

control subsystem and the position control subsystem. Based on the cascaded structure, the formation controller considers the nonlinearity and heterogeneity of the systems and guarantees the global asymptotic convergence for the closed-loop system state.

- 2) The proposed formation control protocol works even when the vehicle network is subject to *switching topologies*. It is shown that switching topologies do not matter if the communication graph contains a directed spanning tree. Furthermore, the proposed control law is *robust to communication delays*. To be precise, we present a generalized Slotine-Li controller for distributed consensus of arbitrary order multi-agent systems. First, a reference velocity trajectory that contains the position error information is defined such that, if the velocity converges to the reference velocity, the position error will also converge to zero. Next, a controller is designed to stabilize the (reduced-order) velocity error system. The reference velocity trajectory in this work is defined by integration. As a result, the reference velocity trajectory is always continuous due to the integral action even under switching topologies. Based on the generalized Slotine-Li transformation, the control design is reduced to stabilize an integrator chain.
- 3) Instead of requiring the relative positions, the proposed control protocol requires the *bearing angle information* of the neighbor vehicles. Using the distributed sliding mode observers, the ranges between the vehicle and its neighbors are estimated in finite time based on the bearing, attitude, and local velocity measurements. It should be emphasized that the bearing angles of the neighbors can be easily measured by onboard monocular cameras, which are much cheaper and lighter than LiDARs. Furthermore, the proposed distributed control law requires only neighbor-to-neighbor information exchange, and all the measurements are performed by onboard sensors. The controller also has a simple structure, and thus, is practical and easy to implement.

Compared with existing results in the literature and in contrast to existing controllers in [61, 78, 91, 136], which are applicable only to *homogeneous* quadcopter networks, the approach proposed in this article can be applied to *heterogeneous* spatial underactuated vehicle networks. In contrast to the existing methods in [81–84], the approach proposed in this article does not simplify the model and considers the full nonlinear vehicle dynamics. In contrast to the existing methods in [58, 121, 137, 138], the proposed approach is robust to *switching topologies* and *communication delays*. In contrast to the traditional bearing-based formation methods in [139–141], where the target formation is required to be *rigid* and the group leaders are required to move at a common *constant* velocity, the approach proposed in this article only requires the existence of *directed spanning tree* topology.

6.2 Range Observer Design

In this section, we present a distributed finite-time sliding mode observer for range estimation among spatial vehicles based on the relative bearing, attitude, and local velocity measurements in the formation. Observer design for the range estimation problem between a spatial robot and a *static* feature point is presented in [142, 143]. Compared to the observers presented in [143], the sliding mode observer proposed in this work can be applied to moving objects, avoids open-loop integration, and guarantees finite-time estimation.

We consider a pair of agents (\mathbf{i}, \mathbf{j}) , where agent \mathbf{j} is the leader and agent \mathbf{i} is the follower, as shown in Figure 6.1. In the body-fixed frame $\{\mathcal{B}_i\}$, the relative position vector of agent \mathbf{j} is denoted by

$$\zeta_{ij} = R(\eta_i)^\top (\xi_j - \xi_i). \quad (6.1)$$

We assume that the measurable signal is the bearing angle of vehicle \mathbf{j} in the body-fixed frame $\{\mathcal{B}_i\}$. In other words, we measure the projection of ζ_{ij} on the unit sphere centered at the origin of $\{\mathcal{B}_i\}$, i.e.,

$$\sigma_{ij} = \frac{\zeta_{ij}}{|\zeta_{ij}|} \in \mathbb{S}^2. \quad (6.2)$$

The bearing angle σ_{ij} is well defined for all $|\zeta_{ij}| \neq 0$. The problem is to estimate the range $r_{ij} = |\zeta_{ij}|$ based on the bearing angle σ_{ij} , the attitude, and the velocity measurements.

To start with, we write the error dynamics in the body-fixed frame $\{\mathcal{B}_i\}$. Note that

$$\dot{|\zeta_{ij}|^2} = 2|\zeta_{ij}| \dot{|\zeta_{ij}|} = \dot{\zeta_{ij}^\top \zeta_{ij}} = 2\zeta_{ij}^\top \dot{\zeta_{ij}} = 2r_{ij}\dot{r}_{ij}, \quad (6.3)$$

and $\dot{r}_{ij} = \sigma_{ij}^\top \dot{\zeta_{ij}}$. Taking time derivative of (6.1), and substituting (2.7), we obtain

$$\dot{r}_{ij} = \sigma_{ij}^\top [R(\eta_i)^\top R(\eta_j)v_j - v_i] = \sigma_{ij}^\top w_{ij}, \quad (6.4)$$

where $w_{ij} = R(\eta_i)^\top R(\eta_j)v_j - v_i$, and we used the fact that the matrix $(\omega_i)_\times$ is skew-symmetric. Taking time derivative of (6.2), we have

$$\dot{\sigma}_{ij} = -(\omega_i)_\times \sigma_{ij} + \frac{1}{r_{ij}} (I_3 - \sigma_{ij}\sigma_{ij}^\top) w_{ij}. \quad (6.5)$$

Multiplying by r_{ij} and applying the stable filter $\alpha/(s + \alpha)$ with $\alpha > 0$ to both sides of (6.5) yields

$$\frac{\alpha}{s + \alpha} [r_{ij} \dot{\sigma}_{ij}] = \frac{\alpha}{s + \alpha} [-r_{ij}(\omega_i)_\times \sigma_{ij}] + \frac{\alpha}{s + \alpha} [(I_3 - \sigma_{ij}\sigma_{ij}^\top) w_{ij}]. \quad (6.6)$$

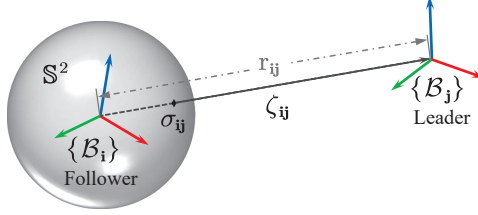


Figure 6.1: Illustration of the bearing and the range of leader \mathbf{j} with respect to follower \mathbf{i} .

Applying Lemma A.3, the left-hand side of (6.6) becomes

$$\alpha G_2[r_{ij}\dot{\sigma}_{ij}] = r_{ij}G_1[\sigma_{ij}] - G_2[\sigma_{ij}^\top w_{ij}G_1[\sigma_{ij}]]. \quad (6.7)$$

where $G_1(s) = \alpha s/(s + \alpha)$ and $G_2(s) = 1/(s + \alpha)$. Substituting (6.7) into (6.6) and applying Lemma A.3 again, we obtain

$$r_{ij}\Phi_{ij} = G_2[\sigma_{ij}^\top w_{ij}\Phi_{ij}] + \alpha G_2[(I_3 - \sigma_{ij}\sigma_{ij}^\top)w_{ij}], \quad (6.8)$$

where $\Phi_{ij} = G_1[\sigma_{ij}] + \alpha G_2[(\omega_i) \times \sigma_{ij}]$ is a continuous measurable signal.

Proposition 6.1. Consider the dynamics (6.4)-(6.5) with input w_{ij} . The sliding mode observer

$$\hat{r}_{ij} = \sigma_{ij}^\top w_{ij} - \gamma \operatorname{sign}\{\Phi_{ij}^\top (\Phi_{ij}\hat{r}_{ij} - G_2[\sigma_{ij}^\top w_{ij}\Phi_{ij}] - \alpha G_2[(I_3 - \sigma_{ij}\sigma_{ij}^\top)w_{ij}])\} \quad (6.9)$$

$$\hat{\zeta}_{ij} = \sigma_{ij}\hat{r}_{ij} \quad (6.10)$$

with $\gamma > 0$ provides a globally finite-time convergent estimate to the relative position error ζ_{ij} , i.e., there exists $T_r > 0$ such that $\hat{\zeta}_{ij}(t) = \zeta_{ij}(t)$ for all $t \geq T_r$, if the signal Φ_{ij}^\top is persistently exciting (PE), i.e., there exist $\mu, T > 0$ such that

$$\int_t^{t+T} \Phi_{ij}(s)^\top \Phi_{ij}(s) \geq \mu, \quad \forall t \geq 0. \quad (6.11)$$

Proof. Define the estimation error $\tilde{r}_{ij} = \hat{r}_{ij} - r_{ij}$. Substituting (6.8) into (6.9), the observation error dynamics are given by

$$\dot{\tilde{r}}_{ij} = -\gamma \operatorname{sign}(\Phi_{ij}^\top \Phi_{ij}) \operatorname{sign}(\tilde{r}_{ij}). \quad (6.12)$$

Consider the Lyapunov candidate $V(\tilde{r}_{ij}) = |\tilde{r}_{ij}|$, where its derivative is calculated as

$$\dot{V} = \begin{cases} -\gamma \operatorname{sign}(\Phi_{ij}^\top \Phi_{ij}) & , \quad \tilde{r}_{ij} \neq 0 \\ 0 & , \quad \tilde{r}_{ij} = 0. \end{cases} \quad (6.13)$$

It should be noted that the function V is continuous, and (6.13) implies that the time derivative of V along trajectories is non-increasing. For each $\tilde{r}_{ij}(0) \neq 0$, we have, along trajectories, $\dot{V}(\tilde{r}_{ij}(t)) = -\gamma$, if $\Phi_{ij}(t)^\top \Phi_{ij}(t) > 0$, and $\dot{V}(\tilde{r}_{ij}(t)) = 0$, if $\Phi_{ij}(t)^\top \Phi_{ij}(t) = 0$. Due to the PE condition (6.11) and the continuity of $\Phi_{ij}(t)$, for each time interval $[t, t+T]$, the measure of the set $\{s \in [t, t+T] : \Phi_{ij}(s)^\top \Phi_{ij}(s) \geq \mu/T\}$ must be (strictly) larger than zero. Define $l_{[a,b]}$ as the measure of the set $\{s \in [a, b] : \Phi_{ij}(s)^\top \Phi_{ij}(s) > 0\}$. We have, for all $t \geq 0$,

$$l_{[t,t+T]} = \operatorname{meas}\{s \in [t, t+T] : \Phi_{ij}(s)^\top \Phi_{ij}(s) > 0\} > \operatorname{meas}\{s \in [t, t+T] : \Phi_{ij}(s)^\top \Phi_{ij}(s) \geq \mu/T\} > 0. \quad (6.14)$$

Integrating both sides of (6.13) along trajectories yields $V(\tilde{r}_{ij}(t)) = V(\tilde{r}_{ij}(0)) - \gamma l_{[0,t]} t$. Therefore, for each $\tilde{r}_{ij}(0) \neq 0$, there exists $T_r = V(\tilde{r}_{ij}(0))/(\gamma l_{[0,t]})$ such that $V(\tilde{r}_{ij}(T_r)) = 0$, which proves the global and finite-time convergence. \square

Remark 6.1. Although we require the excitation condition (6.11) to hold for all $t \geq 0$, it follows from the proof of Proposition 6.1 that, to guarantee the finite-time convergence, the excitation condition is only needed to hold on the time interval $[0, T_r]$. The difference is that the PE condition (6.11) guarantees not only the finite-time convergence but also the *stability* for the error system (6.12). In fact, the function $V(\tilde{r}_{ij})$ is a weak Lyapunov function because $\dot{V} \leq 0$, which shows that the system (6.12) is *globally bounded* and *locally Lyapunov stable*. Together with the PE condition (6.11), which guarantees the *global finite-time convergence*, we conclude that the system has global finite-time stability. In practical applications, to guarantee finite-time *convergence*, only the finite-time excitation condition is required, which is called the interval excitation (IE) condition. Given the initial estimation error $\tilde{r}_{ij}(0)$, the time T_r can be estimated *a priori*. Due to the finite-time convergence, users can implement the excitation condition in advance, and then, apply the control laws after T_r to avoid the transient.

6.3 Formation Control Development

6.3.1 Generalized Slotine-Li Controller

As shown in Remark 2.2, the control objective is to design the virtual control law ν_i and input $\tilde{\tau}_i$ for double-integrator dynamics to achieve the formation. It should be pointed out that

the extension of consensus tracking algorithms from single-integrator dynamics to higher-order dynamics is nontrivial. Lemma A.2 shows that switching topologies do *not* matter for single-integrator systems when the graph contains a spanning tree. However, for higher-order systems, the situation is radically different. For example, even under the time-invariant topology case, the controller parameters need to be selected carefully to achieve the consensus for double-integrator dynamics [2]. Under switching topology, the analysis becomes more complicated. In this section, we present the generalized Slotine-Li control strategy for *arbitrary order integrator dynamics* to solve the consensus tracking problem subject to switching topologies. The main idea of the generalized Slotine-Li control strategy is to convert the consensus tracking problem for a higher-order system into consensus tracking for single-integrator dynamics.

In [144], an adaptive scheme (a.k.a. Slotine-Li controller) was proposed for trajectory tracking control of fully-actuated EL systems with unknown parameters. The main idea of the Slotine-Li controller is to introduce a virtual "reference velocity", and then, PD feedback is employed to steer the velocity variable to the "reference velocity". For illustration, consider the double-integrator dynamics $\ddot{x} = u$. The objective is to design a feedback u such that $x(t)$ tracks the desired trajectory $x_d(t)$. To this end, define the reference velocity $z = \dot{x}_d - (x - x_d)$ and the "sliding variable" $s = \dot{x} - z$. It is clear that if $s(t) \rightarrow 0$ as $t \rightarrow \infty$ (i.e., the velocity $\dot{x}(t)$ converges to the reference velocity $z(t)$), then the position error $x(t) - x_d(t)$ also converges to zero. That is, the tracking control problem for the second-order system is reduced to the stabilization problem of a first-order system, i.e., $\dot{s} = u - \dot{z}$. This objective can be achieved by simply choosing the control $u = \dot{z} - ks$ with $k > 0$.

The Slotine-Li controller also can be used to solve the consensus tracking problem for multi-agent systems. Consider N double-integrator systems, i.e., $\ddot{x}_i = u_i$ with $x_i \in \mathbb{R}^n$, $i = 1, \dots, N$. Define the reference velocity, the sliding variable, and the control input as

$$\begin{cases} z_i = \frac{1}{\sum_{j \in \mathcal{N}_i} a_{ij}} \sum_{j \in \mathcal{N}_i} a_{ij} [\dot{x}_j - (x_i - x_j)], \\ s_i = \dot{x}_i - z_i, \\ u_i = \dot{z}_i - k_i s_i, \end{cases} \quad (6.15)$$

where a_{ij} and \mathcal{N}_i are defined in Chapter 2; $k_i > 0$ is a constant control gain. Noting that the control law $u_i = \dot{z}_i - k_i s_i$ guarantees that $s_i(t) \rightarrow 0$ exponentially, and on the sliding manifold

$\{s_i \equiv 0\}$, the closed-loop dynamics are given by

$$\dot{x}_i = \frac{1}{\sum_{j \in \mathcal{N}_i} a_{ij}} \sum_{j \in \mathcal{N}_i} a_{ij} [\dot{x}_j - (x_i - x_j)]. \quad (6.16)$$

The first-order dynamics (6.16) are exactly the same as (A.26), and thus, it follows from Lemma A.2 that the consensus tracking problem is solved if the communication topology contains a directed spanning tree. In summary, the closed-loop system on the sliding manifold $\{s_i \equiv 0\}$ recovers the classical single-integrator consensus tracking algorithm.

The algorithm (6.15) works well when the communication topology is fixed. However, it has a fatal flaw when the topology is dynamically changing. For instance, under switching topologies, $a_{ij}(t)$ and the reference velocity $z_i(t)$ are no longer continuous. Thus, the control law $u_i = \dot{z}_i - k_i s_i$ cannot be implemented because it involves the time derivative of a discontinuous term. To solve this problem, instead of defining the reference velocity $z_i(t)$ as in (6.15), we define $z_i(t)$ by integration. Consider the following algorithm

$$\begin{cases} \dot{z}_i = \frac{1}{\Xi_i(t)} \sum_{j \in \mathcal{N}_i(t)} a_{ij}(t) [\ddot{x}_j - (\alpha + 1)(\dot{x}_i - \dot{x}_j) - \alpha(x_i - x_j)], \\ s_i = \dot{x}_i - z_i, \\ u_i = \dot{z}_i - k_i s_i, \end{cases} \quad (6.17)$$

where $\alpha > 0$ is a control gain, and $\Xi_i(t)$ is defined in (A.26). It should be pointed out that the reference velocity $z_i(t)$ is differentiable due to the integration action, and thus, the control law $u_i = \dot{z}_i - k_i s_i$ is well defined. The control law $u_i = \dot{z}_i - k_i s_i$ ensures that $s_i(t) \rightarrow 0$ (and $\dot{s}_i(t) \rightarrow 0$) exponentially. Consider the closed-loop dynamics on the manifold $\{\dot{s}_i \equiv 0\}$, which are given by

$$(\ddot{x}_i + \alpha \dot{x}_i) = \frac{1}{\Xi_i(t)} \sum_{j \in \mathcal{N}_i(t)} a_{ij}(t) \{(\ddot{x}_j + \alpha \dot{x}_j) - [(\dot{x}_i + \alpha x_i) - (\dot{x}_j + \alpha x_j)]\}. \quad (6.18)$$

Note that the system (6.18) has the same structure as (A.26). It follows from Lemma A.2 that $(\dot{x}_i + \alpha x_i) - (\dot{x}_j + \alpha x_j) \rightarrow 0$ as $t \rightarrow +\infty$, for all $i, j \in \mathcal{V}$. Therefore, we have

$$(\dot{x}_i - \dot{x}_j) = -\alpha(x_i - x_j) + \epsilon_t, \quad \forall i, j \in \mathcal{V}, \quad (6.19)$$

where $\epsilon_t \rightarrow 0$. It follows from the converging-input converging-state property of stable linear systems that $(x_i - x_j) \rightarrow 0$ as $t \rightarrow \infty$ [92], and thus, the consensus tracking problem is solved. It should be noted that, if the communication topology is fixed, i.e., $a_{ij}(t) \equiv a_{ij}$ for all $i, j \in \mathcal{V}$,

then the control law (6.17) reduces to the Slotine-Li controller (6.15) when $\alpha = 0$.

This idea can be generalized to the m -th order integrator-chain model. The generalized Slotine-Li controller is given by

$$\left\{ \begin{array}{l} z_i^{(m-1)} = \frac{1}{\Xi_i(t)} \sum_{j \in \mathcal{N}_i(t)} a_{ij}(t) \left[x_j^{(m)} - (1 + \alpha_{m-1}) (x_i^{(m-1)} - x_j^{(m-1)}) \right. \\ \quad \left. - (\alpha_{m-1} + \alpha_{m-2}) (x_i^{(m-2)} - x_j^{(m-2)}) - \dots \right. \\ \quad \left. \dots - (\alpha_2 + \alpha_1) (\dot{x}_i - \dot{x}_j) - \alpha_1 (x_i - x_j) \right], \\ s_i = \dot{x}_i - z_i, \\ u_i = z_i^{(m-1)} - k_{1i}s_i - \dots - k_{(m-1)i}s_i^{(m-2)}, \end{array} \right. \quad (6.20)$$

where the parameters $\alpha_1, \dots, \alpha_{m-1}$ are chosen such that the matrix $A(\alpha_1, \dots, \alpha_{m-1})$ is Hurwitz, $k_{1i}, \dots, k_{(m-1)i}$ are chosen such that the matrix $A(k_{1i}, \dots, k_{(m-1)i})$ is Hurwitz, and the matrix $A(\cdot)$ is defined as

$$A(k_1, \dots, k_{m-1}) = \begin{bmatrix} 0 & 1 & 0 & \cdots & 0 \\ 0 & 0 & 1 & \cdots & 0 \\ \vdots & \vdots & \vdots & \ddots & \vdots \\ 0 & 0 & 0 & \cdots & 1 \\ -k_1 & -k_2 & -k_3 & \cdots & -k_{m-1} \end{bmatrix} \in \mathbb{R}^{(m-1) \times (m-1)}. \quad (6.21)$$

Theorem 6.1. Consider the m -th order integrator-chain model $x_i^{(m)} = u_i$, where $x_i \in \mathbb{R}^n$, $i = 1, \dots, N$, and $m, n, N \in \mathbb{Z}_{>0}$. Then, under the generalized Slotine-Li controller (6.20), the consensus tracking problem is solved provided that Assumption 2.1 holds.

Proof. Noting that the reference velocity $z_i(t)$ is differentiable up to $(m-1)$ -th order, we have

$$s_i^{(m-1)} = x_i^{(m)} - z_i^{(m-1)}. \quad (6.22)$$

Substituting $x_i^{(m)} = u_i$ into (6.22) yields $s_i^{(m-1)} = -k_{1i}s_i - \dots - k_{(m-1)i}s_i^{(m-2)}$. The condition $A(k_{1i}, \dots, k_{(m-1)i})$ being Hurwitz implies that $(s_i, \dot{s}_i, \dots, s_i^{(m-1)})(t) \rightarrow 0$ exponentially as $t \rightarrow +\infty$. On the other hand, substituting $z_i^{(m-1)}$ into (6.22), and denoting $q_i = x_i^{(m-1)} + \alpha_{(m-1)}x_i^{(m-2)} + \dots + \alpha_2\dot{x}_i + \alpha_1x_i$, we recover the first-order consensus algorithm

$$\dot{q}_i = \frac{1}{\Xi_i(t)} \sum_{j \in \mathcal{N}_i(t)} a_{ij}(t) [\dot{q}_j - (q_i - q_j)] + s_i^{(m-1)}(t), \quad (6.23)$$

which can be viewed as an exponentially stable linear system (with respect to the equilibrium manifold $\{(x_1, \dots, x_N) : x_i = x_j, \forall i, j \in \mathcal{V}\}$) [2, 145] with an exponentially decaying input $s_i^{(m-1)}(t)$. It follows from Lemma A.2 and the converging-input converging-state property for stable linear systems that the exponential consensus is achieved for variable q_i [92]. That is, $|q_i(t) - q_j(t)| \rightarrow 0$ exponentially as $t \rightarrow +\infty$, for all $i, j \in \mathcal{V}$. Finally, it follows from the condition $A(\alpha_1, \dots, \alpha_{m-1})$ being Hurwitz that $|x_i(t) - x_j(t)| \rightarrow 0$ exponentially as $t \rightarrow +\infty$, for all $i, j \in \mathcal{V}$, where the consensus tracking problem is solved under switching topologies. \square

Remark 6.2. Lemma A.2 shows that switching topologies do not matter for single-integrator systems when the graph contains a spanning tree. However, as shown in [2], the consensus tracking problem for double-integrator systems, let alone the m -th order integrator-chain, is far more complicated than single integrator systems, especially considering *directed* switching topologies [67, 145]. The generalized Slotine-Li controller proposed in this section solves the consensus tracking problem under switching topologies for *arbitrary order* integrator-chain dynamics by reducing the closed-loop dynamics into the form of the first-order consensus system (6.23), and thus, switching topologies do not matter when the graph contains a spanning tree. It should be pointed out that $z_i^{(m-1)}$ in (6.20) is derived from the linear consensus algorithm (A.26). It also can be generalized to other nonlinear forms by considering different first-order nonlinear consensus algorithms such as finite-time consensus protocol [69], bounded control input consensus algorithm [2, Sec. 3.3.2], etc. The control law u_i in (6.20) can also be generalized to other nonlinear forms. For example, the first-order sliding mode control law $u_i = \dot{z}_i - k_i \text{sign}(s_i)$ guarantees $s_i(t) \rightarrow 0$ in finite time and is robust to bounded matched disturbances; or adaptive neural network control law can be used to compensate unknown dynamics.

Remark 6.3. Another advantage of the first-order linear consensus algorithm (6.23) is, as shown in [3] (Thm. 10.8), that under communication delays, for all $i, j \in \mathcal{V}$, $|q_i(t) - q_j(t)|$ is uniformly ultimately bounded (UUB) no matter how large the communication delay is if the graph contains a spanning tree. Thus, a direct corollary from the proof of Theorem 6.1 is that, under communication delays, $|q_i(t) - q_j(t)|$ is UUB, and thus, $|x_i(t) - x_j(t)|$ is also UUB. That is, for the m -th order integrator-chain network, the generalized Slotine-Li algorithm (6.20) is robust to communication delays.

Remark 6.4. As shown in Theorem 6.1, the generalized Slotine-Li control strategy is applicable to m -th order integrator-chain model. It is well-known that, under full-state measurements, all fully-actuated systems can be feedback linearized into double-integrator dynamics, and then, the generalized Slotine-Li control strategy can be applied directly. However, it is

impossible to use preliminary feedback to convert an *underactuated* system into the double-integrator dynamics. So the generalized Slotine-Li strategy may only be applied to a part of the system dynamics. For some underactuated systems with nonholonomic constraints, such as mobile robots and surface vessels, stabilization *cannot* be achieved by using continuous time-invariant state-feedback due to the violation of Brockett's necessary condition. As a result, the generalized Slotine-Li strategy, which is essentially a continuous time-invariant state-feedback, may not be applicable to such systems.

6.3.2 Formation Control Design

We apply the proposed finite-time sliding mode observer, attitude resolution, and the generalized Slotine-Li design to the formation control problem for heterogeneous spatial underactuated vehicle networks.

Position control design. Consider the position dynamics (2.18) and the finite-time sliding mode observer (6.9)-(6.10). We propose the following observer-based generalized Slotine-Li control law for ν_i

$$\begin{cases} \dot{\mathbf{z}}_{1i} = \frac{1}{\Xi_i(t)} \sum_{j \in \mathcal{N}_i(t)} a_{ij}(t) \left[\ddot{\xi}_j - (\alpha_1 + 1)(\dot{\xi}_i - \dot{\xi}_j) + \alpha_1 \left(R(\eta_i) \hat{\zeta}_{ij} + d_{ij} \right) \right], \\ s_{1i} = \dot{\xi}_i - \dot{\mathbf{z}}_{1i}, \\ \nu_i = \dot{\mathbf{z}}_{1i} - k_{1i}s_{1i}, \end{cases} \quad (6.24)$$

where $\alpha_1, k_{1i} > 0$ are the control gains and $\hat{\zeta}_{ij}(t)$ is the output of the sliding mode observer (6.9)-(6.10).

Attitude control design. Consider the attitude subsystem (2.12). It is clear that the attitude dynamics are decoupled and controlled by three independent control inputs, i.e., $\tilde{\tau}_i = [\tilde{\tau}_{\phi i}, \tilde{\tau}_{\theta i}, \tilde{\tau}_{\psi i}]^\top$. For the three cases discussed in Section 4.1, we apply the generalized Slotine-Li control law to the independently controlled attitude variable. Specifically, for **Case 1**, ϕ_i is independently controlled, and we propose

$$\begin{cases} \dot{\mathbf{z}}_{2i} = \frac{1}{\Xi_i(t)} \sum_{j \in \mathcal{N}_i(t)} a_{ij}(t) \left[\ddot{\phi}_j - (\alpha_2 + 1)(\dot{\phi}_i - \dot{\phi}_j) - \alpha_2 (\phi_i - \phi_j) \right], \\ s_{2i} = \dot{\phi}_i - \dot{\mathbf{z}}_{2i}, \\ \tilde{\tau}_{\phi i} = \dot{\mathbf{z}}_{2i} - k_{2i}s_{2i}, \end{cases} \quad (6.25)$$

where $\alpha_2, k_{2i} > 0$ are the control gains. Then, the thrust $u_i(t)$ and the other two desired attitude signals $(\theta_{id}(t), \psi_{id}(t))$ are given by (2.19)-(2.21). Given the desired trajectories

$(\theta_{id}(t), \psi_{id}(t))$, the trajectory tracking control design is trivial for double-integrator (θ_i, ψ_i) -subsystems. Here, we choose the sliding mode control because of its simplicity and robustness

$$\tilde{\tau}_{\theta i} = -\lambda_1 \dot{\tilde{\theta}}_i - k_{3i} \text{sign}(s_{3i}), \quad s_{3i} = \dot{\tilde{\theta}}_i + \lambda_1 \tilde{\theta}_i, \quad (6.26)$$

$$\tilde{\tau}_{\psi i} = -\lambda_2 \dot{\tilde{\psi}}_i - k_{4i} \text{sign}(s_{4i}), \quad s_{4i} = \dot{\tilde{\psi}}_i + \lambda_2 \tilde{\psi}_i, \quad (6.27)$$

where $\tilde{\theta}_i = \theta_i - \theta_{id}$; $\tilde{\psi}_i = \psi_i - \psi_{id}$; and $\lambda_1 > 0$, $\lambda_2 > 0$, $k_{3i} > \sup\{|\ddot{\theta}_{id}(t)|\}$, and $k_{4i} > \sup\{|\ddot{\psi}_{id}(t)|\}$ are control gains. It should be pointed out that other control strategies such as linear PD+ controller or higher-order sliding mode controller also can be used to solve the trajectory tracking control problem. For **Case 2** and **Case 3**, replace the independently controlled attitude variable ϕ in (6.25) by θ and ψ , respectively; generate thrust and desired attitude signals using (2.22)-(2.24) and (2.25)-(2.27), respectively; and replace (θ, ψ) in (6.26)-(6.27) by (ϕ, ψ) and (ϕ, θ) , respectively.

Theorem 6.2. *Consider the vehicle dynamics (2.18), (2.12). Suppose that Assumption 2.1 holds. Then, the controller (6.24)-(6.27), together with the finite-time sliding mode observer (6.9)-(6.10), solves the formation tracking problem.*

Proof. The vehicle dynamics (2.18), (2.12) is in the (ξ_i, η_i) -cascaded structure. For the η_i -subsystem, substituting (6.26)-(6.27) into (2.12), yields $\dot{s}_{3i} = -k_{3i} \text{sign}(s_{3i}) - \ddot{\theta}_{id}(t)$ and $\dot{s}_{4i} = -k_{4i} \text{sign}(s_{4i}) - \ddot{\psi}_{id}(t)$. Then, conditions $k_{3i} > \sup\{|\ddot{\theta}_{id}(t)|\}$ and $k_{4i} > \sup\{|\ddot{\psi}_{id}(t)|\}$ imply that $s_{3i}(t) \rightarrow 0$ and $s_{4i}(t) \rightarrow 0$ in finite time. On the sliding manifolds $\{s_{3i} = 0\}$ and $\{s_{4i} = 0\}$, we have $\dot{\tilde{\theta}}_i = -\lambda_1 \tilde{\theta}_i$, and $\dot{\tilde{\psi}}_i = -\lambda_2 \tilde{\psi}_i$, which implies that $\theta_i(t) - \theta_{id}(t) \rightarrow 0$ and $\psi_i(t) - \psi_{id}(t) \rightarrow 0$ exponentially as $t \rightarrow +\infty$, and thus, we conclude that $|\eta_i(t) - \eta_{id}(t)| \rightarrow 0$ exponentially. In **Case 2**, we have $\phi_i(t) - \phi_{id}(t) \rightarrow 0$ and $\psi_i(t) - \psi_{id}(t) \rightarrow 0$ exponentially as $t \rightarrow +\infty$, and in **Case 3**, we have $\phi_i(t) - \phi_{id}(t) \rightarrow 0$ and $\theta_i(t) - \theta_{id}(t) \rightarrow 0$ exponentially as $t \rightarrow +\infty$. Therefore, the same conclusion $|\eta_i(t) - \eta_{id}(t)| \rightarrow 0$ also can be obtained for both **Case 2** and **Case 3**. Furthermore, the interconnection term $g_i(\eta_i(t), u_i(t), \dot{\xi}_i(t), \nu_i(t)) \rightarrow 0$ as $t \rightarrow +\infty$ as mentioned in Remark 2.2. Moreover, it follows from Proposition 6.1 that the finite-time sliding mode observer (6.9)-(6.10) guarantees the global finite-time convergence of $\hat{\zeta}_{ij}(t) - \zeta_{ij}(t) \rightarrow 0$. Thus, after a finite time T_r , $\hat{\zeta}_{ij}(t) \equiv \zeta_{ij}(t) \equiv R(\eta_j)^\top (\xi_j - \xi_i)$. Replace $\hat{\xi}_{ij}(t)$ with $\xi_{ij}(t)$ in (6.24), which recovers the generalized Slotine-Li controller structure (6.17). Also note that the controller (6.25) is exactly the same as the generalized Slotine-Li controller (6.17). Therefore, it follows from Theorem 6.1 that $\phi_i(t) - \phi_j(t) \rightarrow 0$ as $t \rightarrow +\infty$. Note that the dynamics $\dot{s}_{1i} = \ddot{\xi}_i - \dot{\zeta}_{1i} = -k_{1i}s_{1i} + g_i(\eta_i(t), u_i(t), \dot{\xi}_i(t), \nu_i(t))$ can be viewed as a stable linear system with an input term g_i , and the last term $g_i(\eta_i(t), u_i(t), \dot{\xi}_i(t), \nu_i(t)) \rightarrow 0$ as $t \rightarrow +\infty$. The converging-input converging-state property of linear systems implies that $s_{1i}(t) \rightarrow 0$ [92].

Finally, it follows from Theorem 6.1 that the control objective (2.17) is achieved, which completes the proof. \square

In contrast to existing robust control methods for underactuated systems in the literature where the error converges to zero under bounded model uncertainties, we do not *explicitly* consider model uncertainties. Although any first-order consensus algorithm can be used, in this paper, we choose the first-order *linear* consensus algorithm (A.26) for simplicity, which guarantees *asymptotic* convergence of the formation error under switching topologies, and guarantees *bounded* formation error under bounded uncertainties, disturbances, and time delays. However, in order to achieve *asymptotic* convergence of the formation error under model uncertainties and disturbances, as claimed in Remark 6.2, the method also can be generalized to first-order *nonlinear* consensus algorithms.

6.4 Numerical Simulation

In this section, we apply the proposed range observer-based formation control strategy to a heterogeneous spatial underactuated vehicle network including one AUV and four quadrotor unmanned aerial vehicles (UAVs). We provide numerical simulation results to verify the performance of the proposed formation control law. All parameters are given in SI units.

The four quadrotors are numbered **1** to **4** and the AUV is agent **5**. Note that the model of the AUV can be classified into **Case 1** and the model of quadrotors can be classified into **Case 3**.

We assume that the desired formation shape is an inverted quadrangular pyramid. Specifically, the desired formation shape of the group of quadrotors is a horizontal square with the leader vehicle **1** located at its upper-left corner, as shown in Figure 6.2. The length of the square sides is 5 m. The desired XY position of the AUV **5** is the center of the square in the formation, and the desired vertical position is 15 m lower than the horizontal square. In the simulation, the group leader is commanded to follow a circle of radius 1 m centered at $(0, 0, 10)$ and a constant speed of 1 rad/s. The desired yaw angle for the leader vehicle is 1 rad. The

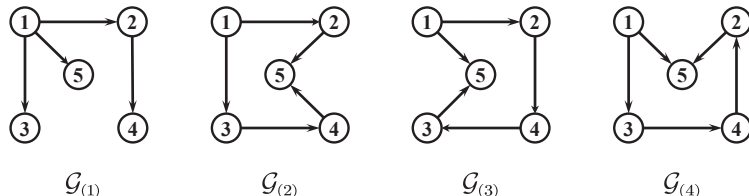


Figure 6.2: *Directed switching topologies in the numerical simulation.*

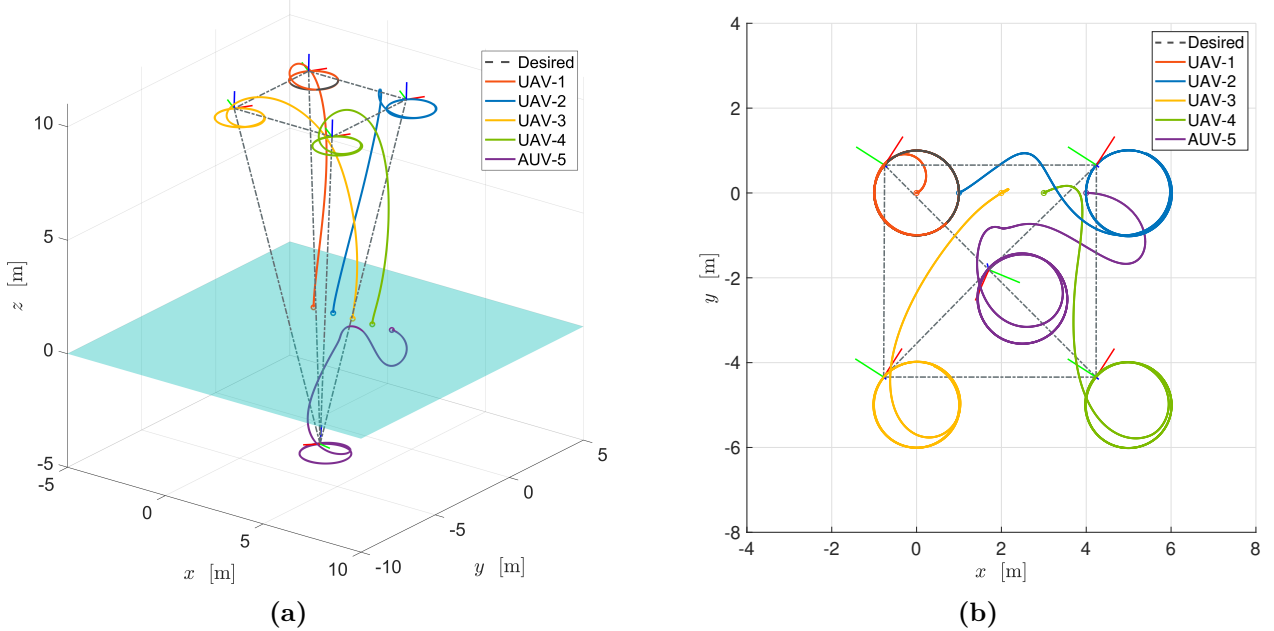
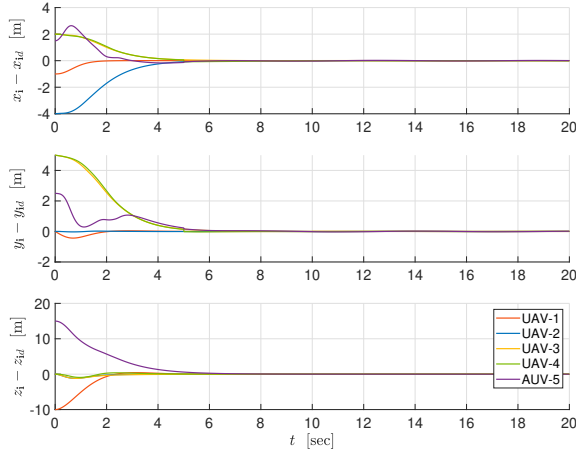


Figure 6.3: The trajectories of the five vehicles in three-dimensional space (left) and the top view (right).

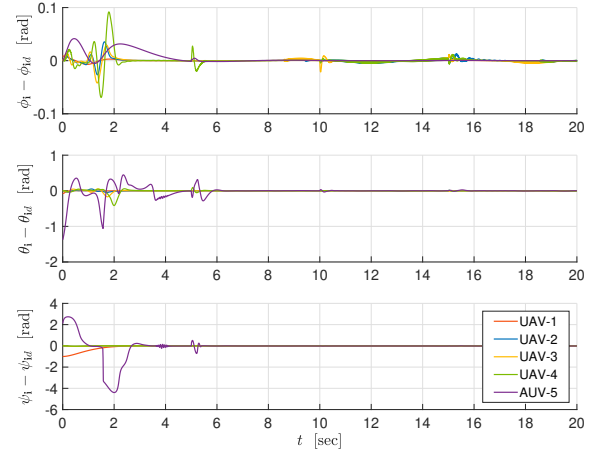
quadrotor parameters are selected as: $m_i = 1 \text{ kg}$, $I_i = \text{diag}\{0.0127, 0.0125, 0.0227\} \text{ kg}\cdot\text{m}^2$, $D_{vi} = \text{diag}\{0, 0, 0\}$, $D_{\omega i} = \text{diag}\{0, 0, 0\}$ for $i = 1, \dots, 4$. The AUV parameters are selected as: $m_5 = 11.85 \text{ kg}$, $I_5 = \text{diag}\{0.26, 2.51, 0.27\} \text{ kg}\cdot\text{m}^2$, $D_{v5} = \text{diag}\{0.85, 3.11, 0.24\}$, $D_{\omega 5} = \text{diag}\{0.01, 1.61, 1.28\}$. The buoyancy force of the AUV is 114.2 N. The gravity acceleration $g = 9.81 \text{ kg/s}^2$. All vehicles start from rest at the initial positions shown in Figure 6.3 and the initial Euler angles are 0. The directed communication graph $\mathcal{G}(t)$ switches every 5 seconds from $\mathcal{G}_{(1)}$ to $\mathcal{G}_{(2)}$ to $\mathcal{G}_{(3)}$ and to $\mathcal{G}_{(4)}$, as shown in Figure 6.2. The components of the adjacency matrix are $a_{ij}(t) = 1$ if $(j, i) \in \mathcal{E}(t)$ and $a_{ij}(t) = 0$ otherwise.

The observer parameters in the simulation are selected as $\alpha = 5$ and $\gamma = 5$. The control parameters for the four quadrotors are selected as $k_{1i} = 3$, $k_{2i} = 3$, $k_{3i} = 20$, $k_{4i} = 20$ for $i = 1, \dots, 4$, $\alpha_1 = 2$, $\alpha_2 = 3$, $\lambda_1 = 3$, $\lambda_2 = 3$. The control parameters for the AUV are selected as: $k_{15} = 2$, $k_{25} = 1$, $k_{35} = 25$, $k_{45} = 25$, $\alpha_1 = 1$, $\alpha_2 = 1$, $\lambda_1 = 5$, $\lambda_2 = 5$.

Simulation results are illustrated in Figures 6.3-6.6. Figure 6.3 shows the paths of all five vehicles in three-dimensional space and the \$XY\$ plane (i.e. the top view) with the formation illustrated at $t = 20 \text{ s}$. Figure 6.4 shows the time history of the configuration errors of the five vehicles in the formation, where $\xi_{id} = [x_{id}, y_{id}, z_{id}]^\top = (1/\Xi_i(t)) \sum_{j \in \mathcal{N}_i(t)} a_{ij}(t)(\xi_j + d_{ij})$. It can be seen from Figure 6.4 that the convergence is exponential and the formation is achieved after about 6 seconds. Figure 6.5 shows the time history of the Euler angles of the five vehicles in the formation. The yaw angles of all four quadrotors are in consensus and converge to the



(a)



(b)

Figure 6.4: Time history of the configuration errors of the five vehicles in the formation: position errors (left), attitude errors (right).

desired angle (1 rad). The roll angle of the AUV converges to the desired trajectory assigned by the quadrotors, while its yaw angle linearly increases as time tends to infinity due to continuous rotation around its circular path. It is noted that all the roll and pitch angles are in the interval $(-\pi/2, \pi/2)$. The estimation errors of the range observers for the four follower vehicles are shown in Figure 6.6. It can be seen that the convergence is achieved in finite time, and the estimated ranges converge to the actual ranges in 4 seconds. The numerical simulation demonstrates the effectiveness and robustness of the proposed formation controller under switching communication topologies.

Remark 6.5. It can be seen from the proof of Proposition 6.1 that the parameter $\gamma > 0$ determines the convergence time T_r of the observer. That is, the larger γ , the quicker convergence of the observer. In practice, the two observer parameters α and γ are suggested to be selected moderately in order to avoid aggressive transient. Furthermore, the control parameters $k_{1i}, k_{2i}, \lambda_1$, and λ_2 determine the speed that trajectories converge to the sliding surface, and are also suggested to be selected moderately in order to avoid overshooting. The parameters α_1 and α_2 are usually selected as small values to guarantee the transient performance. Finally, the parameters k_{3i}, k_{4i} are gains of sliding mode control, which are suggested to be chosen larger to guarantee robustness.

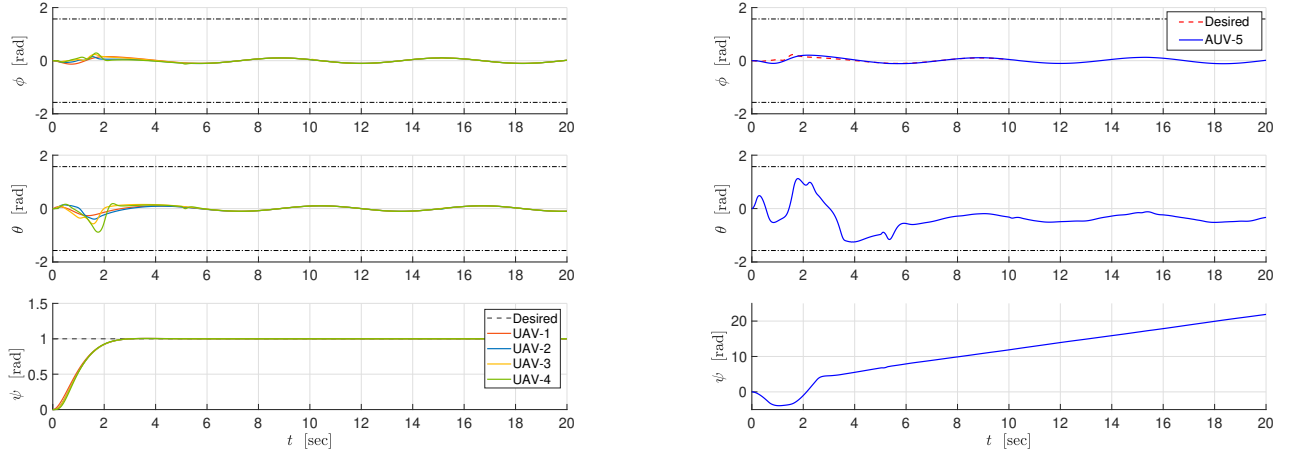


Figure 6.5: Time history of the Euler angles of the five vehicles in the formation; UAVs (left), AUV (right).

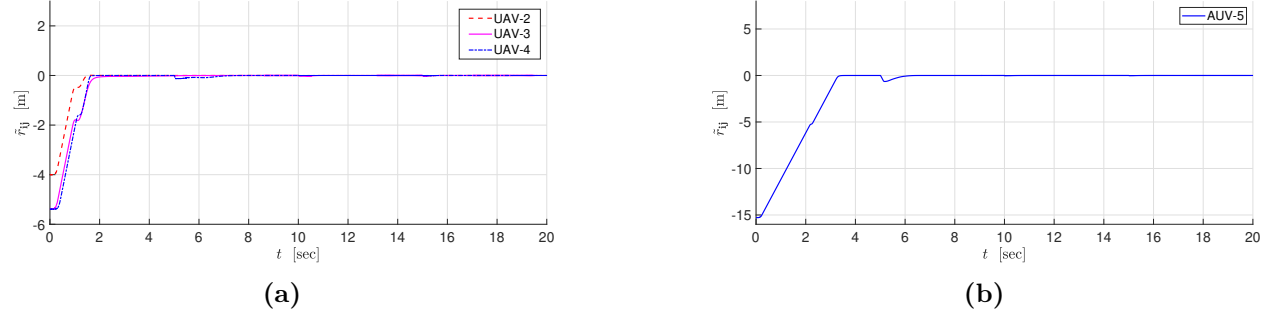


Figure 6.6: Time history of the estimation errors of the finite-time range observers; follower UAVs (left), AUV (right).

6.5 Conclusions

The formation control problem for a team of heterogeneous spatial underactuated vehicles subject to switching topologies and communication delays has been addressed without requiring any relative position measurements. The spatial vehicle model is assumed to have two degrees of underactuation, which include underwater vehicles and quadrotors. A distributed sliding mode observer is used to estimate ranges between vehicles in finite time based on bearing angles, vehicle attitude, and local velocity measurements. Then, the generalized Slotine-Li controller is presented to deal with switching topologies. Global asymptotic convergence is proved for the closed-loop system based on the cascaded structure of the vehicle systems. The simulation results show the effectiveness of the proposed formation control law.

Chapter 7

Conclusions & Future Work

7.1 Conclusions

This dissertation mainly considers the problem of distributed coordination and formation control for heterogeneous underactuated multi-vehicle systems.

Robust Formation Control for Planar Multi-vehicle Systems

- In Chapter 3, we have developed a distributed formation control approach for networks of planar underactuated vehicles without requiring global position measurements. All vehicles in the network are modeled as generic three degree of freedom planar rigid bodies with two control inputs and are allowed to have non-identical dynamics.
- A transformation is proposed to reduce the order of error dynamics and then two sliding mode control laws are employed to stabilize the error dynamics. It is shown that the approach can be applied to networks of nonholonomic mobile robots, underactuated surface vessels with various modeling complexities, and planar air vehicles. We successfully apply the proposed approach to a time-varying formation control problem for a complex network of heterogeneous mobile robots and surface vessels.

Formation Stabilization and Tracking Control for Planar Multi-vehicle Systems

- In Chapter 4, we have presented a distributed control framework to *simultaneously* address the formation stabilization and tracking control problem for heterogeneous planar underactuated vehicle networks without global position measurements. The control design is developed based on partial stability theory, Matrosov's theorem, and $u\delta$ -PE, and guarantees GAS for the origin of the closed-loop system.

Source Seeking for Planar Underactuated Vehicles

- In Chapter 5, we developed a source seeking scheme for generic force-controlled planar underactuated vehicles by surge force tuning. The control design is based on symmetric product approximations, averaging, passivity, and partial-state stability theory. The controller does not require any position or velocity measurements but only real-time measurements of the source signal at the current position. The P-SPUAS is proven for the closed-loop source seeking system.

Range Observer-Based Formation Control for Spatial Underactuated Vehicles

- In Chapter 6, we solve the distributed formation control problem for a class of heterogeneous spatial underactuated vehicle networks with a directed communication graph. It is shown that switching topologies do not matter if the communication graph contains a directed spanning tree. Furthermore, the proposed control law is robust to communication delays.
- Instead of requiring the relative positions, the proposed control protocol requires the bearing angle information of the neighbor vehicles. Using the distributed sliding mode observers, the ranges between the vehicle and its neighbors are estimated in finite time based on the bearing, attitude, and local velocity measurements. It should be emphasized that the bearing angles of the neighbors can be easily measured by onboard monocular cameras, which are much cheaper and lighter than LiDARs.

7.2 Future Work

In this section, we outline the opportunities for future work.

On Prescribe-Time Formation Design for Underactuated Vehicle Systems

- In the future, one might investigate the finite-time and/or prescribed-time formation control design for both heterogeneous planar and spatial underactuated vehicle networks. It is useful to have finite-time convergence or prescribed-time convergence of the formation error in practical applications. Furthermore, finite-time and/or prescribed-time obstacle avoidance problems also can be investigated by combining the approaches proposed in this dissertation and the time transformation approach.

On Source Seeking for Planar Underactuated Vehicles by Torque Tuning

- Compared with the forward motion-tuning approach, the angular motion-tuning approach seems to be more efficient and elegant—it avoids back-and-forth (or acceleration-and-deceleration) motion during the seeking process. For some planar aircraft, it is even unrealistic to generate back-and-forth trajectories in practice. Moreover, angular motion-tuning source seeking algorithms exist in nature. For example, it was shown that sperm chemotaxis is a biological implementation of the angular motion-tuning source seeking algorithm. Therefore, it is reasonable to expect angular motion-tuning source seeking algorithms for autonomous vehicles. One might investigate the angular motion-tuning algorithm for a generic planar underactuated vehicle. Lie bracket approximation and singular perturbation analysis may be used in the design.

On Cooperative Control for Both Planar and Spatial Underactuated Vehicles

- In the future, one might explore the design of integrating the approaches presented in this dissertation so that a multi-vehicle system containing both planar and spatial vehicles can work cooperatively to achieve a common task. One might consider the formation control problem for a group of vehicles containing both planar and spatial vehicles. With an appropriate formation motion planning algorithm, one might also explore the formation control design with collision/obstacle avoidance ability.

Appendix A

Basic Notions

A.1 Partial-State Stability Notions

Consider the nonlinear interconnected system

$$\dot{x}_1 = f_1(x_1, x_2), \quad x_1(t_0) = x_{10}, \quad t \geq t_0, \quad (\text{A.1})$$

$$\dot{x}_2 = f_2(x_1, x_2), \quad x_2(t_0) = x_{20}. \quad (\text{A.2})$$

where $f_1 : \mathbb{R}^{n_1} \times \mathbb{R}^{n_2} \rightarrow \mathbb{R}^{n_1}$ is such that, for every $x_2 \in \mathbb{R}^{n_2}$, $f_1(0, x_2) = 0$ and $f_1(x_1, x_2)$ is locally Lipschitz in x_1 uniformly in x_2 ; $f_2 : \mathbb{R}^{n_1} \times \mathbb{R}^{n_2} \rightarrow \mathbb{R}^{n_2}$ is such that for every $x_1 \in \mathbb{R}^{n_1}$, $f_2(x_1, x_2)$ is locally Lipschitz in x_2 uniformly in x_1 . Let $x_1(\cdot) := x_1(\cdot, x_{10}, x_{20})$ and $x_2(\cdot) := x_2(\cdot, x_{10}, x_{20})$ denote the solution of the initial value problem (A.1)-(A.2). We define the *partial-state stability* as stability with respect to x_1 for system (A.1)-(A.2).

Definition A.1 (P-UGAS). The system (A.1)-(A.2) is *globally asymptotically stable (GAS) with respect to x_1 uniformly in x_{20}* if the following conditions are satisfied:

- 1) *Partial-State Uniform Stability (P-US)*: For each $\varepsilon > 0$, there exists $\delta(\varepsilon)$ such that

$$|x_{10}| \leq \delta(\varepsilon) \implies |x_1(t)| \leq \varepsilon, \quad \forall t \geq 0, \quad \forall x_{20} \in \mathbb{R}^{n_2}.$$

- 2) *Partial-State Uniform Global Boundedness (P-UGB)*: For each $r > 0$, there exists $R(r)$ such that

$$|x_{10}| \leq r \implies |x_1(t)| \leq R(r), \quad \forall t \geq 0, \quad \forall x_{20} \in \mathbb{R}^{n_2}.$$

- 3) *Partial-State Uniform Global Attractivity (P-UGA)*: For each $r > 0$, for each $\sigma > 0$, there

exists $T(r, \sigma)$ such that

$$|x_{10}| \leq r \implies |x_1(t)| \leq \sigma, \quad \forall t \geq T(r, \sigma), \quad \forall x_{20} \in \mathbb{R}^{n_2}.$$

We present Lyapunov conditions for P-UG(A)S of (A.1)-(A.2). Given a function $V(x_1, x_2)$, define $\dot{V}(x_1, x_2) = (\partial V / \partial x)f(x_1, x_2)$, where $x = \text{col}(x_1, x_2)$ and $f = \text{col}(f_1, f_2)$.

Theorem A.1 ([146]). *Consider the interconnected system (A.1)-(A.2). If there exist a function $V : \mathbb{R}^{n_1} \times \mathbb{R}^{n_2} \rightarrow \mathbb{R}_{\geq 0}$ of class C^1 , class- \mathcal{K}_∞ functions α_1, α_2 such that for all $(x_1, x_2) \in \mathbb{R}^{n_1} \times \mathbb{R}^{n_2}$,*

$$\alpha_1(|x_1|) \leq V(x_1, x_2) \leq \alpha_2(|x_1|), \quad (\text{A.3})$$

$$\dot{V}(x_1, x_2) \leq 0, \quad (\text{A.4})$$

then the system (A.1)-(A.2) is US and UGB with respect to x_1 uniformly in x_{20} . Furthermore, if exists a positive definite function α_3 such that for all $(x_1, x_2) \in \mathbb{R}^{n_1} \times \mathbb{R}^{n_2}$,

$$\dot{V}(x_1, x_2) \leq -\alpha_3(|x_1|), \quad (\text{A.5})$$

then (A.1)-(A.2) is UGAS with respect to x_1 uniformly in x_{20} .

We present sufficient conditions for UGAS of time-varying interconnected systems with partial-state stability. Consider the following time-varying interconnected system

$$\Sigma_1 : \dot{x}_1 = f_1(t, x_1, x_2), \quad x_1(t_0) = x_{10}, \quad t_0 \geq 0, \quad (\text{A.6})$$

$$\Sigma_2 : \dot{x}_2 = f_2(t, x_1, x_2), \quad x_2(t_0) = x_{20}, \quad (\text{A.7})$$

where $x = \text{col}(x_1, x_2) \in \mathbb{R}^{n_1} \times \mathbb{R}^{n_2}$. We assume that the functions f_1, f_2 are continuous in their arguments, locally Lipschitz in (x_1, x_2) , uniformly in t , and the origin $(x_1, x_2) = (0, 0)$ is an equilibrium point.

Theorem A.2. *Suppose that f_2 is continuously differentiable. Then, the origin of the interconnected system (A.6)-(A.7) is UGAS if the following conditions hold.*

1) (P-UGAS with respect to x_1) There exist a C^1 function $V_1 : \mathbb{R} \times \mathbb{R}^{n_1} \times \mathbb{R}^{n_2} \rightarrow \mathbb{R}_{\geq 0}$, functions $\alpha_1, \alpha_2 \in \mathcal{K}_\infty$, and a positive definite function $W_1 : \mathbb{R}^{n_1} \rightarrow \mathbb{R}$ such that

$$\alpha_1(|x_1|) \leq V_1(t, x_1, x_2) \leq \alpha_2(|x_1|), \quad (\text{A.8})$$

$$\dot{V}_1(t, x_1, x_2) \leq -W_1(x_1), \quad (\text{A.9})$$

for all $(t, x_1, x_2) \in \mathbb{R} \times \mathbb{R}^{n_1} \times \mathbb{R}^{n_2}$.

2) (0-UGAS of Σ_2) There exist a C^1 function $V_2 : \mathbb{R} \times \mathbb{R}^{n_2} \rightarrow \mathbb{R}_{\geq 0}$, functions $\alpha_3, \alpha_4 \in \mathcal{K}_\infty$, function $\alpha_5 \in \mathcal{K}$, and a positive definite function $W_2 : \mathbb{R}^{n_2} \rightarrow \mathbb{R}$ such that

$$\alpha_3(|x_2|) \leq V_2(t, x_2) \leq \alpha_4(|x_2|), \quad (\text{A.10})$$

$$\frac{\partial V_2}{\partial t} + \frac{\partial V_2}{\partial x_2} f_2(t, 0, x_2) \leq -W_2(x_2), \quad (\text{A.11})$$

$$\left| \frac{\partial V_2}{\partial x_2} \right| \leq \alpha_5(|x_2|), \quad (\text{A.12})$$

for all $(t, x_2) \in \mathbb{R} \times \mathbb{R}^{n_2}$.

3) ($|x_1|$ is small order of W_1) The function W_1 satisfies

$$\lim_{|x_1| \rightarrow \infty} \frac{|x_1|}{W_1(x_1)} = 0. \quad (\text{A.13})$$

Proof. Along the trajectories of (A.6), (A.7), we have

$$\begin{aligned} \dot{V}_2 &\leq -W_2(x_2) + \left[\frac{\partial V_2}{\partial x_2} f_2(t, x_1, x_2) - \frac{\partial V_2}{\partial x_2} f_2(t, 0, x_2) \right] \\ &\leq -W_2(x_2) + \left| \frac{\partial V_2}{\partial x_2} \right| \left| \frac{\partial f_2}{\partial x_1} \right| |x_1|. \end{aligned}$$

Since V_2 is continuously differentiable and f_2 is continuous and Lipschitz, it follows that for each $r > 0$ there exist $c_1 > 0$ and $c_2 > 0$ such that $|\partial V_2 / \partial x_2| \leq c_1$ and $|\partial f_2 / \partial x_1| \leq c_2$ for all $t \geq 0$ and for all $(x_1, x_2) \in \bar{\mathcal{B}}_r$. Then, consider a Lyapunov candidate $V = \kappa V_1 + V_2$, where κ is a positive constant. Along the trajectories of (A.6), (A.7), we have

$$\dot{V}(t, x_1, x_2) \leq -\kappa W_1(x_1) \left[1 - \frac{c_1 c_2}{\kappa W_1(x_1)} |x_1| \right] - W_2(x_2). \quad (\text{A.14})$$

It follows from (A.13), (A.14) that the system (A.6), (A.7) is uniformly globally bounded (UGB) by choosing κ sufficiently large. It follows from [147, Theorem 3.1] that the origin of system (A.6), (A.7) is uniformly asymptotically stable. Thus, there exists $\delta > 0$ such that $|x(t_0)| < \delta \Rightarrow |x(t, t_0, x(t_0))| \rightarrow 0$ as $t \rightarrow \infty$. The uniform global attractivity follows from the fact that κ can be chosen arbitrarily large such that the trajectory of (A.6), (A.7) with initial conditions starting in $\bar{\mathcal{B}}_r$ enters the domain of attraction \mathcal{B}_δ for any $r > 0$. \square

We define *partial-state practical stability* for interconnected systems that depends on a

small parameter $\varepsilon > 0$,

$$\dot{x}_1 = f_1^\varepsilon(t, x_1, x_2), \quad x_1^\varepsilon(t_0) = x_{10}, \quad t \geq t_0, \quad (\text{A.15})$$

$$\dot{x}_2 = f_2^\varepsilon(t, x_1, x_2). \quad x_2^\varepsilon(t_0) = x_{20}, \quad (\text{A.16})$$

Let $x_1^\varepsilon(\cdot) := x_1^\varepsilon(\cdot, t_0, x_{10}, x_{20})$ and $x_2^\varepsilon(\cdot) := x_2^\varepsilon(\cdot, t_0, x_{10}, x_{20})$ denote the solution of the initial value problem (A.15)-(A.16).

Definition A.2 (P-SPUAS). The system (A.15)-(A.16) said to be *semi-globally practically asymptotically stable (SPAS) with respect to x_1 uniformly in (t_0, x_{20})* if for every compact set $\bar{\mathcal{B}}_r^{n_2} \subset \mathbb{R}^{n_2}$, the following conditions are satisfied:

- 1) For every $c_2 > 0$, there exists c_1 and $\hat{\varepsilon}(r) > 0$ such that for all $(t_0, x_{20}) \in \mathbb{R}_{\geq 0} \times \bar{\mathcal{B}}_r^{n_2}$ and for all $\varepsilon \in (0, \hat{\varepsilon})$,

$$|x_{10}| \leq c_1 \implies |x_1^\varepsilon(t)| \leq c_2, \quad \forall t \geq t_0.$$

- 2) For every $c_1 > 0$, there exists c_2 and $\hat{\varepsilon}(r) > 0$ such that for all $(t_0, x_{20}) \in \mathbb{R}_{\geq 0} \times \bar{\mathcal{B}}_r^{n_2}$ and for all $\varepsilon \in (0, \hat{\varepsilon})$,

$$|x_{10}| \leq c_1 \implies |x_1^\varepsilon(t)| \leq c_2, \quad \forall t \geq t_0.$$

- 3) For all $c_1 > 0$, $c_2 > 0$, there exists $T(c_1, c_2)$ and $\hat{\varepsilon}(r) > 0$ such that for all $(t_0, x_{20}) \in \mathbb{R}_{\geq 0} \times \bar{\mathcal{B}}_r^{n_2}$ and for all $\varepsilon \in (0, \hat{\varepsilon})$,

$$|x_{10}| \leq c_1 \implies |x_1^\varepsilon(t)| \leq c_2, \quad \forall t \geq t_0 + T(c_1, c_2).$$

The notion of P-SPUAS is an extension of the notion of SPUAS [118, 131, 148]. It is well known that, under the assumption that trajectories of (A.15)-(A.16) converge to trajectories of (A.1)-(A.2) uniformly on compact time intervals as $\varepsilon \rightarrow 0$, if (A.1)-(A.2) is GAS, then the origin of (A.15)-(A.16) is SPUAS [131, 148]. We extend this claim to interconnected systems with partial-state stability.

Definition A.3 (Partial Converging Trajectories Property). The systems (A.1)-(A.2) and (A.15)-(A.16) are said to satisfy the *partial converging trajectories property* if for every $T > 0$, for every compact set $K \subset \mathbb{R}^{n_1} \times \mathbb{R}^{n_2}$, and for every $d > 0$, there exists ε^* such that for all $t_0 \geq 0$, for all $(x_{10}, x_{20}) \in K$ and for all $\varepsilon \in (0, \varepsilon^*)$,

$$|x_1^\varepsilon(t) - x_1(t)| < d, \quad \forall t \in [t_0, t_0 + T]. \quad (\text{A.17})$$

Proposition A.1. Assume that for the system (A.1)-(A.2), the flow $(x_1(\cdot), x_2(\cdot))$ is forward complete, and that the systems (A.1)-(A.2) and (A.15)-(A.16) satisfy the partial converging trajectories property. If (A.1)-(A.2) is GAS with respect to x_1 uniformly in x_{20} , then (A.15)-(A.16) is SPAS with respect to x_1 uniformly in (t_0, x_{20}) .

Proof. We successively prove that conditions 1, 2, and 3 of Definition A.2 are satisfied.

- 1) Take an arbitrary $c_2 > 0$, and let $b_2 \in (0, c_2)$. By the P-US property, there exists c_1 such that

$$|x_{10}| \leq c_1 \implies |x_1(t)| \leq b_2, \quad \forall t \geq t_0, \quad \forall x_{20} \in \mathbb{R}^{n_2}.$$

Let $b_1 \in (0, c_1)$, and by the P-UGA property, there exists T such that

$$|x_{10}| \leq c_1 \implies |x_1(t)| \leq b_1, \quad \forall t \geq t_0 + T, \quad \forall x_{20} \in \mathbb{R}^{n_2}.$$

Let $d = \min\{c_1 - b_1, c_2 - b_2\}$ and $K = \{(x_1, x_2) \in \mathbb{R}^{n_1} \times \mathbb{R}^{n_2} : |x_1| \leq c_1, |x_2| \leq r\}$, where $r > 0$ is an arbitrary number. By the partial converging trajectory property, there exists ε^* such that for all $(x_{10}, x_{20}) \in K$ and for all $\varepsilon \in (0, \varepsilon^*)$,

$$|x_1^\varepsilon(t) - x_1(t)| < d, \quad \forall t \in [t_0, t_0 + T].$$

Thus, we conclude that for all $t_0 \in \mathbb{R}_{\geq 0}$, for all $(x_{10}, x_{20}) \in K$ and for all $\varepsilon \in (0, \varepsilon^*)$,

$$\begin{aligned} |x_1^\varepsilon(t)| &< c_2, & \forall t \in [t_0, t_0 + T], \\ |x_1^\varepsilon(t)| &< c_1, & \text{for } t = t_0 + T. \end{aligned} \tag{A.18}$$

Since $|x_1^\varepsilon(t_0 + T)| < c_1$, a repeated application of (A.18) yields that for all $(x_{10}, x_{20}) \in K$ and for all $\varepsilon \in (0, \varepsilon^*)$, we have $|x_1^\varepsilon(t)| < c_2, \forall t \geq t_0$.

- 2) Take an arbitrary $c_1 > 0$, and let $b_1 \in (0, c_1)$. By the P-UGB and P-UGA properties, there exist b_2 and T such that for all $t_0 \in \mathbb{R}_{\geq 0}$ and for all $x_{20} \in \mathbb{R}^{n_2}$,

$$\begin{aligned} |x_{10}| \leq c_1 &\implies |x_1(t)| \leq b_2, & \forall t \geq t_0, \\ |x_{10}| \leq c_1 &\implies |x_1(t)| \leq b_1, & \forall t \geq t_0 + T. \end{aligned}$$

Let $c_2 > b_2$, and by the partial converging trajectory property again, we conclude that there exists ε^* such that for all $(x_{10}, x_{20}) \in K$ and for all $\varepsilon \in (0, \varepsilon^*)$, we have $|x_1^\varepsilon(t)| < c_2, \forall t \geq t_0$.

- 3) Take arbitrary $c_1, c_2 > 0$. By the Item 1 proven above, there exist c_3 and ε^* such that for

all $t_0 \in \mathbb{R}_{\geq 0}$, for all $\varepsilon \in (0, \varepsilon^*)$,

$$|x_{10}| \leq c_3 \implies |x_1^\varepsilon(t)| < c_2, \forall t \geq t_0, \forall x_{20} \in \bar{\mathcal{B}}_r^{n_2}. \quad (\text{A.19})$$

Let $b_3 \in (0, c_3)$, and by the P-UGA property, there exists T such that for all $x_{20} \in \mathbb{R}^{n_2}$,

$$|x_{10}| \leq c_1 \implies |x_1(t)| \leq b_3, \quad \forall t \geq t_0 + T.$$

Let $d = c_3 - b_3$. Then, by the partial converging trajectory property, there exists $\varepsilon^\#$ such that for all $\varepsilon \in (0, \varepsilon^\#)$ and for all $x_{20} \in \bar{\mathcal{B}}_r^{n_2}$,

$$|x_{10}| \leq c_1 \implies |x_1^\varepsilon(t) - x_1(t)| < d, \quad \forall t \in [t_0, t_0 + T],$$

which implies that for all $\varepsilon \in (0, \varepsilon^\#)$ and for all $x_{20} \in \bar{\mathcal{B}}_r^{n_2}$,

$$|x_{10}| \leq c_1 \implies |x_1^\varepsilon(t_0 + T)| < c_3.$$

Finally, together with (A.19), we conclude that for all $t_0 \in \mathbb{R}_{\geq 0}$, for all $\varepsilon \in (0, \min\{\varepsilon^*, \varepsilon^\#\})$, and for all $x_{20} \in \bar{\mathcal{B}}_r^{n_2}$,

$$|x_{10}| \leq c_1 \implies |x_1^\varepsilon(t)| < c_2, \quad \forall t \geq t_0 + T,$$

which completes the proof. □

A.2 Technical Lemmas

Consider the differential equation $\dot{x} = f(t, x)$ with an equilibrium point at the origin.

Definition A.4 (Non-zero definiteness [149]). *A continuous function $w : \mathbb{R}_{\geq 0} \times \bar{\mathcal{B}}_\rho \rightarrow \mathbb{R}$ is said to be non-zero definite on the set $M \subset \bar{\mathcal{B}}_\rho$ if for any pair of numbers δ and R such that $0 < \delta < R \leq \rho$ there exist positive numbers Δ and μ such that*

$$\left. \begin{array}{l} |x| \in [\delta, R] \\ |x|_M < \Delta \\ t \geq 0 \end{array} \right\} \implies |w(t, x)| > \mu, \quad (\text{A.20})$$

where $|x|_M := \inf_{z \in M} |x - z|$.

Theorem A.3 (Matrosov's theorem [149]). *Suppose that there exist a continuous function $V^* : \mathbb{R}^n \rightarrow \mathbb{R}_{\geq 0}$, continuously differentiable functions $V : \mathbb{R}_{\geq 0} \times \mathbb{R}^n \rightarrow \mathbb{R}$ and $W : \mathbb{R}_{\geq 0} \times \mathbb{R}^n \rightarrow \mathbb{R}$, functions $\alpha_1, \alpha_2 \in \mathcal{K}_\infty$, and for each $R > 0$, there exists $L > 0$ such that*

(a) *W and f satisfy*

$$\max \{|W(t, x)|, |f(t, x)|\} \leq L, \quad \forall (t, x) \in \mathbb{R}_{\geq 0} \times \bar{\mathcal{B}}_R; \quad (\text{A.21})$$

(b) *V is positive definite decrescent and \dot{V} is negative semi-definite, i.e., for all $(t, x) \in \mathbb{R}_{\geq 0} \times \mathbb{R}^n$*

$$\alpha_1(|x|) \leq V(t, x) \leq \alpha_2(|x|), \quad (\text{A.22})$$

$$\dot{V}(t, x) \leq -V^*(x) \leq 0; \quad (\text{A.23})$$

(c) *the function $\dot{W}(t, x)$ is non-zero definite on*

$$M := \{x \in \bar{\mathcal{B}}_R : V^*(x) = 0\}. \quad (\text{A.24})$$

Then, the origin of $\dot{x} = f(t, x)$ is UGAS.

Lemma A.1 ([150, restated]). *Consider the following system*

$$\begin{aligned} \dot{x}_1 &= f(t, x_1) + \omega(t)x_2, \\ \dot{x}_2 &= -p\omega(t)^\top \left[\frac{\partial V}{\partial x_1} \right]^\top, \end{aligned} \quad (\text{A.25})$$

where $x_1 \in \mathbb{R}^{n_1}$, $x_2 \in \mathbb{R}$, $f : \mathbb{R}_{\geq 0} \times \mathbb{R}^{n_1} \rightarrow \mathbb{R}^{n_1}$, $\omega : \mathbb{R}_{\geq 0} \rightarrow \mathbb{R}^{n_1}$, $V : \mathbb{R}_{\geq 0} \times \mathbb{R}^{n_1} \rightarrow \mathbb{R}_{\geq 0}$ and $p > 0$ is a constant. Let the following assumptions A1-A3 hold.

A1.) *There exist class \mathcal{K}_∞ functions $\alpha_1(\cdot)$ and $\alpha_2(\cdot)$, and a positive definite function $\alpha_3(\cdot)$ such that, for all $t \geq 0$, and $x_1 \in \mathbb{R}^{n_1}$,*

$$\begin{aligned} \alpha_1(|x_1|) &\leq V(t, x_1) \leq \alpha_2(|x_2|), \\ \frac{\partial V}{\partial t} + \frac{\partial V}{\partial x_1} f(t, x_1) &\leq -\alpha_3(|x_1|), \text{ a.e.} \end{aligned}$$

A2.) *There exists a continuous nondecreasing function $\beta : \mathbb{R}_{\geq 0} \rightarrow \mathbb{R}_{\geq 0}$ such that, for all*

$t \geq 0$, and $x_1 \in \mathbb{R}^{n_1}$,

$$\max \left\{ |f(t, x_1)|, \left| \frac{\partial V(t, x_1)}{\partial x_1} \right| \right\} \leq \beta(|x_1|) |x_1|, \text{ a.e.}$$

A3.) The function $\omega(\cdot)$ is bounded with a bounded first derivative, smooth and persistently exciting (PE), i.e., there exists $T > 0, \mu > 0$ such that

$$\int_t^{t+T} |\omega(\tau)|^2 d\tau \geq \mu, \quad \forall t \geq 0.$$

Then the origin of (A.25) is UGAS. Furthermore, if the origin of system $\dot{x}_1 = f(t, x_1)$ is UGES then the origin of (A.25) is UGES.

Lemma A.2 ([2], Theorem 3.11). Consider the single-integrator dynamics $\dot{x}_i = u_i$, where $x_i \in \mathbb{R}^n$, $i = 1, \dots, N$ with the network communication graph satisfying Assumption 2.1. Then, under the control law

$$u_i = \frac{1}{\Xi_i(t)} \sum_{j \in \mathcal{N}_i(t)} a_{ij}(t) [\dot{x}_j - \alpha(x_i - x_j)], \quad i = 1, \dots, N, \quad (\text{A.26})$$

where $\Xi_i(t) = \sum_{j \in \mathcal{N}_i(t)} a_{ij}(t)$, and $\alpha > 0$ is a constant, the consensus tracking problem is solved.

Lemma A.3 (Swapping lemma [151]). For continuous differentiable signals $x, y : \mathbb{R}_{\geq 0} \rightarrow \mathbb{R}$, the following holds for any $\alpha > 0$

$$\frac{\alpha}{s + \alpha}[xy] = y \frac{\alpha}{s + \alpha}[x] - \frac{1}{s + \alpha} \left[\dot{y} \frac{\alpha}{s + \alpha}[x] \right]. \quad (\text{A.27})$$

A.3 The Variation of Constants Formula

Consider the dynamic system

$$\dot{x} = g(t, x), \quad x(0) = x_0, \quad (\text{A.28})$$

where the vector field $g(t, x)$ is locally Lipschitz in x uniformly in t . The flow map $\Phi_{0,t}^g(\cdot)$ is a diffeomorphism, which describes the solution of (A.28) at time t , i.e., $x(t) = \Phi_{0,t}^g(x_0)$.

Given a diffeomorphism ϕ and a vector field f , the pull back of f along ϕ , denoted by $\phi^* f$, is the vector field

$$(\phi^* f)(x) := \left(\frac{\partial \phi^{-1}}{\partial x} \circ f \circ \phi \right) (x), \quad (\text{A.29})$$

where $(f \circ \phi)(x) = f(\phi(x))$. The variation of constants formula [86, 152] characterizes the relationship between the flow of $f + g$ and the flows of f and g .

Theorem A.4 (Variation of constants formula). *Consider the dynamic system*

$$\dot{x} = f(t, x) + g(t, x), \quad x(0) = x_0, \quad (\text{A.30})$$

where $f, g : \mathbb{R}_{\geq 0} \times \mathbb{R}^n \rightarrow \mathbb{R}^n$ are smooth vector fields. If $z(t)$ is the solution of the system

$$\dot{z}(t) = ((\Phi_{0,t}^g)^* f)(t, z), \quad z(0) = x_0, \quad (\text{A.31})$$

then the solution $x(t)$ of the initial value problem

$$\dot{x} = g(t, x), \quad x(0) = z(t) \quad (\text{A.32})$$

is the solution of system (A.30).

System (A.31) is called the *pull back system*. Furthermore, if f is a time-invariant vector field and g is a time-varying vector field, then the pull back of f along $\Phi_{0,t}^g$ is given by

$$((\Phi_{0,t}^g)^* f)(t, x) = f(x) + \sum_{k=1}^{\infty} \int_0^t \cdots \int_0^{s_{k-1}} (\text{ad}_{g(s_k, x)} \cdots \text{ad}_{g(s_1, x)} f(x)) \, ds_k \cdots ds_1. \quad (\text{A.33})$$

Bibliography

- [1] Z. Sun, *Cooperative coordination and formation control for multi-agent systems*. Cham, Switzerland: Springer, 2018.
- [2] W. Ren and R. W. Beard, *Distributed Consensus in Multi-Vehicle Cooperative Control*. London, UK: Springer, 2008.
- [3] W. Ren and Y. Cao, *Distributed Coordination of Multi-Agent Networks: Emergent Problems, Models, and Issues*. London, UK: Springer, 2011.
- [4] Y. Cao, W. Yu, W. Ren, and G. Chen, “An overview of recent progress in the study of distributed multi-agent coordination,” *IEEE Trans. Ind. Inform.*, vol. 9, no. 1, pp. 427–438, 2012.
- [5] K.-K. Oh, M.-C. Park, and H.-S. Ahn, “A survey of multi-agent formation control,” *Automatica*, vol. 53, pp. 424–440, 2015.
- [6] J. Qin, Q. Ma, Y. Shi, and L. Wang, “Recent advances in consensus of multi-agent systems: A brief survey,” *IEEE Transactions on Industrial Electronics*, vol. 64, no. 6, pp. 4972–4983, 2016.
- [7] S. Zuo, Y. Song, F. L. Lewis, and A. Davoudi, “Adaptive output formation-tracking of heterogeneous multi-agent systems using time-varying \mathcal{L}_2 -gain design,” *IEEE Contr. Syst. Lett.*, vol. 2, no. 2, pp. 236–241, 2018.
- [8] E. Panteley and A. Loría, “Synchronization and dynamic consensus of heterogeneous networked systems,” *IEEE Trans. Autom. Contr.*, vol. 62, no. 8, pp. 3758–3773, 2017.
- [9] Y. Liu and H. Yu, “A survey of underactuated mechanical systems,” *IET Control Theory Appl.*, vol. 7, no. 7, pp. 921–935, 2013.
- [10] R. W. Brockett, “Asymptotic stability and feedback stabilization,” in *Differential geometric control theory*, pp. 181–191, 1983.
- [11] J.-B. Pomet, “Explicit design of time-varying stabilizing control laws for a class of controllable systems without drift,” *Syst. Control Lett.*, vol. 18, no. 2, pp. 147–158, 1992.

- [12] A. Astolfi, “Discontinuous control of nonholonomic systems,” *Syst. Control Lett.*, vol. 27, no. 1, pp. 37–45, 1996.
- [13] A. Bloch, M. Reyhanoglu, and N. McClamroch, “Control and stabilization of nonholonomic dynamic systems,” *IEEE Trans. Autom. Contr.*, vol. 37, no. 11, pp. 1746–1757, 1992.
- [14] I. Kolmanovsky and N. H. McClamroch, “Developments in nonholonomic control problems,” *IEEE Control Syst.*, vol. 15, no. 6, pp. 20–36, 1995.
- [15] C. Canudas-de Wit, H. Khenouf, C. Samson, and O. J. Sordalen, “Nonlinear control design for mobile robots,” in *Recent Trends in Mobile Robots* (Y. F. Zheng, ed.), vol. 11, pp. 121–156, World Scientific Ser. Robot. Intelligent Syst., 1993.
- [16] M. Aicardi, G. Casalino, A. Bicchi, and A. Balestrino, “Closed loop steering of unicycle like vehicles via lyapunov techniques,” *IEEE Robot. Autom. Mag.*, vol. 2, no. 1, pp. 27–35, 1995.
- [17] D. A. Lizárraga, “Obstructions to the existence of universal stabilizers for smooth control systems,” *Math. Control Signals Syst.*, vol. 16, no. 4, pp. 255–277, 2004.
- [18] Z.-P. Jiang and H. Nijmeijer, “Tracking control of mobile robots: A case study in backstepping,” *Automatica*, vol. 33, no. 7, pp. 1393–1399, 1997.
- [19] E. Panteley, E. Lefeber, A. Loria, and H. Nijmeijer, “Exponential tracking control of a mobile car using a cascaded approach,” *IFAC Proceedings Volumes*, vol. 31, no. 27, pp. 201–206, 1998.
- [20] W. E. Dixon, D. M. Dawson, E. Zergeroglu, and A. Behal, *Nonlinear control of wheeled mobile robots*, vol. 175. London, UK: Springer, 2001.
- [21] G. Oriolo, A. De Luca, and M. Vendittelli, “WMR control via dynamic feedback linearization: design, implementation, and experimental validation,” *IEEE Trans. Control Syst. Technol.*, vol. 10, no. 6, pp. 835–852, 2002.
- [22] Z. Wang, S. Li, and S. Fei, “Finite-time tracking control of a nonholonomic mobile robot,” *Asian J. Control*, vol. 11, no. 3, pp. 344–357, 2009.
- [23] J. Pliego-Jiménez, R. Martínez-Clark, C. Cruz-Hernández, and A. Arellano-Delgado, “Trajectory tracking of wheeled mobile robots using only cartesian position measurements,” *Automatica*, vol. 133, p. 109756, 2021.
- [24] Z.-P. Jiang, “Controlling underactuated mechanical systems: A review and open problems,” in *Advances in the theory of control, signals and systems with physical modeling*, pp. 77–88, Springer, 2010.

- [25] T.-C. Lee, K.-T. Song, C.-H. Lee, and C.-C. Teng, “Tracking control of unicycle-modeled mobile robots using a saturation feedback controller,” *IEEE Trans. Control Syst. Technol.*, vol. 9, no. 2, pp. 305–318, 2001.
- [26] K. D. Do, Z.-P. Jiang, and J. Pan, “A global output-feedback controller for simultaneous tracking and stabilization of unicycle-type mobile robots,” *IEEE Trans. Robot. Automat.*, vol. 20, no. 3, pp. 589–594, 2004.
- [27] K. D. Do, Z.-P. Jiang, and J. Pan, “Simultaneous tracking and stabilization of mobile robots: an adaptive approach,” *IEEE Trans. Autom. Contr.*, vol. 49, no. 7, pp. 1147–1151, 2004.
- [28] Y. Wang, Z. Miao, H. Zhong, and Q. Pan, “Simultaneous stabilization and tracking of nonholonomic mobile robots: A Lyapunov-based approach,” *IEEE Trans. Control Syst. Technol.*, vol. 23, no. 4, pp. 1440–1450, 2015.
- [29] Z. Wang, G. Li, X. Chen, H. Zhang, and Q. Chen, “Simultaneous stabilization and tracking of nonholonomic WMRs with input constraints: Controller design and experimental validation,” *IEEE Trans. Ind. Electron.*, vol. 66, no. 7, pp. 5343–5352, 2018.
- [30] M. Maghenem, A. Loría, and E. Panteley, “A unique robust controller for tracking and stabilisation of non-holonomic vehicles,” *Int. J. Control.*, vol. 93, no. 10, pp. 2302–2313, 2020.
- [31] C. I. Byrnes and A. Isidori, “On the attitude stabilization of rigid spacecraft,” *Automatica*, vol. 27, no. 1, pp. 87–95, 1991.
- [32] M. Reyhanoglu, “Control and stabilization of an underactuated surface vessel,” in *Proc. IEEE Conf. Decis. Control*, vol. 3, pp. 2371–2376, IEEE, 1996.
- [33] K. Y. Pettersen and O. Egeland, “Exponential stabilization of an underactuated surface vessel,” in *Proc. IEEE Conf. Decis. Control*, vol. 1, pp. 967–972, IEEE, 1996.
- [34] K. Pettersen and H. Nijmeijer, “Global practical stabilization and tracking for an underactuated ship-a combined averaging and backstepping approach,” *IFAC Proceedings Volumes*, vol. 31, no. 18, pp. 59–64, 1998.
- [35] F. Mazenc, K. Pettersen, and H. Nijmeijer, “Global uniform asymptotic stabilization of an underactuated surface vessel,” *IEEE Trans. Autom. Contr.*, vol. 47, no. 10, pp. 1759–1762, 2002.
- [36] W. Dong and Y. Guo, “Global time-varying stabilization of underactuated surface vessel,” *IEEE Trans. Autom. Contr.*, vol. 50, no. 6, pp. 859–864, 2005.
- [37] J. Ghommam, F. Mnif, A. Benali, and N. Derbel, “Asymptotic backstepping stabilization of an underactuated surface vessel,” *IEEE Trans. Control Syst. Technol.*, vol. 14, no. 6, pp. 1150–1157, 2006.

- [38] K. Pettersen and H. Nijmeijer, “Tracking control of an underactuated surface vessel,” in *Proc. IEEE Conf. Decis. Control*, vol. 4, pp. 4561–4566, IEEE, 1998.
- [39] Z.-P. Jiang, “Global tracking control of underactuated ships by Lyapunov’s direct method,” *Automatica*, vol. 38, no. 2, pp. 301–309, 2002.
- [40] K. D. Do, Z.-P. Jiang, and J. Pan, “Underactuated ship global tracking under relaxed conditions,” *IEEE Trans. Autom. Contr.*, vol. 47, no. 9, pp. 1529–1536, 2002.
- [41] E. Lefeber, K. Y. Pettersen, and H. Nijmeijer, “Tracking control of an underactuated ship,” *IEEE Trans. Control Syst. Technol.*, vol. 11, no. 1, pp. 52–61, 2003.
- [42] A. Behal, D. M. Dawson, W. E. Dixon, and Y. Fang, “Tracking and regulation control of an underactuated surface vessel with nonintegrable dynamics,” *IEEE Trans. Autom. Contr.*, vol. 47, no. 3, pp. 495–500, 2002.
- [43] K. D. Do, Z.-P. Jiang, and J. Pan, “Universal controllers for stabilization and tracking of underactuated ships,” *Syst. Control Lett.*, vol. 47, no. 4, pp. 299–317, 2002.
- [44] K. D. Do, Z.-P. Jiang, J. Pan, and H. Nijmeijer, “A global output-feedback controller for stabilization and tracking of underactuated ODIN: A spherical underwater vehicle,” *Automatica*, vol. 40, no. 1, pp. 117–124, 2004.
- [45] H. Ashrafiou, S. Nersesov, and G. Clayton, “Trajectory tracking control of planar underactuated vehicles,” *IEEE Trans. Autom. Contr.*, vol. 62, no. 4, pp. 1959–1965, 2016.
- [46] S. Bouabdallah, A. Noth, and R. Siegwart, “PID vs LQ control techniques applied to an indoor micro quadrotor,” in *IEEE/RSJ International Conference on Intelligent Robots and Systems (IROS)*, vol. 3, pp. 2451–2456, IEEE, 2004.
- [47] F. Kendoul, Z. Yu, and K. Nonami, “Guidance and nonlinear control system for autonomous flight of minirotorcraft unmanned aerial vehicles,” *Journal of Field Robotics*, vol. 27, no. 3, pp. 311–334, 2010.
- [48] D. Lee, H. Jin Kim, and S. Sastry, “Feedback linearization vs. adaptive sliding mode control for a quadrotor helicopter,” *Int. J. Control Autom. Syst.*, vol. 7, no. 3, pp. 419–428, 2009.
- [49] R. Xu and Ü. Özgüner, “Sliding mode control of a class of underactuated systems,” *Automatica*, vol. 44, no. 1, pp. 233–241, 2008.
- [50] A. Poultney, C. Kennedy, G. Clayton, and H. Ashrafiou, “Robust tracking control of quadrotors based on differential flatness: Simulations and experiments,” *IEEE ASME Trans. Mechatron.*, vol. 23, no. 3, pp. 1126–1137, 2018.

- [51] T. Lee, M. Leok, and N. H. McClamroch, “Geometric tracking control of a quadrotor uav on $\text{se}(3)$,” in *49th IEEE conference on decision and control (CDC)*, pp. 5420–5425, IEEE, 2010.
- [52] F. Goodarzi, D. Lee, and T. Lee, “Geometric nonlinear pid control of a quadrotor uav on $\text{se}(3)$,” in *2013 European control conference (ECC)*, pp. 3845–3850, IEEE, 2013.
- [53] K. L. Fetzer, S. Nersesov, and H. Ashrafiouon, “Nonlinear control of three-dimensional underactuated vehicles,” *Int. J. Robust Nonlinear Control*, vol. 30, no. 4, pp. 1607–1621, 2020.
- [54] K. L. Fetzer, S. G. Nersesov, and H. Ashrafiouon, “Trajectory tracking control of spatial underactuated vehicles,” *Int. J. Robust Nonlinear Control*, vol. 31, no. 10, pp. 4897–4916, 2021.
- [55] R. W. Beard, J. Lawton, and F. Y. Hadaegh, “A coordination architecture for spacecraft formation control,” *IEEE Trans. Control Syst. Technol.*, vol. 9, no. 6, pp. 777–790, 2001.
- [56] L. Consolini, F. Morbidi, D. Prattichizzo, and M. Tosques, “Leader–follower formation control of nonholonomic mobile robots with input constraints,” *Automatica*, vol. 44, no. 5, pp. 1343–1349, 2008.
- [57] M. Ghasemi, S. G. Nersesov, G. Clayton, and H. Ashrafiouon, “Sliding mode coordination control for multiagent systems with underactuated agent dynamics,” *Int. J. Control*, vol. 87, no. 12, pp. 2615–2633, 2014.
- [58] X. Jin, “Fault tolerant finite-time leader–follower formation control for autonomous surface vessels with los range and angle constraints,” *Automatica*, vol. 68, pp. 228–236, 2016.
- [59] M. A. Maghenem, A. Loría, and E. Panteley, “Cascades-based leader–follower formation tracking and stabilization of multiple nonholonomic vehicles,” *IEEE Trans. Autom. Contr.*, vol. 65, no. 8, pp. 3639–3646, 2019.
- [60] H. Du, W. Zhu, G. Wen, and D. Wu, “Finite-time formation control for a group of quadrotor aircraft,” *Aerosp. Sci. Technol.*, vol. 69, pp. 609–616, 2017.
- [61] L. Dou, C. Yang, D. Wang, B. Tian, and Q. Zong, “Distributed finite-time formation control for multiple quadrotors via local communications,” *Int. J. Robust Nonlinear Control*, vol. 29, no. 16, pp. 5588–5608, 2019.
- [62] W. Dong, “Cooperative control of underactuated surface vessels,” *IET Control Theory Appl.*, vol. 4, no. 9, pp. 1569–1580, 2010.
- [63] W. Dong and J. Farrell, “Formation control of multiple underactuated surface vessels,” *IET Control Theory Appl.*, vol. 2, no. 12, pp. 1077–1085, 2008.

- [64] W. Dong and J. A. Farrell, “Cooperative control of multiple nonholonomic mobile agents,” *IEEE Trans. Autom. Contr.*, vol. 53, no. 6, pp. 1434–1448, 2008.
- [65] K.-K. Oh and H.-S. Ahn, “Formation control of mobile agents based on inter-agent distance dynamics,” *Automatica*, vol. 47, no. 10, pp. 2306–2312, 2011.
- [66] W. Ren and R. W. Beard, “Consensus seeking in multiagent systems under dynamically changing interaction topologies,” *IEEE Trans. Autom. Contr.*, vol. 50, no. 5, pp. 655–661, 2005.
- [67] W. Ren, “On consensus algorithms for double-integrator dynamics,” *IEEE Trans. Autom. Contr.*, vol. 53, no. 6, pp. 1503–1509, 2008.
- [68] G. Antonelli, F. Arrichiello, F. Caccavale, and A. Marino, “Decentralized time-varying formation control for multi-robot systems,” *Int. J. Rob. Res.*, vol. 33, no. 7, pp. 1029–1043, 2014.
- [69] F. Xiao, L. Wang, J. Chen, and Y. Gao, “Finite-time formation control for multi-agent systems,” *Automatica*, vol. 45, no. 11, pp. 2605–2611, 2009.
- [70] J. H. Seo, H. Shim, and J. Back, “Consensus of high-order linear systems using dynamic output feedback compensator: Low gain approach,” *Automatica*, vol. 45, no. 11, pp. 2659–2664, 2009.
- [71] W. Ren, “Distributed attitude consensus among multiple networked spacecraft,” in *Proc. Amer. Contr. Conf.*, (Minneapolis, MN), p. 4237–4242, IEEE, June 2006 2006.
- [72] D. V. Dimarogonas, P. Tsiotras, and K. J. Kyriakopoulos, “Leader-follower cooperative attitude control of multiple rigid bodies,” *Syst. Control Lett.*, vol. 58, no. 6, pp. 429–435, 2009.
- [73] J. Mei, W. Ren, and G. Ma, “Distributed coordinated tracking with a dynamic leader for multiple Euler-Lagrange systems,” *IEEE Trans. Autom. Contr.*, vol. 56, no. 6, pp. 1415–1421, 2011.
- [74] L. Yan and B. Ma, “Adaptive practical leader-following formation control of multiple nonholonomic wheeled mobile robots,” *Int. J. Robust Nonlinear Control*, vol. 30, no. 17, pp. 7216–7237, 2020.
- [75] T. Liu and Z.-P. Jiang, “Distributed formation control of nonholonomic mobile robots without global position measurements,” *Automatica*, vol. 49, no. 2, pp. 592–600, 2013.
- [76] M. A. Kamel, X. Yu, and Y. Zhang, “Real-time fault-tolerant formation control of multiple wmr based on hybrid ga-psa algorithm,” *IEEE Trans. Autom. Sci. Eng.*, 2020.

- [77] M. A. Kamel, X. Yu, and Y. Zhang, “Formation control and coordination of multiple unmanned ground vehicles in normal and faulty situations: A review,” *Annu. Rev. Control*, vol. 49, pp. 128–144, 2020.
- [78] K. D. Do, “Coordination control of quadrotor VTOL aircraft in three-dimensional space,” *Int. J. Control*, vol. 88, no. 3, pp. 543–558, 2015.
- [79] F. Liao, R. Teo, J. L. Wang, X. Dong, F. Lin, and K. Peng, “Distributed formation and reconfiguration control of VTOL UAVs,” *IEEE Trans. Control Syst. Technol.*, vol. 25, no. 1, pp. 270–277, 2016.
- [80] X. Yu, Z. Liu, and Y. Zhang, “Fault-tolerant formation control of multiple uavs in the presence of actuator faults,” *Int. J. Robust Nonlinear Control*, vol. 26, no. 12, pp. 2668–2685, 2016.
- [81] Y. Zhang, X. Wang, S. Wang, and X. Tian, “Three-dimensional formation–containment control of underactuated auvs with heterogeneous uncertain dynamics and system constraints,” *Ocean Eng.*, vol. 238, p. 109661, 2021.
- [82] B. Mu, K. Zhang, and Y. Shi, “Integral sliding mode flight controller design for a quadrotor and the application in a heterogeneous multi-agent system,” *IEEE Trans. Ind. Electron.*, vol. 64, no. 12, pp. 9389–9398, 2017.
- [83] B. Mu and Y. Shi, “Distributed lqr consensus control for heterogeneous multiagent systems: Theory and experiments,” *IEEE ASME Trans. Mechatron.*, vol. 23, no. 1, pp. 434–443, 2018.
- [84] N. Wang and C. K. Ahn, “Coordinated trajectory-tracking control of a marine aerial-surface heterogeneous system,” *IEEE ASME Trans. Mechatron.*, vol. 26, no. 6, pp. 3198–3210, 2021.
- [85] M. W. Spong, S. Hutchinson, and M. Vidyasagar, *Robot modeling and control*. New York, NY, USA: Wiley, 2006.
- [86] F. Bullo and A. D. Lewis, *Geometric Control of Mechanical Systems: Modeling, Analysis, and Design for Simple Mechanical Control Systems*. New York, NY, USA: Springer, 2005.
- [87] R. Ortega, J. A. L. Perez, P. J. Nicklasson, and H. J. Sira-Ramirez, *Passivity-based control of Euler-Lagrange systems: mechanical, electrical and electromechanical applications*. London, UK: Springer-Verlag, 1998.
- [88] M. Ghasemi, S. G. Nersesov, and G. Clayton, “Finite-time tracking using sliding mode control,” *J. Franklin Institute*, vol. 351, no. 5, pp. 2966–2990, 2014.
- [89] S. Sastry, *Nonlinear Systems: Analysis, Stability, and Control*. New York, NY, USA: Springer, 2013.

- [90] L. R. G. Carrillo, A. E. D. López, R. Lozano, and C. Pégard, *Quad rotorcraft control: vision-based hovering and navigation*. London, UK: Springer Science & Business Media, 2012.
- [91] H. Du, W. Zhu, G. Wen, Z. Duan, and J. Lü, “Distributed formation control of multiple quadrotor aircraft based on nonsmooth consensus algorithms,” *IEEE Trans. Cybern.*, vol. 49, no. 1, pp. 342–353, 2019.
- [92] C. A. Desoer and M. Vidyasagar, *Feedback Systems: Input-Output Properties*. Philadelphia, PA, USA: SIAM, 1975.
- [93] H. K. Khalil, *Nonlinear Systems*. Englewood Cliffs, NJ, USA: Prentice Hall, 3 ed., 2002.
- [94] J. Yang, W.-H. Chen, and S. Li, “Non-linear disturbance observer-based robust control for systems with mismatched disturbances/uncertainties,” *IET Control Theory Appl.*, vol. 5, no. 18, pp. 2053–2062, 2011.
- [95] L. Guo and W.-H. Chen, “Disturbance attenuation and rejection for systems with non-linearity via dobc approach,” *Int. J. Robust Nonlinear Control*, vol. 15, no. 3, pp. 109–125, 2005.
- [96] J. Yang, S. Li, and X. Yu, “Sliding-mode control for systems with mismatched uncertainties via a disturbance observer,” *IEEE Trans. Ind. Electron.*, vol. 60, no. 1, pp. 160–169, 2013.
- [97] E. Cruz-Zavala, J. A. Moreno, and L. M. Fridman, “Uniform robust exact differentiator,” *IEEE Trans. Autom. Contr.*, vol. 56, no. 11, pp. 2727–2733, 2011.
- [98] L. K. Vasiljevic and H. K. Khalil, “Error bounds in differentiation of noisy signals by high-gain observers,” *Syst. Control Lett.*, vol. 57, no. 10, pp. 856–862, 2008.
- [99] J. A. Moreno and M. Osorio, “Strict Lyapunov functions for the super-twisting algorithm,” *IEEE Trans. Autom. Contr.*, vol. 57, no. 4, pp. 1035–1040, 2012.
- [100] A. Teel, E. Panteley, and A. Loría, “Integral characterizations of uniform asymptotic and exponential stability with applications,” *Math. Control Signals Syst.*, vol. 15, no. 3, pp. 177–201, 2002.
- [101] Y. Shtessel, C. Edwards, L. Fridman, and A. Levant, *Sliding Mode Control and Observation*. New York, NY, USA: Birkhauser, 2014.
- [102] T. I. Fossen, *Marine Control Systems: Guidance, Navigation, and Control of Ships, Rigs and Underwater Vehicles*. Trondheim, Norway: Marine Cybernetics, 2002.
- [103] J.-H. Li, P.-M. Lee, B.-H. Jun, and Y.-K. Lim, “Point-to-point navigation of underactuated ships,” *Automatica*, vol. 44, no. 12, pp. 3201–3205, 2008.

- [104] B. Lu, Y. Fang, and N. Sun, “Continuous sliding mode control strategy for a class of nonlinear underactuated systems,” *IEEE Trans. Autom. Contr.*, vol. 63, no. 10, pp. 3471–3478, 2018.
- [105] J. Huang, S. Ri, T. Fukuda, and Y. Wang, “A disturbance observer based sliding mode control for a class of underactuated robotic system with mismatched uncertainties,” *IEEE Trans. Autom. Contr.*, vol. 64, no. 6, pp. 2480–2487, 2019.
- [106] H.-S. Ahn, *Formation Control: Approaches for Distributed Agents*. Cham, Switzerland: Springer, 2020.
- [107] B. Paden and R. Panja, “Globally asymptotically stable ‘PD+’ controller for robot manipulators,” *Int. J. Control.*, vol. 47, no. 6, pp. 1697–1712, 1988.
- [108] B. Wang, S. Nersesov, and H. Ashrafiou, “A unified approach to stabilization, trajectory tracking, and formation control of planar underactuated vehicles,” in *Proc. Amer. Contr. Conf.*, (Denver, CO, USA), pp. 5269–5274, IEEE, 2020.
- [109] B. Wang, S. Nersesov, and H. Ashrafiou, “Formation regulation and tracking control for nonholonomic mobile robot networks using polar coordinates,” *IEEE Contr. Syst. Lett.*, vol. 6, pp. 1909–1914, 2021.
- [110] A. Loría, E. Panteley, D. Popovic, and A. R. Teel, “A nested Matrosov theorem and persistency of excitation for uniform convergence in stable nonautonomous systems,” *IEEE Trans. Autom. Contr.*, vol. 50, no. 2, pp. 183–198, 2005.
- [111] K. B. Ariyur and M. Krstić, *Real-time optimization by extremum-seeking control*. Hoboken, New Jersey: John Wiley & Sons, 2003.
- [112] M. Krstić and H.-H. Wang, “Stability of extremum seeking feedback for general nonlinear dynamic systems,” *Automatica*, vol. 36, no. 4, pp. 595–602, 2000.
- [113] Y. Tan, D. Nešić, and I. Mareels, “On non-local stability properties of extremum seeking control,” *Automatica*, vol. 42, no. 6, pp. 889–903, 2006.
- [114] C. Zhang, A. Siranosian, and M. Krstić, “Extremum seeking for moderately unstable systems and for autonomous vehicle target tracking without position measurements,” *Automatica*, vol. 43, no. 10, pp. 1832–1839, 2007.
- [115] M. S. Stanković and D. M. Stipanović, “Discrete time extremum seeking by autonomous vehicles in a stochastic environment,” in *Proc. 48th IEEE Conf. Decis. Control held jointly with 2009 28th Chin. Control Conf.*, pp. 4541–4546, IEEE, 2009.
- [116] C. Zhang, D. Arnold, N. Ghods, A. Siranosian, and M. Krstić, “Source seeking with non-holonomic unicycle without position measurement and with tuning of forward velocity,” *Syst. Control Lett.*, vol. 56, no. 3, pp. 245–252, 2007.

- [117] J. Cochran and M. Krstić, “Nonholonomic source seeking with tuning of angular velocity,” *IEEE Trans. Autom. Contr.*, vol. 54, no. 4, pp. 717–731, 2009.
- [118] H.-B. Dürr, M. S. Stanković, C. Ebenbauer, and K. H. Johansson, “Lie bracket approximation of extremum seeking systems,” *Automatica*, vol. 49, no. 6, pp. 1538–1552, 2013.
- [119] R. Suttner, “Extremum seeking control for an acceleration controlled unicycle,” *IFAC-PapersOnLine*, vol. 52, no. 16, pp. 676–681, 2019.
- [120] R. Suttner and M. Krstić, “Acceleration-actuated source seeking without position and velocity sensing,” *IFAC-PapersOnLine*, vol. 53, no. 2, pp. 5348–5355, 2020.
- [121] B. Wang, H. Ashrafiou, and S. Nersesov, “Leader-follower formation stabilization and tracking control for heterogeneous planar underactuated vehicle networks,” *Syst. Control Lett.*, vol. 156, p. 105008, 2021.
- [122] A. Scheinker and M. Krstić, “Extremum seeking with bounded update rates,” *Syst. Control Lett.*, vol. 63, pp. 25–31, 2014.
- [123] H.-B. Dürr, M. Krstić, A. Scheinker, and C. Ebenbauer, “Extremum seeking for dynamic maps using Lie brackets and singular perturbations,” *Automatica*, vol. 83, pp. 91–99, 2017.
- [124] S. Michalowsky and C. Ebenbauer, “The multidimensional n-th order heavy ball method and its application to extremum seeking,” in *Proc. 53rd IEEE Conf. Decis. Control*, pp. 2660–2666, IEEE, 2014.
- [125] S. Michalowsky and C. Ebenbauer, “Model-based extremum seeking for a class of nonlinear systems,” in *Proc. 2015 American Control Conf.*, pp. 2026–2031, IEEE, 2015.
- [126] A. Scheinker, “Extremum seeking for force and torque actuated systems,” in *Proc. 57th IEEE Conf. Decis. Control*, pp. 7107–7111, IEEE, 2018.
- [127] R. Suttner, “Extremum seeking control for a class of mechanical systems,” *IEEE Trans. Autom. Contr.*, vol. Early Access, 2022.
- [128] S.-J. Liu and M. Krstic, “Stochastic averaging in continuous time and its applications to extremum seeking,” *IEEE Trans. Autom. Contr.*, vol. 55, no. 10, pp. 2235–2250, 2010.
- [129] N. Monshizadeh, P. Monshizadeh, R. Ortega, and A. van der Schaft, “Conditions on shifted passivity of port-hamiltonian systems,” *Syst. Control Lett.*, vol. 123, pp. 55–61, 2019.
- [130] V. Grushkovskaya, A. Zuyev, and C. Ebenbauer, “On a class of generating vector fields for the extremum seeking problem: Lie bracket approximation and stability properties,” *Automatica*, vol. 94, pp. 151–160, 2018.

- [131] A. R. Teel, J. Peuteman, and D. Aeyels, “Semi-global practical asymptotic stability and averaging,” *Syst. Control Lett.*, vol. 37, no. 5, pp. 329–334, 1999.
- [132] P. E. Crouch, “Geometric structures in systems theory,” *IEE Proc.*, vol. 128, no. 5, pp. 242–252, 1981.
- [133] F. Bullo, N. E. Leonard, and A. D. Lewis, “Controllability and motion algorithms for underactuated lagrangian systems on Lie groups,” *IEEE Trans. Autom. Contr.*, vol. 45, no. 8, pp. 1437–1454, 2000.
- [134] W. Hahn, *Stability of motion*. New York, NY, USA: Springer, 1967.
- [135] Z.-P. Jiang, A. R. Teel, and L. Praly, “Small-gain theorem for ISS systems and applications,” *Math. Control Signals Syst.*, vol. 7, no. 2, pp. 95–120, 1994.
- [136] E. Restrepo, A. Loria, I. Sarras, and J. Marzat, “Robust consensus of high-order systems under output constraints: Application to rendezvous of underactuated UAVs,” *IEEE Trans. Autom. Contr.*, vol. Early access, pp. 1–1, 2022.
- [137] B. Wang, S. G. Nersesov, and H. Ashrafiou, “Time-varying formation control for heterogeneous planar underactuated multivehicle systems,” *ASME J. Dyn. Syst. Meas. Contr.*, vol. 144, no. 4, p. 041006, 2022.
- [138] B. Wang, S. Nersesov, and H. Ashrafiou, “Robust formation control and obstacle avoidance for heterogeneous underactuated surface vessel networks,” *IEEE Trans. Control Netw. Syst.*, 2022.
- [139] S. Zhao, Z. Li, and Z. Ding, “Bearing-only formation tracking control of multiagent systems,” *IEEE Trans. Autom. Contr.*, vol. 64, no. 11, pp. 4541–4554, 2019.
- [140] Z. Li, H. Thunay, S. Zhao, W. Meng, S. Q. Xie, and Z. Ding, “Bearing-only formation control with prespecified convergence time,” *IEEE Trans. Cybern.*, 2020.
- [141] K. Wu, J. Hu, B. Lennox, and F. Arvin, “Finite-time bearing-only formation tracking of heterogeneous mobile robots with collision avoidance,” *IEEE Trans. Circuits Syst. II Express Briefs*, vol. 68, no. 10, pp. 3316–3320, 2021.
- [142] T. Hamel and C. Samson, “Position estimation from direction or range measurements,” *Automatica*, vol. 82, pp. 137–144, 2017.
- [143] B. Yi, C. Jin, and I. R. Manchester, “Globally convergent visual-feature range estimation with biased inertial measurements,” *arXiv preprint arXiv:2112.12325*, 2021.
- [144] J.-J. Slotine and W. Li, “On the adaptive control of robot manipulators,” *Int. J. Rob. Res.*, vol. 6, no. 3, pp. 49–59, 1987.

- [145] E. Panteley, A. Loria, and S. Sukumar, “Strict lyapunov functions for consensus under directed connected graphs,” in *Proc. Euro. Control Conf.*, pp. 935–940, *Proc. Euro. Control Conf.*, IEEE, 2020.
- [146] W. M. Haddad and V. Chellaboina, *Nonlinear Dynamical Systems and Control: A Lyapunov-Based Approach*. Princeton, NJ, USA: Princeton University Press, 2011.
- [147] B. Wang, H. Ashrafiou, and S. G. Nersesov, “The use of partial stability in the analysis of interconnected systems,” *ASME J. Dyn. Syst. Meas. Contr.*, vol. 143, p. 044501, 2021.
- [148] L. Moreau and D. Aeyels, “Practical stability and stabilization,” *IEEE Trans. Autom. Contr.*, vol. 45, no. 8, pp. 1554–1558, 2000.
- [149] N. Rouche, P. Habets, and M. Laloy, *Stability theory by Liapunov’s direct method*. New York, NY, USA: Springer, 1977.
- [150] E. Panteley, A. Loria, and A. Teel, “Relaxed persistency of excitation for uniform asymptotic stability,” *IEEE Trans. Autom. Contr.*, vol. 46, no. 12, pp. 1874–1886, 2001.
- [151] S. Sastry and M. Bodson, *Adaptive control: stability, convergence, and robustness*. Englewood Cliffs, NJ, USA: Prentice-Hall, 1989.
- [152] F. Bullo, “Averaging and vibrational control of mechanical systems,” *SIAM J. Control Optim.*, vol. 41, no. 2, pp. 542–562, 2002.